NANYANG TECHNOLOGICAL UNIVERSITY

SYNTHESIS, STRUCTURES AND PROPERTIES OF FUNCTIONAL POLYHEDRAL OLIGOMERIC SILSESQUIOXANE (POSS)-BASED CONJUGATED MATERIALS

XIAO YANG

SCHOOL OF MATERIALS SCIENCE & ENGINEERING (MSE)

2010

SYNTHESIS, STRUCTURES AND PROPERTIES OF FUNCTIONAL POLYHEDRAL OLIGOMERIC SILSESQUIOXANE (POSS)-BASED CONJUGATED MATERIALS

XIAO YANG

School of Materials Science & Engineering (MSE)

A thesis submitted to the Nanyang Technological University
in fulfillment of the requirement for the degree of
Doctor of Philosophy

2010

Acknowledgements

I am grateful to the Agency for Science, Technology and Research (A*Star) for the Scientific Staff Development Award (SSDS) which awards the sponsorship for, and allows me to undertake the Ph. D programme.

I would like to express my deepest gratefulness and respect to my supervisor, A/P Lu Xuehong for giving me this opportunity to pursue a Ph. D degree in NTU. Also thanks Prof Lu for her endless patience and warmest encouragement as well as in detailed guidance throughout my study. I would also like to thank my co-supervisor, Dr He Chaobin, for his nomination and support for my application for SSDS. I have been sincerely appreciating Dr He's supervision for many years and grateful to his inspiring and expert guidance. I am really grateful to Dr He for providing me the comprehensive training plan and research freedom. Special thanks shown to Dr He for his patience, tolerance, and gentleness.

Thanks to all the staff and students working in organic synthesis lab under Dr Chen Zhikuan's supervision, especially thanks to Ms Chang Soon Yee for her daily support and lab management as well as assistance in HPLC, GPC, MDTF, DSC, and TGA testing. I would also like to thank Dr Zhang Xinhai for his valuable discussion and effort in time-resolved photoluminescence analysis. I sincerely appreciate the help given by Dr Tripathy Sudhiranjan in Raman spectroscopy analysis. Thanks to Ms Tan Li Wei and Mr. Ong Kian Soo for device fabrication and testing.

Thanks to my parents, husband, and daughter for their unconditional love and support.

TABLE OF CONTENTS

Summary

Polyhedral oligomeric silsesquioxane (POSS) is a cage-like molecule with a well-defined and highly symmetric structure having a size of 0.5 nm diagonally. The POSS material demonstrates a truly hybrid inorganic core / organic shell architecture with one or more vertexes covalently substituted by a wide range of functional groups which render materials with versatile properties for many applications. Recent studies indicate POSS incorporated conjugated polymers show improved performance due to less aggregation caused by the cubic cage which interrupts close packed linear polymers. Our previous work indicated that molecules consisting of a POSS cage and rigid organic short chains exhibit strong quantum confinement effects which imply organic-quantum-dot-like properties.

In this research, a systematic study on the effect of incorporation of POSS on the properties, especially optical characteristics, of luminescent nano-particles and hyper-branched polymers was conducted in three areas: 1) Well defined blue POSS luminescent dots were designed and synthesized where conjugated oligomers are directly grafted onto eight vertexes of POSS cage. It was found that excitons are confined in each arm of emissive units and hence excitons are confined within each dot and isolated chromospheres are obtained. 2) Highly regioselective bromination of octaphenyl-POSS was achieved. The green POSS light emitting dots based on this structure were synthesized to achieve well defined nano-particles with precisely controlled structures and sizes. The structures demonstrated quantum confined characteristics as both intra- and inter- molecular interactions are prevented and exciton decay time remained same regardless the molecules were in solid form, solution state or solid solutions blended with other polymers. 3). Functional POSS was incorporated into red hyper-branched conjugated polymers. As a result, POSS based hyper-

branched polymers demonstrated greatly improved performances compared to the parent polymer before incorporating with POSS.

In summary, isolated organic chromospheres are first achieved, by using a rigid POSS cage and well defined organic moieties which are protected by alkyl/alkoxy shielding chains. The isolated chromospheres can be in condensed solid form as well as in solution. The achievement is significant for exciton dynamic studies, optical physics, as well as organic-light-emitting-diodes and solar cell applications. Combining inorganic cores and functionalized organic moieties, one can build nano-structured molecules with desired novel properties neither pure inorganic nor organic molecules possess.

CHAPTER ONE

INTRODUCTION

1.1 POSS materials

1.1.1 Structure of POSS materials

Silsesquioxane includes all structures with the formula $RSiO_{1.5,}$ where R can be H, a halogen atom, or any organic group.[1] Oligomeric silsesquioxanes are compounds with the general formula $(RSiO1.5)_n$, where n is an even number ($n \geq 4$) and R is same as the above mentioned.[2] Although the first oligomeric silsesquioxane was obtained in 1946,[3] the interest in silsesquioxanes chemistry continues to increase. In particular, in the past two decades, most attention has been centered on the oligomeric silsesquioxanes with cage structures, as shown in scheme 1.1, and these polyhedral oligomeric silsesquioxanes have been designated by the abbreviation POSS.[4] In recent years the term POSS has gradually been narrowed down to indicate T8 $(RSiO_{1.5})_8$ due to the high popularity and unique advantages of its properties as well as easy production methods.

POSS compounds represent a typical inorganic / organic hybrid molecule which contains an inner inorganic cage which is externally substituted by organic moieties. These organic groups can be either totally hydrocarbon (including pure hydrogen) in nature or functional groups. The cage has a well-defined and highly symmetric structure having a size of 0.5 nm diagonally and is roughly 1.5 nm in dimension when the eight alkyl groups on vertexes are included. The POSS molecule can be considered as the smallest silica particle. Each POSS molecule contains organic substituents on its eight vertexes that make the POSS nanostructure compatible with biological systems，polymers, or surfactants. Furthermore, these groups can be specially designed to be active or non-reactive.

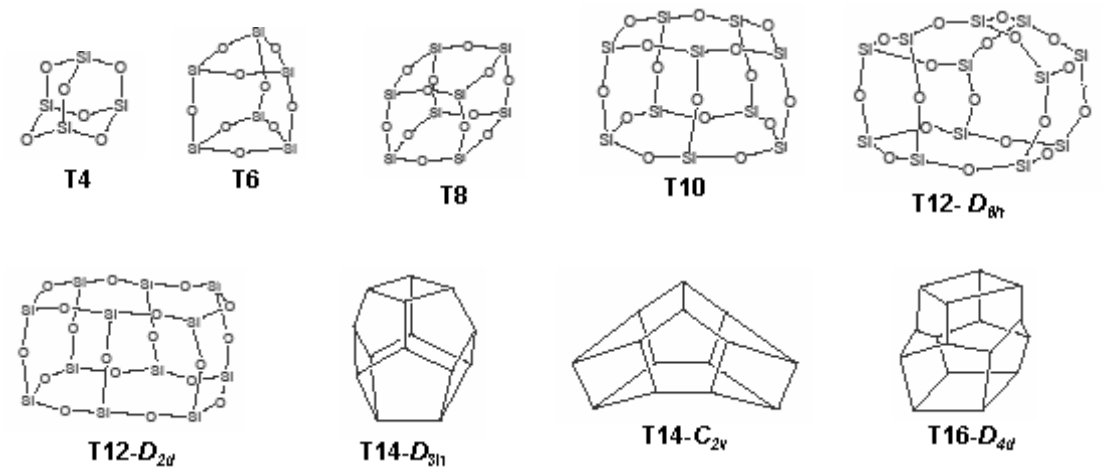

Scheme 1.1.[4] POSS structures of T_4-T_{16}. For easy review the R group connected to Si atom was not drawn. T_{14} and T_{16} are line drawings in which each vertex represents a Si–H or Si-R unit and each edge represents a Si-O-Si link.

1.1.2 Unique properties

POSS with its unique cage-like structure and nano-meter scale of dimensions are of particular interest. The inorganic core can be attached by a wide range of functional groups onto each vertex, leading to its use in a variety of different applications.[5-7] Depending on application, mono- or multi- functionalized POSS can be prepared. The mono-functionalized POSS materials, with seven inert groups and one reactive group, including polysiloxane,[8] poly(methyl methacrylate),[9] poly(4-methyl styrene),[10,11] epoxy,[12,13] polynorbornene,[14,15]and polyurethane[16] have been developed as reinforced filler, which can be grafted to or copolymerized with matrix polymers. POSS with eight reactive functional groups that could be used to form a cross-linking network has been prepared and studied as a filler to enhance

the mechanical property of polymer matrix. Theses functional POSS materials include epoxy,[17-20] amine,[21,22] methacryloyl,[23] vinyl,[24] alkyl halide,[25] hydrido,[24] and isocyanate.[26] It is well known that when the size of the filler is decreased to nano-meter scale, the surface to volume ratio of the filler significantly increases. As a results, the molecular interaction between the fillers and matrix will become a dominant factor in influencing the property of the resulting nano-composite, which could lead to significant improvements in physical properties such as thermal stability, elasticity, mechanical properties, gas barrier, and oxidative retardance.[27–31] For example, the incorporation of a POSS cage into linear polymer chains or polymer networks changes the local molecular interactions and local molecular morphology as well as polymer segmental mobility,[32] leading to improvement in modulus, strength, glass transition temperature, thermal stability, and dimensional stability.[33] POSS molecules can be inserted into polymer systems physically, i.e. non-reactively, or chemically, e.g. form copolymer or cross linking network. In the bottom-up approach, which was realized by chemical reaction, a good dispersion of POSS cage into polymers can be achieved through covalent linkage and the reinforcement occurs via self-assembly or aggregation as well as crystallization.[34]

1.1.3 Applications

Due to their unique structure and excellent properties, POSS materials have a variety of applications. POSS can improve the oxidative stability and flame retardance of polymers in terrestrial applications.[35–37] POSS can also be used as photo-resist coatings,[38-42] barrier materials,[43] dielectric and protective coating films for semiconductor devices,[44-48] liquid crystal display elements,[49] chemosensors,[50] optical fiber coatings,[51] gas separation

membranes,[52] drugs.[53] Recently, there are reports on applications as dental adhesives,[54] lubricants.[55] POSS nanostructures have also shown significant promise for use in catalyst supports[56-59] and in biomedical applications as scaffolds for drug delivery,[60] imaging reagents,[61] and combinatorial drug development.[62] Indeed, many other applications have also been emerged for POSS-based materials including fuel cell and battery membranes.[63-65] All of these applications exploit the unique characteristic of functional POSS materials, i.e. an organic-inorganic hybrid with well defined nano-structures which is easy to be modified with different groups.

The POSS cage has been incorporated into polymer-light-emitting-diodes (PLEDs) applications due to the unique properties of POSS cage and the intrinsic challenges encountered in PLEDs.

1.2 PLED materials

1.2.1 Light emitting materials

Since discovery by Heeger and co-workers as highly conductive polyacetylene (PA) in 1977, PLEDs have attracted intense and long lasting interest.[66] In 1990 Friend and co-workers reported a green electroluminescent device based on a layer of pure conjugated poly(*p*-phenylene vinylene)(PPV) placed between indium tin oxide (ITO) and Al electrodes[67]. The device efficiency and relatively low turn-on voltage sparked an intensive study in PLEDs because of the promised commercial applications in large-area flat-panel displays. The advantages of PLED include solution processing which can be applied to a large area and flexible displays at much lower cost compared to inorganic and small molecular displays; fine tailor-able polymer properties by modification of structures; light weight; and

easy producing. These properties inspired a passion of generating new materials for PLED applications. It is clear that the sophisticated control of the materials in emissive color, efficiency, balanced charge injection and charge transportation are crucial and directly affect the performance of devices. In past decade a large number of different classes of light-emitting conjugated polymers have been developed[68], e.g. poly(fluorene)s (PFs)[69], PPVs[70], poly(p-phenylene) (PPP)[71], poly(phenylene ethnylenes)[72] (PPE), and poly(thiophene)s (PTs)[73], and their derivatives, as shown in Scheme 1.2.

Under photo-excitation a conjugated molecule will be excited from a vibrational level in the electronic ground state to one of the many vibrational levels in the electronic excited state, as shown in Scheme 1.3. A molecule in a higher vibrational level of the excited state will quickly relax to the lowest vibrational level of this state by transferring energy to other molecules through collision. When the molecule returns from excited singlet state to ground state a photon will be emitted and this whole process is called photoluminescence (PL). Of course there are many other ways for molecules to release absorbed energy non-emissively. These processes are also called radiative and non-radiative energy transfer.

PPVs:

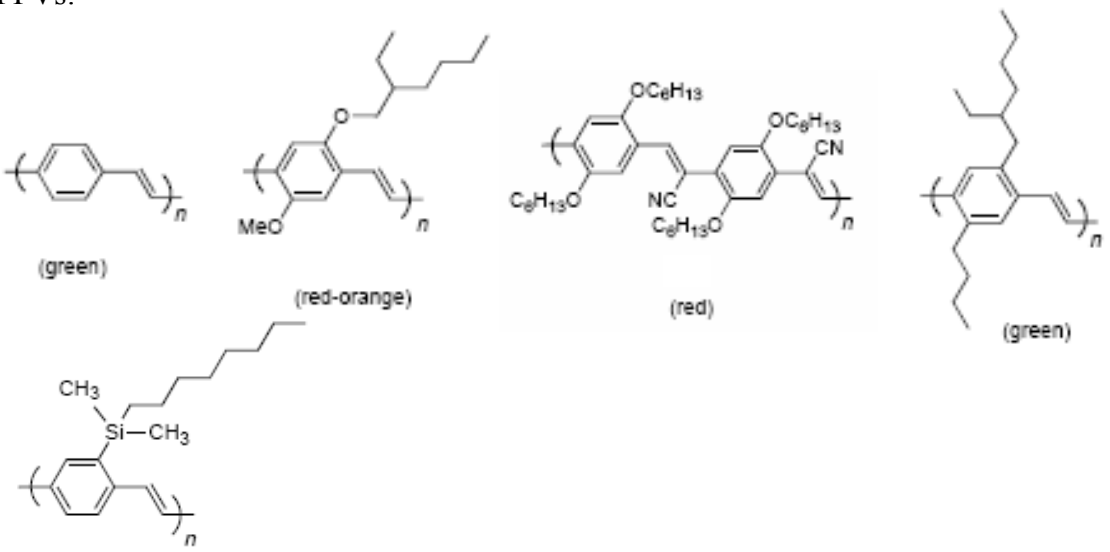

PPPs (ladder type)

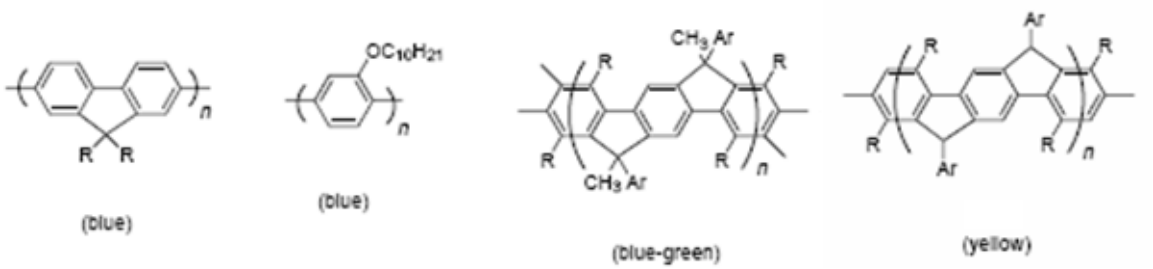

PTs

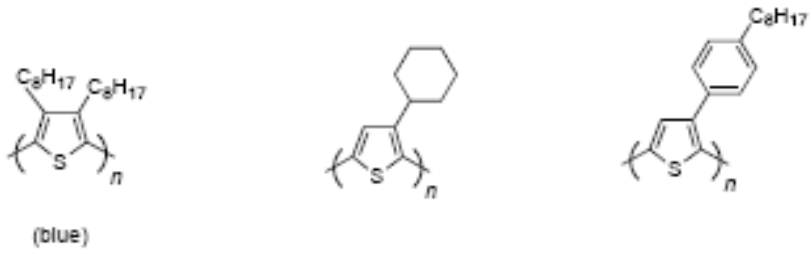

PPEs

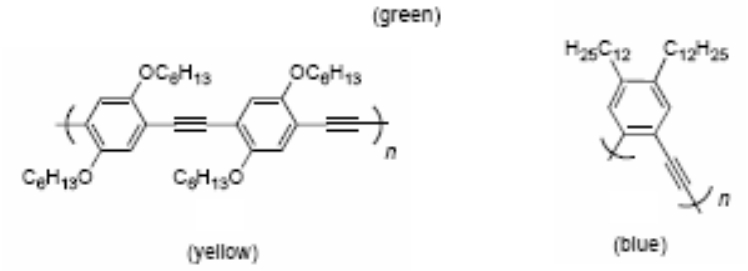

Scheme 1.2. Examples of light-emitting polymers

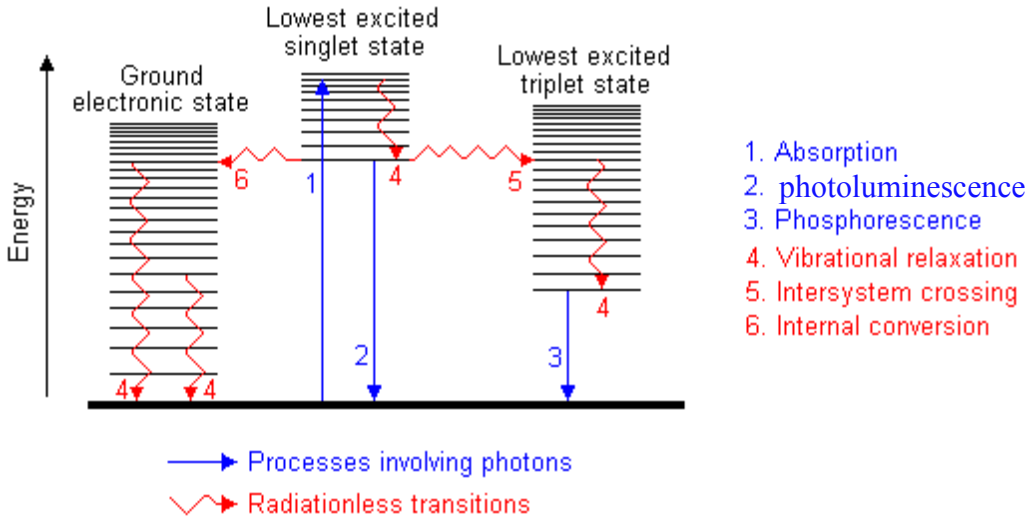

Scheme 1.3. Possible physical process following absorption of a photon by a molecule

Similar with photoluminescence, under electro-excitation a conjugated molecule will absorb energy released from the combination of electron and hole and be excited from a vibrational level in the electronic ground state to one of the many vibrational levels in the electronic excited state. When the molecule returns to ground state it will emit light and this whole process is called electroluminescence (EL), as shown in Scheme 1.4.

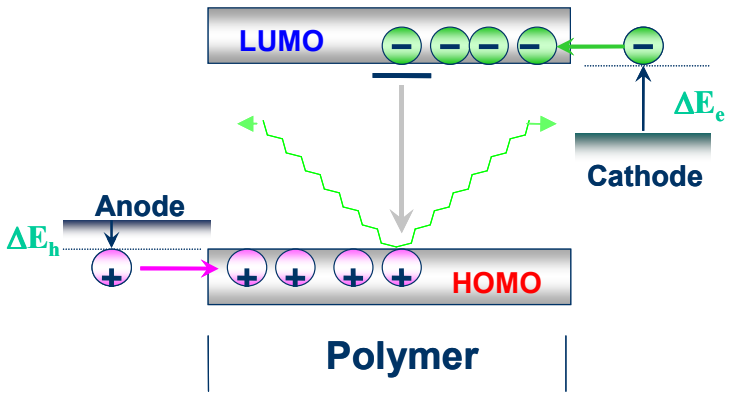

Scheme 1.4. Principle of electroluminescence in a simple device

1.2.2 Light emitting diodes

The PLED device stack was shown in Scheme 1.5. The emissive conjugated polymer film is sandwiched between a cathode and an anode. When direct electric current is run through this device, the cathode releases an electron and the anode releases a hole into the polymer film. Within the polymer film, the electron and the hole recombine and hence release energy that excites the organic material. This excitation emits light in the color characterized by the polymer material. In order for the light to emit outward, either the cathode or the anode must be transparent or translucent. For balanced charge injection and transportation some extra layers would be added in between the emissive layer and the electrodes. In Scheme 1.5 an electron transportation layer (ETL) and hole transportation layer (HTL) were added. The electron (hole) injection layer would be added in between cathode (anode) and ETL (HTL) layers in some other devices as well.

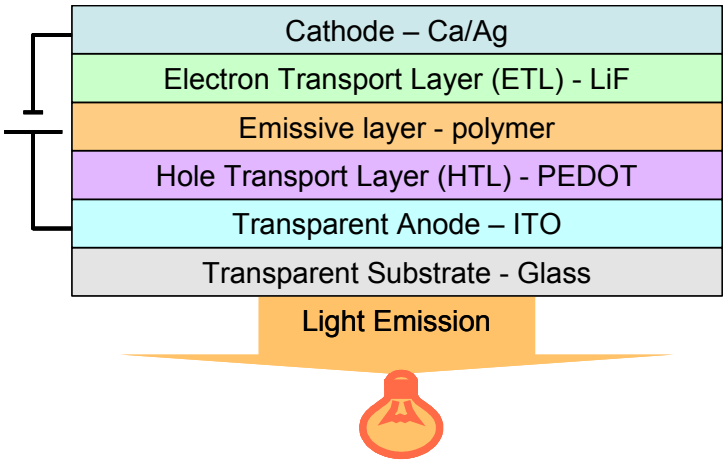

Scheme 1.5. PLED device figure. ITO: Indium Tin Oxide; PEDOT: poly(3,4-ethylenedioxythiophene. PEDOT doped with PPS (Polystyrenesulfonic acid).

1.2.3 Aggregation

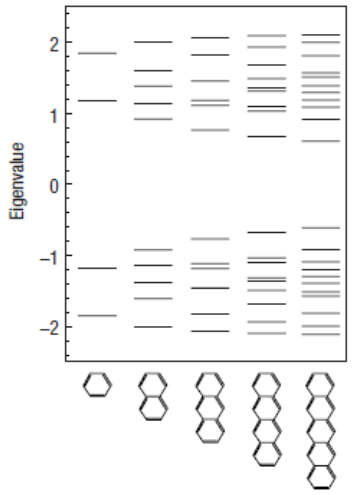

Scheme 1.6. Energy splitting of aggregation of conjugated moieties.[74] Occupied (in the ground state) and virtual molecular orbitals for a series of polyacenes.

HOMO and LUMO are short forms of the highest occupied molecular orbital and lowest unoccupied molecular orbital respectively for conjugated polymers. The energy difference between HOMO and LUMO is defined as the band gap which can serve as a measure of the color the polymer emits and also indicates how easy the molecule can be excited. The HOMO level is the valence band and the LUMO level is the conduction band for inorganic semiconductors. When the molecule forms a dimer or aggregation, the close packing of the orbitals from different polymers or segments leads to a splitting of the HOMO and LUMO energy levels. The simple illustration is shown in Scheme 1.6. This splitting produces vibrational sublevels which each have their own energy, slightly different from one another. There are as many vibrational sublevels as there are molecules that interact together. When there are enough molecules influencing each other (e.g. in an aggregate), there are so many sublevels that we no longer perceive their discrete nature because they form a continuum. We no longer consider energy levels, but energy bands. From Scheme 1.6 we can simply see

the longer the conjugation, or the more the aggregation, the narrower the band gap, and the redder the color of absorbtion and emission by the molecules. In other words, as the conjugation size increases, the band gap decreases.

1.2.4 H and J aggregation

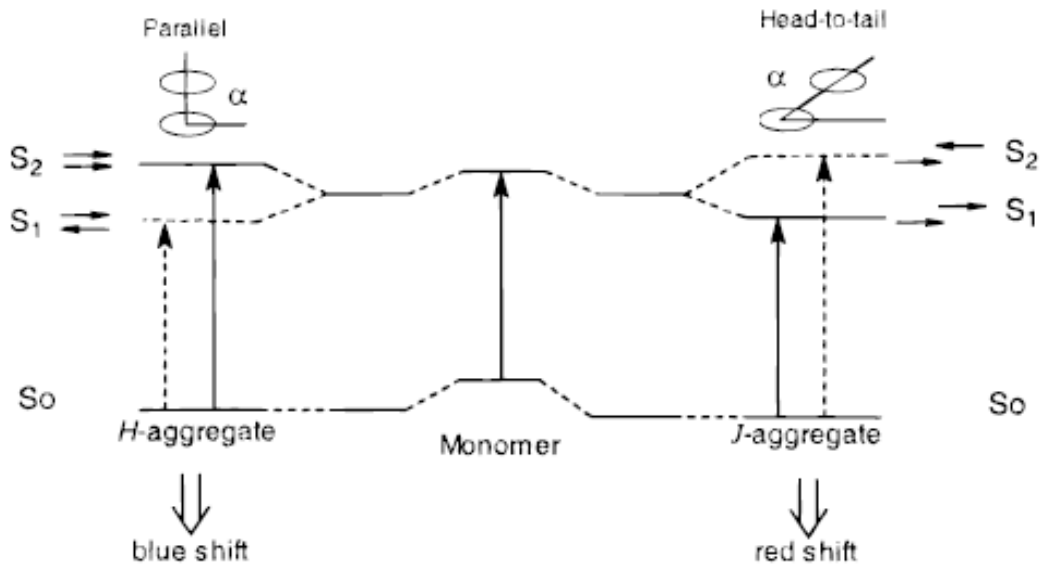

Scheme 1.7. Schematic representation of the relationship between chromophore arrangement and spectral shift based on the molecular exciton theory.

As above mentioned, normal aggregation leads to extension of conjugation, however, if polymer chains or segments aggregate in a way to cause conformation change or backbone twisting, the molecular energy levels will be changed hence two possible consequences will result which is either the band gap enlarges or reduces. The aggregation leading a spectrum red shift is called as J- aggregation and blue shift as H- aggregation.

The first study found that for some dyes the aggregate absorption band is red shifted with respect to that of the monomer and these are the J-aggregates (J for Jelly, one of the first workers who investigated these shifts). By contrast, other dyes showed a shift towards the blue (i.e. higher absorption energies) and were termed H-aggregates (hypsochromic shift). Although dye molecule J-aggregates have been well documented since the early part of this century, conjugated polymer J-aggregates were only reported recently.[75-77] Computational investigations of the effect of intermolecular orientation in aggregates[78] showed that a brick-work arrangement of molecules leads to the characteristic spectral red-shift in J-aggregates. Recent studies of excited state inter-reactions between polymers and large oligomers were confined to aggregates of parallel molecules oriented normally with respect to the intermolecular axis.[79-83]

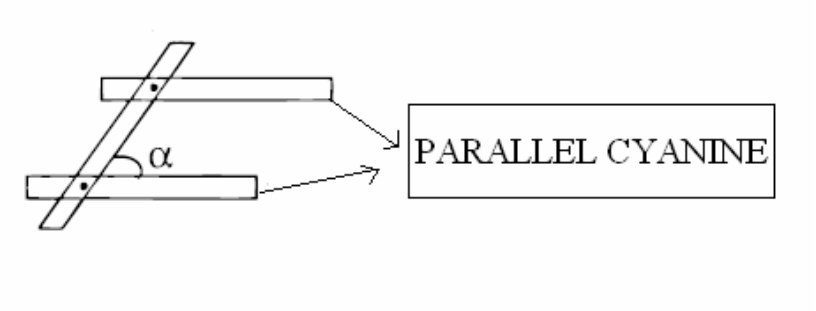

Scheme 1.8. definition of slip angle.[84]

The slippage angle can be defined as the angle between long axis (line passing through the center of the aggregates or parallel to it) and one of the parallel molecule.[84] It is generally agreed that both H and J aggregates are composed of parallel dye molecules stacked plane to plane and end to end and form two dimensional dye crystals molecule. As described above H and J aggregates have their optical properties determined according to their structural

packing. Actually, the difference in structure is due to the different slip angles of the stacked molecules. Large molecular slippage ($\alpha < 32°$) results in a bathochromic shift (J - aggregate), and small slippage ($\alpha > 32°$) results in a hypsochromic shift (H - aggregate).[84] The dye molecules may aggregate in a parallel way (plane to plane stacking) to form a sandwich type arrangement (H dimer) or in a head to tail arrangement (end to end stacking) to form a J dimer.

1.2.5. Challenges of PLEDs

Even though conjugated polymers are promising in applications of PLED, sensors[85], thin-film organic transistors[86], lasers[87], and light-emitting chemical cells[88], they have intrinsic drawbacks. The stability under operating conditions is one of the challenges needing to be overcome. It was also observed that there are challenges in selecting materials for efficient light emitting diode applications because the aggregation effects [89,90] and lower efficiency caused by exciton quenching.[91,92] Beside these, the morphology of polymers has a pronounced effect on the fluorescence yield which can be changed dramatically by using different processing methods.[93] Even though conjugated polymers suffer from considerably lower oxidative stability and lower electroluminescent quantum efficiency compared to inorganic counterparts, they are still attractive as luminescent materials because they promise to have superior processing and thermal properties. Material scientists have been exploring different approaches to achieve high efficiency, high purity, long lifetime, and high stability of polymeric materials which are comparable to the advantages of inorganic or small molecular materials.[94,95]

One of the main challenges to achieve high luminescence quantum efficiency in conjugated polymers is aggregation quenching of the excited state[96-98] because the chromophores are not diluted in solid form as in the diluted solutions. The physical origin of aggregation quenching has been shown to be intra- and inter- chain molecular interactions.[99] Conjugated chains in solid state tend to form aggregates, driven mainly by favorable local π - π interaction and their rigid-rod nature.[100-103] The aggregation in this sense refers to the association of multiple conjugated backbones that results in photo-physical change of the chromophores.[104] Formation of intra- and inter- chain excited state complexes is a non-preventable phenomenon in concentrated solution as well as in the condensed state, especially for those with a lower band gap and flatter backbone structures. These aggregations effectively quench excitons and as a result aggregations tend to be emissive at low efficiency and are therefore a hindrance in realizing optimum luminescence in light-emitting diodes.

The aggregation in conjugated polymers is a very important phenomenon because the polymer chains in aggregated state exhibit electronic properties distinct from that of the isolated chains. The aggregation has been known to cause a red-shift peak in absorption and emission spectra, normally.[105-116] As previously discussed, J aggregation is dominant in conjugated polymers.

1.3 POSS as a building block for light-emitting diode

Polymer intra- and inter- chain interactions and the associated formation of aggregates and excimers are known as sources of degradation in polymer-based devices[117-121]. Due to

the unique structure and properties, POSS has been incorporated into polymer chains to limit / prevent linear chains from aggregation to improve efficiencies of PLEDs.

(I). The first report of incorporating POSS to conjugated polymer system was claimed by Alan J. Heeger and his co-workers[122] in 2003. In this work, they demonstrated semi-conducting polymers, MEH-PPV and PF, with improved thermal stability, reduced chain mobility, and a decrease in the electroluminescent spectral features associated with aggregation/excimer formation, by chemically incorporating bulky POSS into polymer chains. Higher external quantum efficiency (2.2% vs. 1.5%) and luminance (1320 vs. 230 cdm^{-2}) were achieved from the PLED device by using MEH-PPV-POSS compare to neat MEH-PPV. The structures are shown in Scheme 1.9. The molecular weight (*M*w) for MEH-PPV-POSS is 3.5 x 10^5 and PF-POSS is 1.6 x 10^5. It is found that even with a low POSS concentration in polymers, the improvement in device performance is significant.

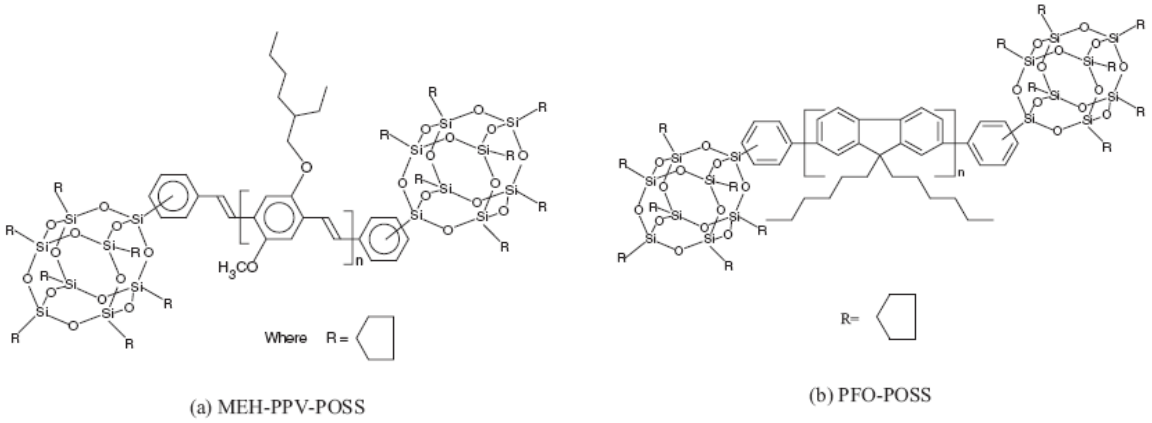

(a) MEH-PPV-POSS (b) PFO-POSS

Scheme 1.9. Structure of (a) MEH-PPV-POSS, and (b) PF-POSS reported in reference 122

(II) The other work was conducted by Hong-Ku Shim and his co-workers in 2004 using mono-functionalizes POSS as a pendent group attached on a PF's side chain to form a co-polymer[123]. The structure is shown in Scheme 1.10. The photoluminescence (PL) spectra of

PF-POSSs showed reduced aggregation / excimer formation because the bulky POSS group inhibited inter- chain interactions. The dilution effect and the high

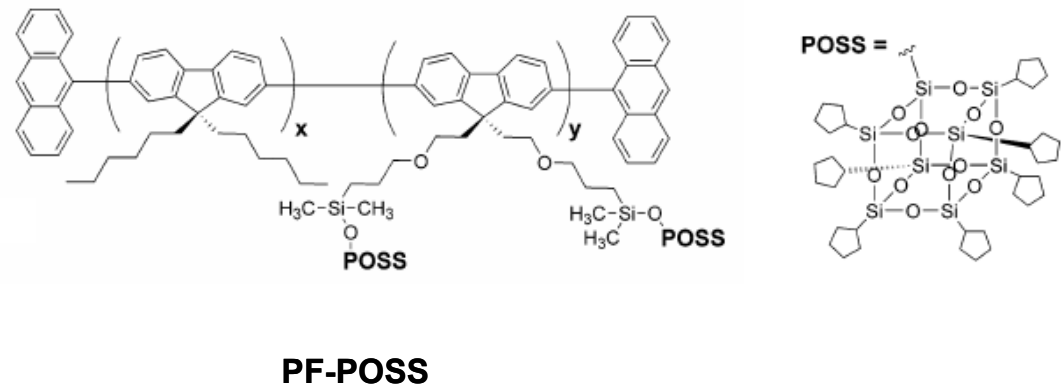

PF-POSS

Scheme 1.10. Structure of PF-POSS reported in reference 123

thermal stability of the POSS unit also improved the color stability of PF-POSS's blue emission after annealing at 150°C. The PL quantum efficiency of PF-POSS both in solution and film are higher than that of PF. The PLED device using the new material as emitting layer showed a very stable blue light emission. The device also showed a low turn-on voltage of 3.7 – 4.4V and brightness of 350 – 1010 cd/m^2.

(III). In 2004 another work studying PF-POSS was reported by Alex K. –Y. Jen[124]. The star-like polymer using POSS as core and a flexible ethylene group connecting Si of POSS and a PF chain in each of the eight vertexes of POSS was synthesized. The incorporation of POSS as core into PF significantly reduced the aggregation and enhanced the thermal stability. The DSC study showed an elimination of the glass transition and crystallization, and a significant reduction of the melting enthalpy for PF-POSS. The stability of the PL

spectra of PF-POSS could be up to 150°C, while PF showed a significant green emission at 530nm. The single layer device fabricated by PF-POSS showed turn-on voltage of 6.0 V, a brightness of 5430 cd/m^2 at 8.8V. The maximum electroluminescent intensity and quantum efficiency of PF-POSS are almost twice as good as those of PF.

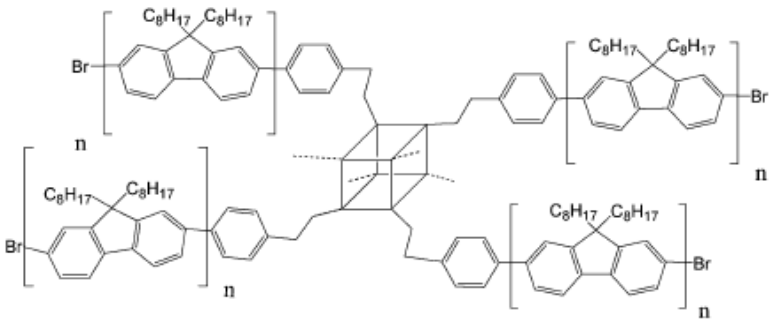

PF-POSS

Scheme 1.11. Structure of PF-POSS reported in reference 124

(IV). In year 2005 Kung-H. Wei and co-workers conducted another work of incorporation of POSS to PF[125]. POSS as pendent group rigidly attached to a PF side chain through an amino phenyl linker, slightly different from that of produced by Hong-Ku Shim's group. The structure of PF-POSS is shown as Scheme 1.12. The improvement of thermal stability and PL, EL quantum efficiency is similar to the results described above in references. The green emission is undesired in PF system but normallyunavoidable. By adding POSS into the system this problem has been resolved. When 5% POSS was included in PF-POSS, the intensity of the blue peak at 425nm increased while the green peak at 530nm remained the same. When 10% POSS was incorporated into PF-POSS, the green emission was reduced

sharply while the blue peak became the major emission. The incorporation of POSS to PF serves a dual function, it not only hinders oxidation of fluorine but also increases the inter-chain distance hence retarding the inter-chain interactions and leading to a reduction of excitons migration to defect sites.

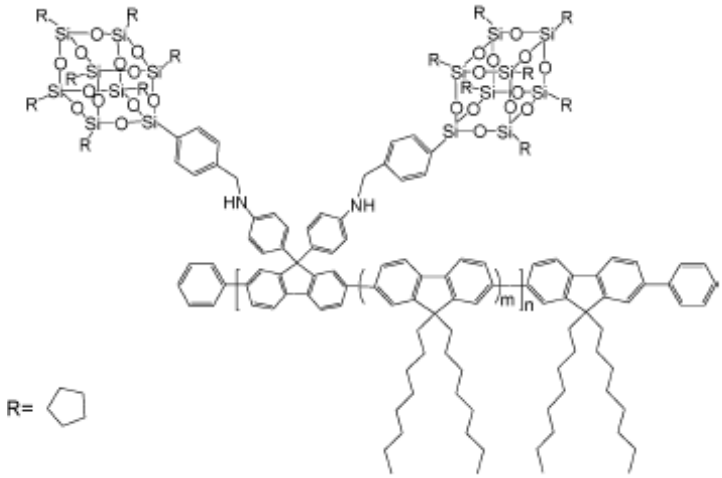

PF-POSS

Scheme 1.12. Structure of PF-POSS reported in reference 125

(V). In same year, 2005, after studying PF-POSS, Kung-H. Wei and co-workers conducted another work of about MEH-PPV[126]. Unlike Alan J. Heeger's work that incorporating POSS at the end of MEH-PPV chain, this time the mono-functionalized POSS as a pendent side group was linked to the copolymer's chain. The structure is shown in Scheme 1.13. Similar with previous reports, incorporation of POSS into a conjugated polymer system increased the thermal stability and PL, EL quantum efficiency due to the reduction of aggregation. By incorporating 10% mole of PPV-POSS into MEH-PPV-POSS system, PL efficiency in thin film increased from 19% to 85% compare to pure MEH-PPV. The device maximum brightness increased from 473 cd/m^2 of MEH-PPV to 2196 cd/m^2 of MEH-PPV-POSS.

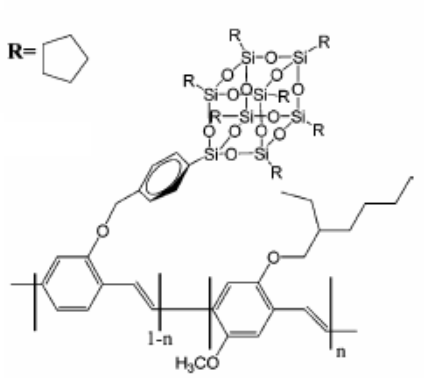

MEH-PPV-POSS

Scheme 1.13. Structure of MEH-PPV-POSS reported in reference 126

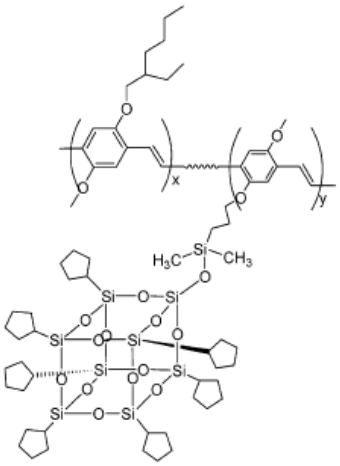

MEH-PPV-POSS

Scheme 1.14. Structure of MEH-PPV-POSS reported in reference 127

(VI). In 2006, Hong-Ku Shim's group reported two pieces of work at same time, one was MEH-PPV-POSS[127] and another was PF-POSS[128]. The structures reported in these two papers are shown in Scheme 1.14 and 1.15. The structure of MEH-PPV-POSS is similar to that described in reference 126. The eight-armed PF-POSS has a maximum PLat 394nm which overlapped with the maximum absorption of PF in solution state, and it was proposed

by the author that using PF-POSS as a dopant to realize energy transfer from PF-POSS to PF to increase the quantum efficiency of PF system.

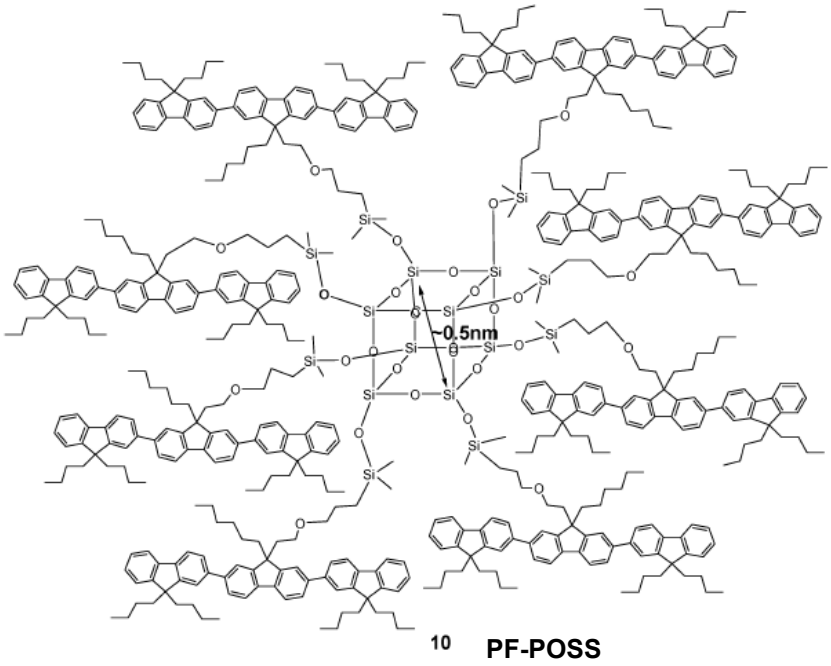

Scheme 1.15. Structure of PF-POSS reported in reference 128

(VII). In 2004, we reported high efficient luminescent organic clusters with quantum dot like properties [129]. The structures reported in this paper are shown in Scheme 1.16. The organic arms work as luminescent centers which are end-capped by alkyl chains to prevent inter-molecular aggregation. To minimize the rotating of phenyl rings, which could cause PL lines broadening, methyl groups are grafted in each α position of the adjacent phenyl ring to increase torsion energy barrier. The most commonly used method for identifying quantum confinement effect for inorganic quantum dot (QD), TEM, UV, PL, Raman, was conducted

on these materials and all of the results indicated these organic cluster materials have QD like properties.

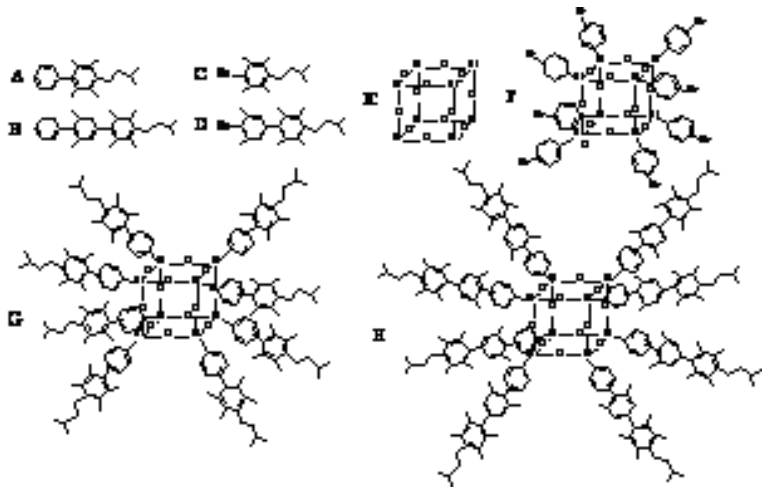

Scheme 1.16. Structure of POSS based molecules reported in reference 129.

In summary, the incorporations of POSS into light-emitting polymers have been proved as an effective approach to achieve higher quantum efficiency of the resulting light emitting polymers. These researches however have been focused mainly on PF and MEH-PPV modification, through a flexible chain linking conjugated polymers with POSS. The modification ranges from end – capping of POSS onto polymer chains to attaching POSS as a pendent group onto a conjugated polymer backbone; from using mono-substituted POSS to using eight vertexes functionalized POSS. The higher the mole ratio of POSS in polymers, the greater the improvement in thermal stability, and the higher the quantum efficiency, the less the aggregation existed in polymer system.

1.4 Quantum confinement effect

1.4.1 Definition of quantum confinement effect

The concept of confinement is all about keeping electrons and holes trapped in a small area where one or more of the dimensions of the nano-crystal approach the Bohr exciton radius which is the size of an exciton in bulk crystal.[130-132] The quantum confinement effect comes in different types. 2D confinement restricts electrons and holes in one dimension and forms a quantum well, which is a structure where the height is about the Bohr exciton radius while the length and breadth can be large. 1D confinement occurs when electrons and holes are restricted in two dimensions and form a quantum wire, the structure where the height and breadth is made small while the length can be long. 0D confinement is found only in the quantum dot where electrons and holes are trapped in three dimensions in which structures in all three dimensions are near the Bohr exciton radius, typically a small sphere.

The quantum confinement of excitons results in blue shift of absorption and emission from that of bulk semiconductors such as LEDs.[133-137] The color of the emitted light is governed by the composition of the inorganic semiconductor material and the band gap of organic material. If the physical size of the semiconductor, regardless organic or inorganic, is considerably reduced to near or smaller than the Bohr radius which is the natural radius of the electron-hole pair, additional energy is required to confine this exciton within the small size, and the higher energy leading to a shift in the emission to shorter wavelengths.

1.4.2 Quantum confinement in inorganic materials

The theoretical calculation of quantum confinement was reported by Efros and Efros in which they assumed spherical micro-crystallites with infinite potential barriers at the

crystallite boundary.[138] They assumed the main energy terms are the electron - hole interaction energy which include the Coulomb interaction and secondly the confinement energy of the electron and hole. The average size of crystallite is R. When R is near to or smaller than a_B (Bohr radius of the bulk semiconductor), by confinement the ground state of the exciton is shifted to higher energies and the shift in energy being proportional to $1/R^2$. The quantum confinement effect results in different optical properties for the quantum confined system, e.g. quantum dot, compare to that of corresponding bulk materials. The most apparent feature is the size effect which means different sizes can emit light of different colors. The physical reason is the quantum confinement effect. A quantum dot with larger size emits a spectrum with lower energy while a smaller dot emits bluer (higher energy) light. Quantitatively speaking, the band gap energy (which determines the color of the fluorescent light) is inversely proportional to the square of the size of the quantum dot. Recent articles in nanotechnology and in other journals have begun to suggest that the shape of the quantum dot may be a factor in the emission as well, but as yet not enough information is available. Furthermore, it was shown[139] that the lifetime of fluorescence is determined by the size of the quantum dot. Larger dots have more closely spaced energy levels in which the electron-hole pair can be trapped. Therefore, electron-hole pairs in larger dots live longer causing larger dots to show a longer lifetime.

Quantum confined systems have diversity of applications. Besides quantum wells and quantum wires, quantum dots alone can be used in different applications such as extremely low threshold laser diodes,[140] bio-detectors,[141] single-electron logic devices,[142] and optical computing quantum units.[143]

However, inorganic quantum confined materials, particularly quantum dots, are highly toxic, which prevents them from being used in many applications such as bio-sensors and solid state lighting applications.

1.4.3 Quantum confinement in organic materials

Organic semiconductors with reduced dimensionality are of growing interest owing to their unique features compared to the inorganic semiconductors. Organic semiconductor materials are not as toxic as inorganic semiconductor materials. Defect-free hetero-structures can be more readily fabricated due to weak Van der Waals interactions between molecules. The smaller dielectric constant of organic molecules compared to inorganic semiconductors could result in strong Coulomb interactions between electrons and holes, leading to large exciton binding energies.[144] However, in spite of many theoretical studies which predicted quantum confinement effects in heterostructured organic semiconductors,[145] clear experimental observation in two dimensions by multi-layer structures[146] and one dimension by diluting polymers from bulk material to single chain[147] were just reported. One major experimental difficulty is the small exciton Bohr radii (a_B) in bulk organic semiconductors (a_B ~ 1.2-2.0 nm) which places severe limitations on suitable techniques for preparing the quantum confined structures.[148] Our previous study has demonstrated that organic quantum-dot-like materials using POSS as a scaffold grafted with conjugated oligomers on eight vertexes is a promising way to reach 0D organic materials.[129]

1.4.4 Organic nano-materials

By definition, nano-materials are functional materials composed of objects with at least one of the three dimensions in the range of 1 - 100 nm. In the past decade many organic

materials with low dimensions have been studied even though the strong quantum confinement effects were not reported. Recently there were reports on using organic dye nano-particles as biomarkers.[149-151] Other nano-particles (0D) have also been studied, such as mono-disperse polystyrene nano- and micro-spheres,[152,153] for the construction of photonic crystals. Nano-spheres can also be obtained from conjugated polymers[154,155] or block copolymers[156,157] by self-assembly. Organic 1D nano-structures have also been widely investigated. Micro- or nano- structured conductive polymers polyaniline[158] and polypyrrole[159] have been studied because of their potential applications in sensors[160] biomedicine[161] and actuators.[162] Conjugated polymer 1D nano-structures (nano-wires) such as PF, PT, PPV, have been intensively studied owing to their novel opto-electronic properties and potential applications such as field effect transistors,[163] lasers,[164] photo-detectors,[165] electroluminescent diodes,[166] bio-sensor and drug delivery applications[167,168].The commonly used preparation methods for polymer nano-wires include electrochemical deposition,[169] electro-spinning,[170] self-assembly,[171] and the template method.[172] DNA molecules have also been used to synthesize nano-wires,[173] as well as to produce and modify nanostructures of other materials.[174,175]

1.5 Nano-particles

Light emitting nano-particles have special advantages compared to conventional rigid and linear conjugated polymers in bio-sensor and bio-imaging applications[176]. By controlling structures at the nano-scale dimensions, one can control and tailor the properties of nanostructures in a very predictable manner to meet the needs of a specific application. The nano-particles can be applied to variety of biomedical applications ranging from diagnosis of

diseases to novel therapies. In particular, they could expand the impact to bio-photonics especially in optical imaging and bio-sensing, by providing more robust contrast agents, fluorescent probes, and sensing substrates[177]. The advantages of using nano-particles in bio-photonic applications could be summarized in three points: 1) The size of nano-particles (1nm- 100nm) is similar to common bio-molecules which makes them interesting for applications such as intracellular tagging, and also makes them appear to be ideal for bio-conjugate applications such as antibody targeting of contrast agents. 2) Typically nano-materials possess optical properties far superior to the conventionally used molecular species – higher quantum efficiencies, greater scattering or absorbance cross sections and 3) The optical activity of nano-particles is more biocompatible in the application wavelength range than conventional molecular species which renders nano-particles substantially greater stability (against photo-bleaching).

There are several successful examples of nano-particles that have been applied to relevant problems in biotechnology and medicine, such as 1) Semiconductor quantum dots used as fluorescent labels.[178,179] 2) Bio-conjugated gold nano-particles and silver plasmon resonant particles used as bioassays, a new innovation based on a traditional bio-conjugate technology[180-182]. 3) Lanthanides, or rare earth metals, with the combination of ligands have been used as markers in all kinds of assays[183-185]. 4) Carbon nano-particles can be visually detected in a semiquantitative way as colored biomarkers[186]. 5) Organic but non-polymeric nano-particles can be used as successful bio-labels after surface functionalization[187,188], just like semiconductor quantum dots. 6) Polymer beads as a matrix can be used as biosensors after bio-conjugation with bio-sensitive molecules and luminescent components[189,190].

1.6 Objective of Research

The main objective for this research is to systematically study the effect of incorporation of POSS cage into organic luminescent subjects on the optical characteristics of conjugated materials.

Earlier research by other groups are mainly focused on grafting POSS to a polymer chain with a single arm or by linking conjugated oligomers/polymers onto eight vertexes of POSS with flexible linkage in between, which, however, will reduce the effectiveness of the rigid POSS core and may lead to a overlapping of polymer chains, while the disadvantage of mono-functionalized POSS is that it has less significant improvement in properties than octa-functionalized POSS does.

In this research, POSS luminescent materials will be designed and synthesized, in which the conjugated oligomers / polymers will be directly linked to eight vertexes of POSS cage with rigid linkages. The effect of POSS on the optical property of organic light emitting diodes will be studied. Our investigation consists of the following three parts:

In chapter 2, well defined POSS light luminescent dots / nano-particles are designed and synthesized, in which a series of conjugated oligomers with precise molecular structure and lengths are grafted onto eight vertexes of POSS cage. As a result, the diameter of POSS light emitting dots could be precisely controlled, which are in the range of 2-4 nm. Based on this unique set of POSS light emitting dots, we could gain a fundamental understanding of the effect of incorporating POSS to organic molecules on the optical characteristics of the resulting light emitting dots and elucidate the exciton recombination mechanism and the quantum confinement effect in these POSS luminescent dots. The synthesis and characterization of POSS light emitting dots and the effect of the conjugated chain length,

side groups, polarity of solvents and alkyl/alkoxy chains on the property of luminescent dots will be studied. The structures are shown as Scheme 1.17.

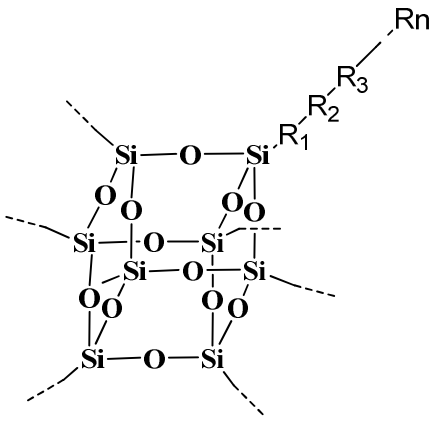

Scheme 1.17. General structure of POSS- luminescent dots. R1, R2..Rn represent aromatic groups substituted by alkyl or alkoxy chains.

The light emitting dots investigated in Chapter 2 mainly emit blue light. In Chapter 3, green light emitting dots based on POSS-oligo-thiophene will be synthesized and investigated. Furthermore, water soluble green light emitting dots will be prepared. The characteristic of the light emitting dots are investigated in detail and a time-resolved PL study will be conducted to gain better understanding of the exciton decay time of the light emitting dot in dilute solution, condensed state, or blended with other polymers. The exciton recombination mechanism and the confinement effect due to the small size of the dots and the unique structure of the molecules are investigated. It is worth mentioning however, that the conjugated oligomers may be grafted onto *meta*- and *para*-positions of the phenyl rings in the octophenyl-POSS, as shown in Scheme 1.18. A question may arise as how such

random grafting of light emitting oligomers could affect the characteristics of a light emitting dot? In order to address this issue, a highly regioselective bromination of octaphenyl-POSS will be prepared, and the POSS light emitting dot based on this structure will be synthesized.

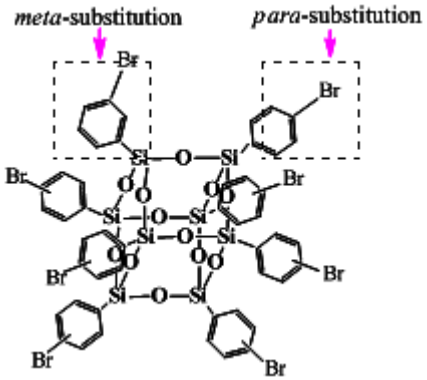

Scheme 1.18. General structure of OBPS (octa-bromophenyl-POSS) with *para*- and *meta*- substitution on phenyl group.

Having understood the effect of incorporating of POSS on the property of light emitting dots, the research will extend to application of POSS in conjugated polymers system. POSS based polymers and their OLED applications will be investigated in chapter 4. Like many other applications that emerged from POSS material research and investigations, POSS materials have been exploited for PLED applications since POSS-LEDs have demonstrated significant improvement in emission efficiencies. This is because the bulky structure of the POSS cage significantly reduced the potential intra- and inter-chain interactions, and hence reduced the chances of non-radiative combination of excitons. In this research, POSS-OLED materials will be designed and synthesized and their characteristics will be investigated. The effect of POSS on the light emitting property of OLED will be studied. Hyper-branched emissive polymers based on POSS will be synthesized and used to demonstrate the

effectiveness of POSS cage in the improvement of luminescent efficiency for a series of red conjugated polymers. Through this investigation, the effect of POSS, either via chemical bond to or physically blended with conjugated polymer on the PL quantum efficiency and device performance will be studied.

1.7 References

1. Baney, R. H., Itoh, M., Sakakibara, A., & Suzuki, T. (1995). Silsesquioxanes. *Chemical Reviews,* 95, 1409-1430.
2. Agaskar, P. A. (1991). New synthetic route to the hydridospherosiloxanes OH-$H_8SI_8O_{12}$ and D_5H-$H_{10}Si_{10}O_{15}$. *Inorganic Chemistry,* 30, 2707-2708.
3. Scott, D. W. (1946). Thermal rearrangement of branched-chain methylpolysiloxanes. *Journal of the American Chemical Society,* 68, 356-358.
4. Lickiss, P. D., & Rataboul F. (2008). Fully condensed polyhedral oligosilsesquioxanes(POSS): From synthesis to application. *Advances in Organometallic Chemistry,* 57, 1-116.
5. Lichtenhan, J. D., Vu, N. Q., Carter, J. A., Gilman, J. W., & Feher, F. J. (1993).Silsesquioxane siloxane copolymers from polyhedral silsesquioxanes. *Macromolecules*, 26, 2141-2142.
6. Lichtenhan, J.D. (1995). Polyhedral oligomeric silsesquioxanes - building-blocks for silsesquioxane-based polymers and hybrid materials. *Comments on Inorganic Chemistry*, 17, 115-130.
7. Voigt, A., Murugavel, R., & Roesky, H. W. (1996). Stannasiloxanes with acyclic, bicyclic, and cubic core structures: X-ray crystal structure of the bicyclic compound

[RSi(OSnPh(2)O)(3)SiR] (R=(2,6-Me(2)C(6)H(3))NSiMe(3)). *Organometallics,* 15, 5097-5101.

8. Li, H. Y., Yu, D. S., & Zhang, J. Y. (2005). A novel and facile method for direct synthesis of cross-linked polysiloxanes by anionic ring-opening copolymerization with Ph-12-POSS/D-4/Ph8D4. *Polymer*, 46, 5317-5323.
9. Gao, F., Tong, Y. H., Schricker, S. R., & Culbertson, B. M. (2001). Evaluation of neat resins based on methacrylates modified with methacryl-POSS, as potential organic-inorganic hybrids for formulating dental restoratives. *Polymers for Advanced Technologies,* 12, 355-360.
10. Haddad, T. S., & Lichtenhan, J. D. (1996). Hybrid organic-inorganic thermoplastics: Styryl-based polyhedral oligomeric silsesquioxane polymers. *Macromolecules,* 29, 7302-7304.
11. Romo-Uribe, A., Mather, P. T., Haddad, T. S., & Lichtenhan, J. D. (1998).Viscoelastic and morphological behavior of hybrid styryl-based polyhedral oligomeric silsesquioxane (POSS) copolymers. *Journal of Polymer Science Part B-Polymer Physics,* 36, 1857-1872.
12. Lee, A., and Lichtenhan, J. D., (1998). Viscoelastic responses of polyhedral oligosilsesquioxane reinforced epoxy systems. *Macromolecules,* 31, 4970-4974.
13. Shockey, E. G., Bolf, A. G., Jones, P. F., Schwab, J. J., Chaffee, K. P., Haddad, T. S., & Lichtenhan, J. D. (1999). Functionalized polyhedral oligosilsesquioxane (POSS) macromers: New graftable POSS hydride, POSS alpha-olefin, POSS epoxy, and POSS chlorosilane macromers and POSS-siloxane triblocks. *Applied Organometallic Chemistry,* 13, 311-327.

14. Mather, P. T., Jeon, H. G., Romo-Uribe, A., Haddad, T. S., & Lichtenhan, J. D. (1999). Mechanical relaxation and microstructure of poly(norbornyl-POSS) copolymers. *Macromolecules* 32, 1194-1203.
15. Bharadwaj, R. K., Berry, R. J., & Farmer, B. L. (2000). Molecular dynamics simulation study of norbornene-POSS polymers. *Polymer*, 41, 7209-7221.
16. Fu, B. X., Hsiao, B. S., Pagola, S., Stephens, P., White, H., Rafailovich, M., Sokolov, J., Mather, P. T., Jeon, H. G., Phillips, S., Lichtenhan, J., & Schwab, J. (2001). Structural development during deformation of polyurethane containing polyhedral oligomeric silsesquioxanes (POSS) molecules. *Polymer*, 42, 599-611.
17. Choi, J., Yee, A. F., & Laine, R. M. (2004). Toughening of cubic silsesquioxane epoxy nanocomposites using core-shell rubber particles: A three-component hybrid system. *Macromolecules,* 37, 3267-3276.
18. Choi, J., Kim, S. G., & Laine, R. M. (2004). Organic/inorganic hybrid epoxy nanocomposites from minophenylsilsesquioxanes. *Macromolecules*, 37. 99-109.
19. Choi, J., Yee, A. F., & Laine, R. M. (2003). Organic/inorganic hybrid composites from cubic silsesquioxanes. Epoxy resins of octa(dimethylsiloxyethylcyclohexylepoxide) silsesquioxane. *Macromolecules.* 36, 5666-5682.
20. Choi, J., Harcup, J., Yee, A. F., Zhu, Q., & Laine, R. M. (2001). Organic/inorganic hybrid composites from cubic silsesquioxanes. Journal of the American Chemical Society. 123, 11420-11430.

21. Tamaki, R., Tanaka, Y., Asuncion, M. Z., Choi, J. W., & Laine, R. M. (2001).Octa(aminophenyl)silsesquioxane as a nanoconstruction site. *Journal of the American Chemical Society,* 123, 12416-12417.
22. Choi, J. W., Tamaki, R., Kim, S. G., & Laine, R. M. (2003). Organic/inorganic imide nanocomposites from aminophenylsilsesquioxanes. *Chemistry of Materials*, 15, 3365-3375.
23. Zhang, C. X., & Laine, R. M. (2000). Hydrosilylation of allyl alcohol with [HSiMe2OSiO1.5](8): Octa(3-hydroxypropyldimethylsiloxy)octasilsesquioxane and its octamethacrylate derivative as potential precursors to hybrid nanocomposites. *Journal of the American Chemical Society*, 122, 6979-6988.
24. Zhang, C. X., Babonneau, F., Bonhomme, C., Laine, R. M., Soles, C. L., Hristov, H. A., & Yee, A. F. (1998). Highly porous polyhedral silsesquioxane polymers. Synthesis and characterization. *Journal of the American Chemical Society*, 120, 8380-8391.
25. Costa, R. O. R., Vasconcelos, W. L., Tamaki, R., & Laine, R. M., (2001). Organic/inorganic nanocomposite star polymers via atom transfer radical polymerization of methyl methacrylate using octafunctional silsesquioxane cores. *Macromolecules,* 34, 5398-5407.
26. Zhou, G., Fragnito, R., & Smid, J. (1989). Siloxanes with aliphatic isocyanate groups - a tetrafunctional cross-linking agent. *Polymer Bulletin, 22, 85-88.*
27. Vollenberg, P.H.T., & Heikens, D. (1989). Particle-size dependence of the young modulus of filled polymers .1. Preliminary experiments. *Polymer* 30, 1656-1662.

28. Petrovic, Z.S., Javni, I., Waddon, A., & B´anhegyi, G. (2000). Structure and properties of polyurethane-silica nanocomposites. *Journal of Applied Polymer Science,* 76, 133-151.
29. Marcadon, V., Herve, & E., Zaoui, A. (2007). Micromechanical modeling of packing and size effects in particulate composites. *International Journal of Solids and Structures,* 44, 8213-8228.
30. Andrady, A.L., Merkel, T.C., & Toy, L.G., (2004). Effect of particle size on gas permeability of filled superglassy polymers. *Macromolecules*, 37, 4329-4331.
31. Cho, K.S., Hong, J.-I., & Chung, C.I. (2004). Effects of ZnO nano particles on thermal stabilization of polymers. *Polymer Engineering and Science,* 44, 1702-1706.
32. Wu, J., & Mather, P. T. (2009). POSS Polymers: Physical Properties and Biomaterials Applications. *Polymer Reviews*, 49, 25-63.
33. Kickelbick, G., (2003). Concepts for the incorporation of inorganic building blocks into organic polymers on a nanoscale. *Progress in Polymer Science,* 28, 83-114.
34. Zheng, L., Hong, S., Cardoen, G., Burgaz, E., Gido, S. P., & Coughlin, E. B. (2004). Polymer nanocomposites through controlled self-assembly of cubic silsesquioxane scaffolds. *Macromolecules*, 37, 8606-8611.
35. Mantz, R. A., Jones, P. F., Chaffee, K. P., Lichtenhan, J. D., Gilman, J. W., Ismail, I. M. K., Burmeister, M. J. (1996). Thermolysis of polyhedral oligomeric silsesquioxane (POSS) macromers and POSS-siloxane copolymers. *Chemistry of Materials,* 8, 1250-1259.

36. Liu, Y.R., Huang, Y.D., & Liu, L. (2007). Influences of monosilanolisobutyl-POSS on thermal stability of polymethylsilxoane. *Journal of Materials Science, 42, 5544-5550.*

37. Liu, Y. R., Huang, Y. D., & Liu, L. (2007). Thermal stability of POSS /methylsilicone nanocomposites. *Composites Science and Technology,* 67, 2864-2876.

38. Lin, H. M., Wu, S. Y., Huang, P. Y., Huang, C. F., Kuo, S. W., & Chang, F. C. (2006). Polyhedral oligomeric silsesquioxane containing copolymers for negative-type photoresists. *Macromolecular Rapid Communications,* 27, 1550-1555.

39. Ali, M.A., Gonsalves, K.E., Agrawal, A., Jeyakumar, A., & Henderson, C.L. (2003). A new nanocomposite resist for low and high voltage electron beam lithography. *Microelectronic Engineering*, 70, 19-29.

40. Eon, D., Cartry, G., Fernandez, V., Cardinaud, C., Tegou, E., Bellas, V., Argitis, P., & Gogolides, E. (2004). Surface segregation of photoresist copolymers containing polyhedral oligomeric silsesquioxanes studied by x-ray photoelectron spectroscopy. *Journal of Vacuum Science & Technology B,* 22, 2526-2532.

41. Ito, H., Truong, H.D., Burns, S.D., Pfeiffer, D., & Medeiros, D.R. (2006). Bilayer resists for 193 nm lithography: SSQ and POSS. *Journal of Photopolymer Science and Technology*. 19, 305-311.

42. Wu, H.P., Hu, Y.Q., Gonsalves, K.E., Yacaman, M.J., (2001). Incorporation of polyhedral oligosilsesquioxane in chemically amplified resists to improve their reactive ion etching resistance. *Journal of Vacuum Science & Technology B,* 19, 851-855.

43. Asuncion, M. Z., & Laine, R. M. (2007). Silsesquioxane barrier materials. *Macromolecules,* 40, 555-562.

44. Leu, C. M., Reddy, G. M., Wei, K. H., & Shu, C. F. (2003). Synthesis and dielectric properties of polyimide-chain-end tethered polyhedral oligomeric silsesquioxane nanocomposites. *Chemistry Of Materials,* 15, 2261-2265.

45. Takala, M., Karttunen, M., Salovaara, P., Kortet, S., Kannus, K., & Kalliohaka, T. (2008). Dielectric properties of nanostructured polypropylene-polyhedral oligomeric silsesquioxane compounds. *IEEE Transactions on Dielectrics and Electrical Insulation*, 15, 40-51.

46. Bian, Y., Pejanovic, S., Kenny, J., & Mijovic, J. (2007). Dynamics of multifunctional polyhedral oligomeric silsesquioxane/poly(propylene oxide) nanocomposites as studied by dielectric relaxation spectroscopy and dynamic mechanical spectroscopy. *Macromolecules,* 40, 6239-6248.

47. Hao, N., Boehning, M., Schoenhals, A., (2007)., Dielectric properties of nanocomposites based on polystyrene and polyhedral oligomeric phenethyl-silsesquioxanes. *Macromolecules* 40, 9672-9679.

48. Liu, Y. L., Liu, C. S., Cho, C. I., & Hwu, M. J. (2007). Polyhedral oligomeric silsequioxane monolayer as a nanoporous interlayer for preparation of low-k dielectric films. 2007 *Nanotechnology* 18, article number 225701.

49. Cui, L., Collet, J. P., Xu, G. Q., Zhu, L., (2006). Supramolecular self-assembly in a disk-cube dyad molecule based on triphenylene and polyhedral oligomeric silsesquioxane (POSS). *Chemistry of Materials,* 18, 3503-3512.

50. Tanaka, K., Inafuku, K., & Chujo, Y. (2008). Ratiometric multimodal chemosensors based on cubic silsesquioxanes for monitoring solvent polarity. *Bioorganic & Medicinal Chemistry*, 16, 10029-10033.

51. Bianucci, P., Rodriguez, J. R., Clements, C. M., Veinot, J. G. C., Meldrum, A., (2009). Silicon nanocrystal luminescence coupled to whispering gallery modes in optical fibers. *Journal of Applied Physics,* 105, Article Number: 023108.

52. Liu, C. Q., Naismith ,N., Huang, Y. Q., & Economy, J. (2003). Synthesis and characterization of novel hyperbranched poly(imide silsesquioxane) membranes. *Journal of Polymer Science Part A-Polymer Chemistry*, 41, 3736-3743.

53. Kannan, R. Y., Salacinski, H. J., Butler, P. E., & Seifalian, A. M. (2005). Polyhedral oligomeric silsesquioxane nanocomposites: The next generation material for biomedical applications. *Accounts of Chemical Research*, 38, 879-884.

54. Soh, M. S., Yap, A. U. J., & Sellinger, A. (2007). Methacrylate and epoxy functionalized nanocomposites based on silsesquioxane cores for use in dental applications. *European Polymer Journal*, 43, 315-327.

55. Joshi, M., Butola, B. S., Simon, G., & Kukaleva, N. (2006). Rheological and viscoelastic behavior of HDPE/octamethyl-POSS nanocomposites. *Macromolecules* 39, 1839-1849.

56. Duchateau, R., Abbenhuis, H. C. L., van Santen, R. A., Thiele, S. K. H., & van Tol, M. F. H. (1998). Half-sandwich titanium complexes stabilized by a novel silsesquioxane ligand: Soluble model systems for silica-grafted olefin polymerization catalysts. *Organometallics,* 17, 5222-5224.

57. Ropartz, L., Morris, R.E., Foster, D.F., & Cole-Hamilton, D.J. (2001). Increased selectivity in hydroformylation reactions using dendrimer based catalysts; a positive dendrimer effect. *Chemical Communications*, 4, 361-362.

58. Letant, S.E., Herberg, J., Dinh, L.N., Maxwell, R.S., Simpson, R.L., & Saab, A.P. (2007). Structure and catalytic activity of POSS-stabilized Pd nanoparticles. *Catalysis Communications*, 8, 2137-2142.

59. He, F.A., Zhang, L.M., (2006). Using inorganic POSS-modified laponite clay to support a nickel alpha-diimine catalyst for in situ formation of high performance polyethylene nanocomposites. *Nanotechnology,* 17, 5941-5946.

60. McCusker, C., Carroll, J. B., & Rotello, V. M. (2005). Cationic polyhedral oligomeric silsesquioxane (POSS) units as carriers for drug delivery processes. *Chemical Communications*, 8, 996-998.

61. Tanaka, K., Inafuku, K., Chujo, Y., (2008). Ratiometric multimodal chemosensors based on cubic silsesquioxanes for monitoring solvent polarity. *Bioorganic & Medicinal Chemistry*, 16, 10029-10033.

62. Pender, M. P., Wolfe, N. P., (2002). Prevention of autoimmune attack and disease progression in multiple sclerosis: current therapies and future prospects. *Internal Medicine Journal*, 32, 554-563.

63. Zhang, H.J., Kulkarni, S., & Wunder, S.L. (2007). Blends of POSS-PEO(n=4)(8) and high molecular weight poly(ethylene oxide) as solid polymer electrolytes for lithium batteries. *Journal Of Physical Chemistry B*, 111, 3583-3590.

64. Zhang, H.J., Kulkarni, S., & Wunder, S.L. (2006). Polyethylene glycol functionalized polyoctahedral silsesquioxanes as electrolytes for lithium batteries. *Journal of the Electrochemical Society*, 153, A239-A248.

65. Maitra, P., & Wunder, S.L. (2004). POSS based electrolytes for rechargeable lithium batteries. *Electrochemical And Solid State Letters*, 7, A88-A92.

66. Chiang, C. K., Fincher, C. R., Park, Y. W., Heeger, A. J., Shirakawa, H., Louis, E. J., Gau, S. C., & Macdiarmid, A. G. (1977). Electrical-conductivity in doped polyacetylene. *Physical Review Letters,* 39, 1098-1101.

67. Burroughes, J. H., Bradley, D. D. C., Brown, A. R., Marks, R. N.,, Mackay, K., Friend, R. H.,, Burns, P. L., & Holmes, A. B. (1990). Light-Emitting-Diodes Based on Conjugated Polymers. *Nature,* 347, 539-541.

68. Kraft, A.; Grimsdale, A. C.; & Holmes, A. B. (1998). Electroluminescent conjugated polymers - Seeing polymers in a new light. *Angewandte Chemie-International Edition*, 37, 402-428.

69. Fukuda, M., Sawada, K., & Yoshino, K. (1993). Synthesis of fusible and soluble conducting polyfluorene derivatives and their characteristics. *Journal of Polymer Science Part A-Polymer Chemistry*, 31, 2465-2471.

70. Greenham, N. C.; Moratti, S. C.; Bradley, D. D. C; Friend, R. H.; & Holmes, A. B. (1993**).** Efficient light-emitting-diodes based on polymers with high electron-affinities. *Nature,* 365. 628-630.

71. Grem, G., Leditzky, G., Ullrich, B., & Leising, G., (1992). Realization of a blue-light-emitting device using poly(para-phenylene). *Advanced Materials.* 4, 36-37.

72. Breen, C. A., Deng T., Breiner, T., Thomas, E. L., & Swager, T. M. (2003). Polarized photoluminescence from poly(p-phenylene-ethynylene) via a block copolymer nanotemplate. *Journal of the American Chemical Society*, 125, 9942-9943.
73. Dyreklev, P., Berggren, M., Inganas, O., Andersson, Mr., Wennerstrom, O., & Hjertberg, T. (1995). Polarized electroluminescence from an oriented substituted polythiophene in a light-emitting diode. *Advanced Materials*, 7, 43-45.
74. Scholes, G. D., & Rumbles, G. (2006). Excitons in nanoscale systems. *Nature Materials,* 5, 683-696.
75. Moliton, A., & Hiorns, R. C. (2004). Review of electronic and optical properties of semiconducting pi-conjugated polymers: applications in optoelectronics. *Polymer International,* 53, 1397-1412.
76. Dautel, O. J., Wantz, G., Almairac, R., Flot, D., Hirsch, L., Lere-Porte, J. P., Parneix, J. P., Serein-Spirau, F., Vignau, L., & Moreau, J. J. E. (2006). Nanostructuration of phenylenevinylenediimide-bridged silsesquioxane: From electroluminescent molecular J-aggregates to photoresponsive polymeric H-aggregates. *Journal of the American Chemical Society*, 128, 4892-4901.
77. Siddiqui, S., & Spano, F.C. (1999). H- and J-aggregates of conjugated polymers and oligomers A theoretical investigation. *Chemical Physics Letters,* 308, 99-105.
78. Czikklely, V., Forsterling, H.D., Kuhn, H., (1970). Extended dipole model for aggregates of dye molecules. *Chemical Physics Letters*, 6, 207-210.
79. Cornil, J., dos Santos, D. A., Crispin, X., Silbey, R., & Bredas, J. L. (1998). Influence of interchain interactions on the absorption and luminescence of conjugated

oligomers and polymers: A quantum-chemical characterization. *Journal of the American Chemical Society*, 120, 1289-1299.

80. Bazan, G. C., Oldham, W. J., Lachicotte, R. J., Tretiak, S., Chernyak, V., & Mukamel, S. (1998). Stilbenoid dimers: Dissection of a paracyclophane chromophore. *Journal of the American Chemical Society*, 120, 9188-9204.
81. McIntire, M.J., Manas, E.S., Spano, F.C., (1997). Spontaneous emission and absorption in model aggregates of pi-conjugated oligomers. *Journal Of Chemical Physics*, 107, 8152-8164.
82. Soos, Z. G., Hayden, G. W., Mcwilliams, P. C. M., & Etemad, S. (1990). Excitation shifts of parallel conjugated polymers due to pi-electron dispersion forces. *Journal of Chemical Physics,* 93, 7439-7448.
83. Meng, H. F. (1998). Excimers in light-emitting conjugated polymers. *Physical Review B*, 58, 3888-3892.
84. Yao, H., Domoto, K., Isohashi, T., & Kimura, K. (2005). In situ detection of birefringent mesoscopic H and J aggregates of thiacarbocyanine dye in solution. *Langmuir* 21, 1067-1073.
85. Heeger, P. S., and Heeger, A. J., (1999). Making sense of polymer-based biosensors. *Proceedings of the National Academy of Sciences of the United States of America*, 96, 12219-12221.
86. Dimitrakopoulos, C. D., and Mascaro, D. J., (2001). Organic thin-film transistors: A review of recent advances. *Ibm Journal Of Research And Development,* 45, 11-27.
87. McGehee, M. D., & (2000). Heeger, A. J. Semiconducting (conjugated) polymers as materials for solid-state lasers. *Advanced Materials,* 12, 1655-1668.

88. Yu, G., Yang, Y., Cao, Y., Pei, Q., Zhang, C., & Heeger, A. J. (1996). Measurement of the energy gap in semiconducting polymers using the light-emitting electrochemical cell. *Chemical Physics Letters*, 259. 465-468.

89. Yan, M., Rothberg, L. J., Papadimitrakopoulos, F., Galvin. Me., & Miller, T. M. (1994). Spatially indirect excitons as primary photoexcitations in conjugated polymers. *Physical Review Letters*, 72, 1104-1107.

90. Samuel, I. D. W., Rumbles, G., Collison, C. J., (1995). Efficient interchain photoluminescence in a high-electron-affinity conjugated polymer. *Physical Review B*, 52, 11573-11576.

91. Yan, M., Rothberg, L. J., Papadimitrakopoulos, F., Galvin, M. E., & Miller, T. M. (1994). Defect quenching of conjugated polymer luminescence. *Physical Review Letters*, 73, 744-747.

92. Sun, R. G., Wang, Y. Z., Wang, D. K., Zheng, Q. B., Kyllo, E. M., Gustafson, T. L., Wang, F. S., & Epstein, A. J. (2000). High PL quantum efficiency of poly(phenylene vinylene) systems through exciton confinement. *Synthetic Metals*, 111, 595-602.

93. Son, S., Dodabalapur, A., Lovinger, A. J., & Galvin, M. E. (1995). Luminescence enhancement by the introduction of disorder into poly(p-phenylene vinylene). *Science,* 269, 376-378.

94. Yu, G., & Heeger, A. J. (1997). High efficiency photonic devices made with semiconducting polymers. *Synthetic Metals,* 85, 1183-1186.

95. Yan, H., Huang, Q. L., Cui, J., Veinot, J. G. C., Kern, M. M., & Marks, T. J. (2003). High-brightness blue light-emitting polymer diodes via anode modification using a self-assembled monolayer. *Advanced Materials,* 15, 835-838.

96. Jung, Y. K., Kim, H., Park, J. H., Lee, J., Lee, S. K., Lee, Y. S., & Shim, H. K. (2008). Alternating fluorene copolymers containing isothianaphthene derivatives: A study of their aggregation properties and small band gap. *Journal of Polymer Science Part A-Polymer Chemistry,* 46, 3573-3590.

97. Conwell, E. (1997). Excimer formation and luminescence in conducting polymers. *Trends in Polymer Science*, 5, 218-222.

98. Huang, W. Y., Yun, H., Lin, H. S., Kwei, T. K., & Okamoto, Y. (1999). Enhancement of fluorescent intensities of poly(quinoline)s in solution and in the solid state. *Macromolecules*, 32, 8089-8093

99. Yan, M., Rothberg, L. J., Kwock, E. W., Miller, T. M. (1995). Interchain excitations in conjugated polymers. *Physical Review Letters,* 75, 1992-1995.

100. Bunz, U. H. F., Enkelmann, V., Kloppenburg ,L., Jones, D., Shimizu, K. D., Claridge, J. B., zur Loye, H. C., & Lieser, G. (1999). Solid-state structures of phenyleneethynylenes: Comparison of monomers and polymers. *Chemistry Of Materials,* 11, 1416-1424.

101. Chen, S. H., Su, A. C., Chou, H. L., & Peng, K. Y., (2004). Phase Behavior and molecular aggregation in bulk poly(2-methoxy-5-(2 '-ethylhexyloxy)-1,4-phenylenevinylene). *Macromolecules,* 37, 167-173.

102. Chen, S. H., Su, C. H., Su, A. C., & Chen, S. A. (2004). Molecular aggregation and luminescence behavior of bulk poly(2,5,2 ',5 '-tetrahexyloxy-8,7 '-dicyano-di-p-phenylenevinylene). *Journal Of Physical Chemistry B,* 108, 8855-8861.

103. Yang, C. Y., Hide, F., Diaz-Garcia, M. A., Heeger, A. J., & Cao, Y. (1998).Microstructure of thin films of photoluminescent semiconducting polymers. *Polymer,* 39, 2299-2304.

104. Belletete, M., Bouchard, J., Leclerc, M., & Durocher, G. (2005). Photophysics and solvent-induced aggregation of 2,7-carbazole-based conjugated polymers. *Macromolecules,* 38, 880-887.

105. Ding, L., Bo, Z. S., Chu, Q. H., Li, J., Dai, L. M., Pang, Y., Karasz, F. E., & Durstock, M. E. (2006). Photophysical and electroluminescent properties of hyperbranched polyfluorenes. *Macromolecular Chemistry and Physics*, 207, 870-878.

106. Ding, L. M., Karasz, F. E., Lin, Y., Pang, Y., & Liao, L. (2003). Photoluminescence and electroluminescence study of violet-blue and green emitting polymers and their blend. *Macromolecules*, 36, 7301-7307.

107. Qu, J. Q., Zhang, J. Y., Grimsdale, A. C., Mullen, K., Jaiser, F., Yang, X. H., & Neher, D. (2004). Dendronized perylene diimide emitters: Synthesis, luminescence, and electron and energy transfer studies. *Macromolecules,* 37, 8297-8306.

108. Johal, M. S., Howland, M., Robinson, J. M., Casson, J. L., Wang, H. L. (2004). Photoluminescent studies of spin-assembled MPS-PPV/dendrimer multilayers. *Chemical Physics Letters,* 383, 276-281.

109. Jakubiak, R., Collison, C. J., Wan, W. C., Rothberg, L. J., Hsieh, B. R., (1999). Aggregation quenching of luminescence in electroluminescent conjugated polymers. *Journal of Physical Chemistry A,* 103, 2394-2398.

110. Menon, A., Galvin, M., Walz, K. A., & Rothberg, L. (2004). Structural basis for the spectroscopy and photophysics of solution-aggregated conjugated polymers. *Synthetic Metals*, 141, 197-202.

111. Collison, C. J., Rothberg, L. J., Treemaneekarn, V., & Li, Y. (2001). Conformational effects on the photophysics of conjugated polymers: A two species model for MEH-PPV spectroscopy and dynamics. *Macromolecules* 34, 2346-2352.

112. Breitenkamp, R. B., & Tew, G. N. (2004). Aggregation of poly(p-phenylene ethynylene)s containing nonpolar and amine side chains. *Macromolecules* 37, 1163-1165.

113. Li, K., & Wang, Q. (2004). Synthesis and solution aggregation of polystyrene-oligo(p-phenyleneethynylene)-polystyrene triblock copolymer. *Macromolecules* 37, 1172-1174.

114. Hsu, J, H., Fann, W. S., Tsao, P. H., Chuang, K. R., & Chen, S. A. (1999). Fluorescence from conjugated polymer aggregates in dilute poor solution. *Journal of Physical Chemistry A*, 103, 2375-2380.

115. Samuel, I. D. W., Rumbles, G., Collison, C. J., Moratti, S. C., & Holmes, A. B. (1998). Intra-and inter-molecular photoexcitations in a cyano-substituted poly(p-phenylenevinylene). *Chemical Physics,* 227, 75-82.

116. Halkyard, C. E., Rampey, M. E., Kloppenburg, L., Studer-Martinez, S. L., Bunz, U. H. F., (1998). Evidence of aggregate formation for 2,5-dialkylpoly(p-phenyleneethynylenes) in solution and thin films. *Macromolecules* 31, 8655-8659.

117. Jenekhe, S. A., & Osaheni, J. A. (1994). Excimers and exciplexes of conjugated polymers. *Science* 265, 765-768.

118. Weinfurtner, K. H., Fujikawa, H., Tokito, S., & Taga, Y. (2000). Highly efficient pure blue electroluminescence from polyfluorene: Influence of the molecular weight distribution on the aggregation tendency. *Applied Physics Letters*, 76, 2502-2504.

119. Lee, J. I., Klaerner, G., & Miller, R. D. (1999). Oxidative stability and its effect on the photoluminescence of poly(fluorene) derivatives: End group effects. *Chemistry Of Materials*, 11, 1083-1088.

120. Lupton, J. M. Schouwink, P., Keivanidis, P. E., Grimsdale, A. C., & Mullen, K. (2003). Influence of dendronization on spectral diffusion and aggregation in conjugated polymers. *Advanced Functional Materials,* 13, 154-158.

121. Lim, E., Jung, B. J., & Shim, H. K., (2003). Synthesis and characterization of a new light-emitting fluorene-thieno[3,2-b]thiophene-based conjugated copolymer. *Macromolecules* 36, 4288-4293.

122. Xiao, S. Nguyen, M. Gong, X., Cao, Y., Wu, H. B., Moses, D., & Heeger, A. J. (2003). Stabilization of semiconducting polymers with silsesquioxane. *Advanced Functional Materials.* 13, 25-29.

123. Lee, J., Cho, H. J., Jung, B. J., Cho, N. S., & Shim, H. K. (2004). Stabilized blue luminescent polyfluorenes: Introducing polyhedral oligomeric silsesquioxane. *Macromolecules,* 37, 8523-8529.

124. Lin, W. J., Chen, W. C., Wu, W. C., Niu, Y. H., & Jen, A. K. Y. (2004). Synthesis and optoelectronic properties of starlike polyfluorenes with a silsesquioxane core. *Macromolecules* 37, 2335-2341.

125. Chou, C. H., Hsu, S. L., Dinakaran, K., Chiu, M. Y., & Wei, K. H., (2005). Synthesis and characterization of luminescent polyfluorenes incorporating side-chain-tethered polyhedral oligomeric silsesquioxane units *Macromolecules 38*, 745-751.

126. Chou, C. H., Hsu, S. L., Yeh, S. W., Wang, H. S., & Wei, K. H. (2005). Enhanced luminance and thermal properties of poly(phenylenevinylene) copolymer presenting side-chain-tethered silsesquioxane units. *Macromolecules*, 38, 9117-9123.

127. Kang, J. M., Cho, H. J., Lee, J., Lee, J. I., Lee, S. K., Cho, N. S., Hwang, D. H., & Shim, H. K., (2006). Highly bright and efficient electroluminescence of new PPV derivatives containing polyhedral oligomeric silsesquioxanes (POSSs) and their blends. *Macromolecules,* 39, 4999-5008.

128. Cho, H. J., Hwang, D. H., Lee, J. I., Jung, Y. K., Park, J. H., Lee, J., Lee, S. K., & Shim, H. K. (2006). Electroluminescent polyhedral oligomeric silsesquioxane-based nanoparticle. *Chemistry of Materials*, 3780-3787.

129. He, C. B., Xiao, Y., Huang, J. C., Lin, T. T., Mya, K. Y., & Zhang, X. H. (2004). Highly efficient luminescent organic clusters with quantum dot-like properties. *Journal of the American Chemical Society*, 126, 7792-7793.

130. Yoffe, A. D., (2002). Low-dimensional systems: quantum size effects and electronic properties of semiconductor microcrystallites (zero-dimensional systems) and some quasi-two-dimensional systems. *Advances in Physics*, 51, 799-890.

131. Bhattacharya, P., Ghosh, S., & Stiff-Roberts, A. D. (2004). Quantum dot opto-electronic devices. *Annual Review of Materials Research*, 34, 1-40.

132. Bukowski, T. J., Simmons, J. H., (2002). Quantum dot research: Current state and future prospects. *Critical Reviews In Solid State And Materials Sciences*, 27, 119-142.

133. Gotoh, H., Ando, H., (1997). Excitonic quantum confinement effects and exciton electroabsorption in semiconductor thin quantum boxes. *Journal of Applied Physics*. 82, 1667-1677.

134. Uozumi, T., & Kayanuma, Y. (2002). Excited states of an electron-hole pair in spherical quantum dots and their optical properties. *Physical Review B*, 65, Article Number: 165318.

135. Potter, B. G., Simmons, J. H., Kumar, P., & Stanton, C. J. (1994). Quantum-size effects on the band-edge of cdte clusters in glass. *Journal of Applied Physics,* 75, 8039-8046.

136. Hall D.W., & Borrelli, N.F. (1988). Absorption saturation in commercial and quantum-confined cdsexs1-x-doped glasses. *Journal Of The Optical Society Of America B-Optical Physics*, 5, 1650-1654.

137. Pauthe, M., Bernstein, E., Dumas, J., Saviot, L., Pradel A., & Ribes, M. (1999). Preparation and characterisation of Si nanocrystallites embedded in a silica matrix. *Journal Of Materials Chemistry,* 9, 187-191.

138. Efros, A. L., & Efros, A. L. (1982). Interband absorption of light in a semiconductor sphere. *Soviet Physics Semiconductors-Ussr*, 16, 772-775.

139. van Driel, A. F., Allan, G., Delerue, C., Lodahl, P., Vos, W. L., & Vanmaekelbergh, D. (2005). Frequency-dependent spontaneous emission rate from CdSe and CdTe

nanocrystals: Influence of dark states. *Physical Review Letters*, 95, Article Number: 236804.

140. Fafard, S., Hinzer, K., Raymond, S., Dion, M., McCaffrey, J., Feng, Y., & Charbonneau, S. (1996). Red-emitting semiconductor quantum dot lasers. *Science* 274, 1350-1353.
141. Chan, W. C. W., & Nie, S. M. (1998). Quantum dot bioconjugates for ultrasensitive nonisotopic detection. *Science,* 281, 2016-2018.
142. Nakajima, F., Miyoshi, Y., Motohisa, J., & Fukui, T. (2003). Single-electron AND/NAND logic circuits based on a self-organized dot network. *Applied Physics Letters,* 83, 2680-2682.
143. White, I., Tin, A. E., Williams, K., Wang, H. B., Wonfor, A., & Penty, R. (2009). Scalable optical switches for computing applications. *Journal Of Optical Networking*, 8, 215-224.
144. Gallagher, F. B., & Mazumdar, S. (1997). Excitons and optical absorption in one-dimensional extended Hubbard models with short- and long-range interactions. *Physical Review B*, 56, 15025-15039.
145. Seel, M., Liegener, C. M., Forner, W., & Ladik, J. (1988). (ambn)x Copolymers - a computational study of electronic and excitonic properties of quasi-one-dimensional superlattices. *Physical Review B*, 37, 956-964.
146. Ohmori, Y., Fujii, A., Uchida, M., Morishima, C., & Yoshino, K. (1993). Fabrication and optical characteristics of an organic multilayer structure utilizing 8-hydroxyquinoline aluminium/aromatic diamine and its application for an electroluminescent diode. *Journal of Physics-Condensed Matter,* 5, 7979-7986.

147. Joshi, H. S., Jamshidi, R., & Tor, Y. (1999). Conjugated 1,10-phenanthrolines as tunable fluorophores. *Angewandte Chemie-International Edition*, 38, 2722-2725.

148. So, F. F., Forrest, S. R., (1991). Evidence for exciton confinement in crystalline organic multiple quantum-wells. *Physical Review Letters*, 66, 2649-2652.

149. Yang, W. J., Trau, D., Renneberg, R., Yu, N. T., & Caruso, F. (2001). Layer-by-layer construction of novel biofunctional fluorescent microparticles for immunoassay applications. *Journal of Colloid and Interface Science.* 234, 356-362.

150. Chan, C. P. Y., Bruemmel, Y., Seydack, M., Sin, K. K., Wong, L. W., Merisko-Liversidge, E., Trau, D., & Renneberg, R. (2004). Nanocrystal biolabels with releasable fluorophores for immunoassays. *Analytical Chemistry.* 76, 3638-3645.

151. Bruemmel, Y., Chan, C.P. Y., Renneberg, R., Thuenemann, A., & Seydack, M. (2004). On the influence of different surfaces in nano- and submicrometer particle based fluorescence immunoassays. *Langmuir* 20, 9371-9379.

152. Jiang, P., Bertone, J. F., Hwang, K. S., & Colvin, V. L. (1999). Single-crystal colloidal multilayers of controlled thickness. *Chemistry of Materials,* 11, 2132-2140.

153. Okubo, M., Minami, H., & Morikawa, K. (2003). Influence of shell strength on shape transformation of micron-sized, monodisperse, hollow polymer particles. *Colloid and Polymer Science*, 281, 214-219.

154. Landfester, K., Montenegro, R., Scherf, U., Guntner, R., Asawapirom, U., Patil, S., Neher, D., & Kietzke, T. (2002). Semiconducting polymer nanospheres in aqueous dispersion prepared by a miniemulsion process. *Advanced Materials,* 14, 651-655.

155. Szymanski, C., Wu, C. F., Hooper, J., Salazar, M. A., Perdomo, A., Dukes, A., & McNeill, J. (2005). Single molecule nanoparticles of the conjugated polymer MEH-PPV, preparation and characterization by near-field scanning optical microscopy. *Journal of Physical Chemistry B,* 109, 8543-8546.

156. Leclere, P., Parente, V., Bredas, J. L., Francois, B., & Lazzaroni, R. (1998). Organized semiconducting nanostructures from conjugated block copolymer self-assembly. *Chemistry of Materials,* 10, 4010-4014.

157. Chen, F., Kondo, Y., & Hashimoto, T. (2007). Control of nanostructure in mixtures of block copolymers: Curvature control via cosurfactant effects. *Macromolecules* 40, 3714-3723.

158. Huang, J. X., Virji, S., Weiller, B. H., & Kaner, R. B. (2003). Polyaniline nanofibers: Facile synthesis and chemical sensors. *Journal of the American Chemical Society,* 125, 314-315.

159. Berdichevsky, Y., & Lo, Y. H. (2006). Polypyrrole nanowire actuators. *Advanced Materials*, 18, 122-125.

160. Shu, J. H., Qiu, W., & Zheng, S. Q. (2009). Polyaniline/Gold Nanoparticle Composites. *Progress In Chemistry,* 21, 1015-1022.

161. Peng, H., Soeller, C., Cannell, M. B., Bowmaker, G. A., Cooney, R. P., & Travas-Sejdic, J. (2006). Electrochemical detection of DNA hybridization amplified by nanoparticles. *Biosensors & Bioelectronics,* 21, 1727-1736.

162. Smela, E. (2003). Conjugated polymer actuators for biomedical applications. *Advanced Materials,* 15, 481-494.

163. Pinto, N. J., Johnson, A. T., MacDiarmid, A. G., Mueller, C. H., Theofylaktos, N., Robinson, D. C., & Miranda, F. A. (2003). Electrospun polyaniline/polyethylene oxide nanofiber field-effect transistor. *Applied Physics Letters*, 83, 4244-4246.

164. O'Carroll, D., Lieberwirth, I., & Redmond, G. (2007). Microcavity effects and optically pumped lasing in single conjugated polymer nanowires. *Nature Nanotechnology,* 2, 180-184.

165. O'Brien, G. A., Quinn, A. J., Tanner, D. A., & Redmond, G. (2006). A single polymer nanowire photodetector. *Advanced Materials*, 18, 2379-2383.

166. Granstrom, M., Berggren, M., & Inganas, O. (1995). Micrometer-sized and nanometer-sized polymeric light-emitting-diodes. *Science* 267, 1479-1481.

167. Liu, B, & Bazan, G. C (2004). Interpolyelectrolyte complexes of conjugated copolymers and DNA: Platforms for multicolor biosensors. *Journal of the American Chemical Society*. 126, 1942-1943.

168. Liu, B., & Bazan, G. C. (2005). Methods for strand-specific DNA detection with cationic conjugated polymers suitable for incorporation into DNA chips and microarrays. *Proceedings of the National Academy of Sciences of the United States of America,* 102, 589-593.

169. Ramanathan, K., Bangar, M. A., Yun, M. H., Chen, W. F., Mulchandani, A., & Myung, N. V. (2004). Individually addressable conducting polymer nanowires array. *Nano Letters,* 4, 1237-1239.

170. Wang, L., Topham, P. D., Mykhaylyk, O. O., Howse, J. R., Bras, W., Jones, R. A. L., & Ryan, A. J. (2007). Electrospinning pH-responsive block copolymer nanofibers. *Advanced Materials*, 19, Pages: 3544-3548.

171. Kim, D. H., Han, J. T., Park, Y. D., Jang, Y., Cho, J. H., Hwang, M., & Cho, K. (2006). Single-crystal polythiophene microwires grown by self-assembly. *Advanced Materials*, 18, 719-723.

172. Martin, C. R., (1995). Template synthesis of electronically conductive polymer nanostructures. *Accounts of Chemical Research,* 28, 61-68.

173. Nakao, H., Gad, M., Sugiyama, S., Otobe, K., Ohtani, T., (2003). Transfer-printing of highly aligned DNA nanowires. *Journal of The American Chemical Society*, 125, 7162-7163.

174. Medalsy, I., Dgany, O., Sowwan, M., Cohen, H., Yukashevska, A., Wolf, S. G., Wolf, A., Koster, A., Almog, O., Marton, I., Pouny, Y., Altman, A., Hoseyov, O. S., & Porath, D. (2008). SP1 protein-based nanostructures and arrays. *Nano Letters,* 8, 473-477.

175. Lapierre-Devlin, M. A., Asher, C. L., Taft, B. J., Gasparac, R., Roberts, M. A., & Kelley, S. O. (2005). Amplified electrocatalysis at DNA-modified nanowires. *Nano Letters*, 5, 1051-1055.

176. Seydack, M., (2005). Nanoparticle labels in immunosensing using optical detection methods. *Biosensors & Bioelectronics*, 20, 2454-2469.

177. de Araujo, A. D., Palomo, J. M., Cramer, J., Kohn, M., Schroder, H., Wacker, R., Niemeyer, C., Alexandrov, K., & Waldmann, H. (2006). Diels-Alder ligation and surface immobilization of proteins. *Angewandte Chemie-International Edition*, 45, 296-301.

178. Bally, M., & Voros, J. (2009). Nanoscale labels: nanoparticles and liposomes in the development of high-performance biosensors. *Nanomedicine*, 4, 447-467.

179. Chan, W. C. W., Maxwell, D. J., Gao, X. H., Bailey, R. E., Han, M. Y., & Nie, S. M. (2002). Luminescent quantum dots for multiplexed biological detection and imaging. *Current Opinion in Biotechnology*, 13, 40-46.

180. Drake, C., Deshpande, S., Bera, D., Seal, S. (2007). Metallic nanostructured materials based sensors. *International Materials Reviews*, 52, 289-317.

181. Elghanian, R., Storhoff, J. J., Mucic, R. C., Letsinger, R. L., & Mirkin, C. A. (1997). Selective colorimetric detection of polynucleotides based on the distance-dependent optical properties of gold nanoparticles. Science 277, 1078-1081.

182. Haes, A. J., & Van Duyne, R. P. (2002). A nanoscale optical blosensor: Sensitivity and selectivity of an approach based on the localized surface plasmon resonance spectroscopy of triangular silver nanoparticles. *Journal Of The American Chemical Society*, 124, 10596-10604.

183. Koshi, Y., Nakata, E., & Hamachi, I. (2005). Luminescent saccharide biosensor by using lanthanide-bound lectin labeled with fluorescein. *Chembiochem*, 6, 1349-1352.

184. Hemmila, I., & Laitala, V. (2005). Progress in lanthanides as luminescent probes. *Journal of Fluorescence,* 15, 529-542.

185. Yuan, J. L., & Wang, G. L. (2006). Lanthanide-based luminescence probes and time-resolved luminescence bioassays. *Trac-Trends In Analytical Chemistry*, 25, 490-500.

186. Lonnberg, M., & Carlsson, J. (2001). Quantitative detection in the attomole range for immunochromatographic tests by means of a flatbed scanner. *Analytical Biochemistry*, 293, 224-231.

187. Wang YY, Liu B., (2009). Conjugated polymer as a signal amplifier for novel silica nanoparticle-based fluoroimmunoassay. *Biosensors & Bioelectronics*, 24, 3293-3298.

188. Chan, C. P. Y., Bruemmel, Y., Seydack, M., Sin, K. K., Wong, L. W., Merisko,-Liversidge, E., Trau, D., & Renneberg, R. (2004). Nanocrystal biolabels with releasable fluorophores for immunoassays. *Analytical Chemistry*, 76, 3638-3645. Published: JUL 1 2004 .

189. Park, J., Kurosawa, S., Watnanbe, J., & Ishihara, K. (2004). Evaluation of 2-methacryloyloxyethyl phosphorylcholine polymeric nanoparticle for immunoassay of c-reactive protein detection. *Analytical Chemistry*, 76, 2649-2655.

190. Siiman, O., Burshteyn, A., & Insausti, M. E. (2001). Covalently bound antibody on polystyrene latex beads: Formation, stability, and use in analyses of white blood cell populations. *Journal of Colloid And Interface Science*, 234, 44-58.

Chapter Two

Nano-Hybrid Luminescent Dot: Synthesis, Characterization and Optical Properties

2.1. Introduction

In the past decade, low dimensional organic semiconductor materials and inorganic semiconductor nano-crystals (quantum dots) have attracted enormous interest in virtually all areas of materials and physical sciences, since these materials have great potential to be used in solar cells and OLED[1-3] as well as biomarkers.[4-6] The advantages of using nano-particles in photonic applications such as bio-detections could be threefolds:[7] firstly, the size of nano-particles is similar to common bio-molecules which makes them appear to be ideal for bio-conjugate applications such as antibody targeting of contrast agents; secondly, typically nano-materials possess optical properties far superior to the conventionally used molecular species – higher quantum efficiencies, greater scattering or absorbance cross sections and thirdly, the optical activity of nano-particles exhibits better biocompatible wavelength regimes than conventional molecular species.

Linear conjugated polymers, though have been widely studied and used for many applications, have suffered some drawbacks, particularly when they are applied as light emitting materials. This is because conjugated polymers posses a wide range of molecular length which makes them difficult to be purified and re-produced. Furthermore, the existence of aggregation in solid phase also possesses serious challenges. The effects of π - π overlap between conjugated segments of the same or different polymer chains manifest in red shifts of PL spectrum in condensed state compared with that in dilute good solvents.[8-13]

Incorporating organic-inorganic hybrid materials into fluorescent conjugated polymers provides an alternative way to achieve novel light emitting materials with combined advantages of conventional small molecules and conjugated polymers. The brightness and quantum efficiency of polyfluorene and MEH-PPV can be improved by incorporating a bulky polyhedral oligomeric silsesquioxane (POSS) into the chain end.[14-19] The star-like polyfluorene with POSS as core has been reported which showed significantly reduced aggregation as well as enhanced thermal stability.[20,21]

POSS cage, with a diameter of about 1 nm proved to be an excellent candidate for the 'bottom-up' approach to prepare novel luminescent nano-particles via grafting oligo-conjugated molecules onto the eight corners of the POSS cage. The resulting hybrid luminescent nano-particles can also be further encapsulated with alkyl /alkoxy chains which make them individually separated from other nano-particles and could potentially be used in OLED or bio-detection applications.

In this study, a series of oligophenylene functionalized POSS nano-materials were synthesized. They combined the advantages of small molecules and polymers, e.g. precise conjugated length, decent molecular weight, soluble in most of organic solvents, non-crystalline, no obvious Tg, easy purification and tunable properties. The unique structure of these materials significantly reduced aggregation. Moreover, their photoluminescence (PL) is even blue shifted in condensed state compare to that in most of organic solvents. The photoluminescent quantum efficiency (PLQE) of conjugated molecules have been significantly increased with incorporation of POSS. Modeling studies indicated that the frontier molecular orbital, e.g. HOMO (highest occupied molecular orbital) and LUMO (lowest unoccupied molecular orbital), are localized on organic conjugated chains instead of

extension from organic chains to POSS cage. POSS cage is purely functioned as a nano-filler or a scaffold for conjugated linear chains. The thermal properties, chemical structure induced optical property changes, solvent effect, and molecular orbital simulations were also reported in this chapter.

2.2. Objectives and working scope

The main objectives of this chapter are:

(1) To synthesize luminescent nano-dot materials using 'bottom-up' approach, in which POSS is used as a core and conjugated molecules are grafted onto eight vertexes of POSS cage. The aromatic moieties will be directly linked to the cage vertexes without any flexible connection in between. The size of luminescent nano-dots will be controlled in a range of 2-4 nm. To study size effects, one group of molecules (**1b** – **3b**) will be designed in which conjugated chains in different sizes but the side groups remain same. To investigate side group effects, another group of molecules (**4b** – **6b**) will be designed in which molecular sizes maintain same but side groups change accordingly. At such small size, the properties of the light emitting dot may be distinct from that of bulk materials.

(2) To study the property of the light emitting dots in solution and condensed state. In addition, the effect of solvent polarity on the light emitting property will be addressed, in comparison with inorganic QDs which are sensitive to the change of dielectric constant of surrounding medium.[22] When the particle size reduced to nanometer scale, the high surface area will amplify the solvent-particle interaction, which results in modulation of the light emitting property of nano-dots. This is one of the characteristics observed in inorganic quantum dots.

(3) To investigate the effect of incorporation of POSS on the frontier molecular orbitals of conjugated oliogmers using molecular modeling method. For hybrid nano-particles, one basic question will be raised is whether the inorganic core (POSS) involves the formation of molecular orbitals and how much does it contribute to the frontier molecular orbitls of the resulting light emitting dot? This is important in design and tailor-making light emitting dot. In order to elucidate this issue, molecular modeling of a series of molecules will be performed and oligophenylene are selected as the conjugated oligomers due to its rigid nature and comparable small twist angle between adjacent phenyl rings which will reduce the uncertainty of band gap caused by rotation of phenyl rings. The rotation between adjacent phenyl groups will cause changing of molecular orbital energy and leading to the fluctuation of band gap, similar with the size changing for inorganic semiconductor quantum dots.

2.3. Experimental Section

2.3.1 Materials

2,5-dimethyl-phenol (99%), 1,4-Dibromobenzene (97%), 4,4'-Dibromobiphenyl (99%), 2,5-Dibromo-p-xylene (98+%), 1,4-dibromo-2,5-dimethoxy-benzene (98%), 2-Ethylhexyl bromide (95%), Bromobenzene (99%), Magnesium turnings (99.9+%), Acetone(95%, TEDIA), CHCl3 (98%, TEDIA) Tetrakis(triphenylphosphine)-palladium(0) [$Pd(PPh)_3$] (99%), were purchased from Aldrich Chemical Co. and were used as received. Tetrahydrofuran (THF) (99.8%, TEDIA) was distilled from sodium/benzophenone. Octa(bromophenyl)octasilsesquioxane (OBPP) was obtained by our previous report.[23]

2.3.2 Characterization

^{1}H, ^{13}C, ^{29}Si nuclear magnetic resonance (NMR) data were obtained by Bruker Avance 400 spectrometer. UV-Vis spectra were recorded on a Shimadzu 3101 spectrophotometer. Fluorescence (PL) measurement was carried out on a Perkin-Elmer LS 50B luminescence spectrometer with a xenon lamp as a light source. Elemental micro-analysis was carried out by the Microanalysis Laboratory of the National University of Singapore. Mass analysis was carried out by the Mass Spectrometry Laboratory of the National University of Singapore. XRD was recorded on a Bruker GADDS under a voltage of 40 kV and a current of 40 mA using CuK_{α} radiation (λ = 0.15418nm). FTIR spectra were recorded on a Bio-Rad FTS 165 spectrometer by dispersing samples in KBr disks. Differential scanning calorimetry (DSC) measurements were performed under nitrogen flow of 30 ml/min on a TA Instruments 2920 differential scanning calorimeter equipped with a cooling accessory and calibrated using indium. Gel permeation chromatography (GPC) analysis was carried out with a Shimadzu SCL-10A and LC-8A system equipped with two Phenogel 5μ 50 and 1000Å columns in series and a refractive detector, using THF as a eluent at a flow rate of 0.3ml/min at 40ºC. Monodispersed poly(ethylene glycol) were used as standards. HPLC analysis was carried out with a Waters 2996 Separation Module linked simultaneously to a Waters 2996 Photodiode Array Detector. The mobile phase is THF/Acetonitrile (80:20 v/v). The column of reverse phase (SymmetryShield^{TM} PP8 5μm, 4.6x150mm) thermostat was set at 30°C. The flow rate was 1ml/min throughout whole the separation. The absorption of the column eluent was monitored at 254nm. PLQE yields (Φ) of materials in solution was recorded by using the diluted quinoline solution in 0.1 N H_2SO_4 as standard, assuming that the PLQE was 55%. PLQE (Φ) of materials in film was recorded by using 9,10-diphenylanthracene (dispersed in

PMMA films with a concentration lower than 1 x 10^{-3} M and a PLQE of 83%) as a standard. Absorption (UV) on-set was defined as the wavelength at which UV and PL intersect. The concentration of dilute solutions of materials for UV and PL analysis is less than 1 x 10^{-3} g/ml. The simulation of optical properties for hybrid dots was conducted by using the density functional theory (DFT) electronic structure program-DMol[3] in The Materials Studio v3.0 package (Accelrys Inc. 2003). Film morphology was examined by field emission scanning electron microscopy (SEM) (JEOL JMS 6700, JAPAN) and Digital Instruments Nanoscope IV multimode AFM (USA). The time-resolved PL measurements were conducted with the excitation of the frequency doubled output of a Ti:sapphire femosecond laser (Sunami, Spectra Physics). The pulses were centered at 400 nm with pulse duration of 100 fs and pulse repetition rate of 82 MHz. The time evolution of the luminescence was recorded using a streak scope (Hamamatsu, C4334) with the time resolution of 15 ps. The samples were kept in vacuum and the experiments were conducted at room temperature. Power of excitation is 12 W/ cm^2.

2.3.3 Synthesis

2.3.3.1 Monomer synthesis

1-Bromo-4-[2-ethylhexyloxy]-p-xylene (1a).[26] A colorless liquid was prepared according to the literature by reaction between 2-Ethylhexyl bromide with 2,5-dimethyl-phenol with NaOH in acetone (yield 90%), followed by brominating at 0-10°C in $CHCl_3$ (yield 98%). ^{1}H NMR ($CDCl_3$, 400 MHz, ppm) δ 7.23 (s, 1H), 6.66 (s, 1H), 3.80 (d, 2H), 2.33 (s, 3H), 2.15 (s, 3H), 1.73 (m, 1H), 1.54(m, 8H), 0.92(m, 6H). ^{13}C ($CDCl_3$) δ 157.9,

136.9, 135.7, 134.1, 127.6, 115.6, 115.4, 113.8. MS (EI, *m/z*): 313.2. Calculate (%) C, 61.34, H, 7.99; Found (%) C, 61.29, H, 8.02.

4-Bromo-4'-[2-ethylhexyloxy]-2',5'-dimethyl-biphenyl (2a). A Grignard reagent of 4-[2-ethylhexyloxy]p-xylene-1-magnesium bromide (31.95mmol) prepared from the reaction of 10g (31,95mmol) of 1-bromo-4-[2-ethylhexyloxy]p-xylene (**1a**) with 0.92g (38.34mmol) of Mg in 80ml of dry THF, was added dropwise into a solution of 1,4-dibromo-benzene (6.28g, 26.62mmol) in 40ml of dry THF containing $Pd(PPh_3)_4$ (0.6mmol) as catalyst over a period of 1 hour. After refluxing for 24 hours, the reaction mixture was quenched with saturated NH_4Cl aqueous solution and extracted with ether. The extract was washed with water two times and with brine once and then dried over anhydrous MgSO4. After removal of solvent, the dark-brown liquid of mixture was subjected to purification by column chromatography on silica gel using hexane as eluant. A 8.45g (yield 68%) of colorless liquid was obtained. ^{1}H NMR ($CDCl_3$, 400 MHz, ppm) δ 7.55 (d, 2H), 7.22 (d, 2H), 7.02(s, 1H), 6.76(s, 1H), 3.94(d, 2H), 2.28 (s, 3H), 2.26 (s, 3H), 1.82 (m, 1H), 1.55(m, 8H), 1.00(m, 6H). ^{13}C ($CDCl_3$) δ 158.2, 142.3, 134.8, 134.0, 133.6, 133.3, 132.4, 131.7, 125.7, 122.0, 121.8, 121.7, 114.8, 113.3. MS (EI, *m/z*): 389.1. Calculate (%) C, 67.87, H, 7.46; Found (%) C, 67.80, H, 7.49.

4-Bromo-4''-[2-ethylhexyloxy]-2'',5''-dimethyl-triphenyl (3a). A white crystalline was obtained following a similar method of obtaining **2a** using 4,4'-Dibromobiphenyl to replace 1,4-dibromo-benzene (yield 51%). ^{1}H NMR ($CDCl_3$, 400 MHz, ppm) δ 7.62 (d, 4H), 7.55 (d, 2H), 7.42(d, 2H), 7.08(s, 1H), 6.770(s, 1H), 3.93(d, 2H), 2.23 (s, 3H), 2.26 (s, 3H), 1.81 (m, 1H), 1.55 (m, 8H), 0.99 (m, 6H). ^{13}C ($CDCl_3$) δ 158.0, 142.7, 141.2, 139.2, 134.0,

132.5, 132.3, 132.1, 130.7, 130.5, 129.1, 128.6, 127.0, 125.5, 122.7, 114.7, 113.2. MS (EI, *m/z*): 466.3. Calculate (%) C, 72.26, H, 7.10; Found (%) C, 72.24, H, 7.13.

4-Bromo-2,5-dimethyl-4'-[2-ethylhexyl]-biphenyl (4a). A colorless liquid was synthesized following a similar method of obtaining **2a** using 2,5-Dibromo-p-xylene and 1-bromo-4-Ethylhexyl-benzene (yield 62%). ^{1}H NMR ($CDCl_3$, 400 MHz, ppm) δ 7.50 (s, 1H), 7.25 (d, 4H), 7.16(s, 1H), 2,65 (d, 2H), 2.44 (s, 3H), 2.28 (s, 3H), 1.69 (m, 1H), 1.38 (m, 8H), 0.97 (m, 6H). ^{13}C ($CDCl_3$) δ 142.5, 142.0, 139.5, 136.2, 135.8, 134.2, 132.7, 131.1, 130.9, 129.5, 129.3, 124.6. MS (EI, *m/z*): 372.1. Calculate (%) C, 70.78, H, 7.78; Found (%) C, 70.89, H, 7.82.

4-Bromo-2,5-dimethyl-4'-[2-ethylhexyloxy]-biphenyl (5a). A colorless liquid was obtained following a similar method of obtaining **2a** using 2,5-Dibromo-p-xylene and 1-bromo-4-Ethylhexyloxy-benzene (yield 59%). ^{1}H NMR ($CDCl_3$, 400 MHz, ppm) δ 7.56 (d, 2H), 7.22 (d, 2H), 7.02 (s, 1H), 6.76 (s, 1H), 3.94 (d, 2H), 2.28 (s, 3H), 2.26 (s, 3H), 1.82 (m, 1H), 1.58 (m, 8H), 1.00 (m, 6H). ^{13}C ($CDCl_3$) δ 159.9, 142.2, 136.2, 135.9, 134.3, 132.7, 132.2, 132.0, 130.6, 124.5, 116.3, 114.8. MS (EI, *m/z*): 388.1. Calculate (%) C, 67.87, H, 7.46; Found (%) C, 67.89, H, 7.45.

4-Bromo-2,5-dimethoxy-4'-[2-ethylhexyloxy]-biphenyl (6a). A colorless liquid was obtained following a similar method of obtaining **2a** using 1,4-dibromo-2,5-dimethoxy-benzene and 1-bromo-4-Ethylhexyloxy-benzene (yield 58%). ^{1}H NMR ($CDCl_3$, 400 MHz, ppm) δ 7.46 (d, 2H), 7.18 (s, 1H), 7.02 (s, 1H), 6.99 (d, 2H), 6.90 (s, 1H), 3.90 (s, 5H), 3.78 (s, 3H), 1.82 (m, 1H), 1.46 (m, 8H), 0.92 (m, 6H). ^{13}C ($CDCl_3$) δ 160.1, 152.1, 151.6, 132.6, 132.5, 131.8, 131.1, 131.0, 119.0, 117.4, 116.8, 116.3, 115.3, 114.7, 111.1. MS (EI, *m/z*): 420.2. Calculate (%) C, 62.71, H, 6.89; Found (%) C, 62.78, H, 6.90.

2.3.3.2 Organic chain synthesis (for comparison with hybrid dots)

4-[2-ethylhexyloxy]-2,5-dimethyl-biphenyl (1c). A colorless liquid was obtained following a similar method of obtaining **2a** using Bromobenzene and **1a** (yield 72%). ^{1}H NMR ($CDCl_3$, 400 MHz, ppm) δ 7.48 (m, 2H), 7.41 (m, 3H), 7.14 (s, 1H), 6.83 (s, 1H), 4.00 (d, 2H), 2.37 (s, 3H), 2.34 (s, 3H), 1.86 (m, 1H), 1.60 (m, 8H), 1.06 (m, 6H). ^{13}C ($CDCl_3$) δ 158.0, 143.5, 135.0, 134.3, 132.8, 131.7, 130.4, 128.8, 127.0, 125.5, 114.8, 113.3. MS (EI, *m/z*): 310.1. Calculate (%) C, 85.16, H, 9.68; Found (%) C, 85.17, H, 9.68.

4-[2-ethylhexyloxy]-2,5-dimethyl-triphenyl (2c). A color-less liquid was obtained following a similar method of obtaining **2a** using Bromobenzene and **2a** (yield 67%). ^{1}H NMR ($CDCl_3$, 400 MHz, ppm) δ 7.80 (m, 4H), 7.58 (m, 4H), 7.50 (t, 1H), 7.27 (s, 1H), 6.94 (s, 1H), 4.09 (d, 2H), 2.50 (s, 3H), 2.44 (s, 3H), 1.95 (m, 1H), 1.72 (m, 8H), 1.16 (m, 6H). ^{13}C ($CDCl_3$ δ 158.1, 142.4, 140.5, 135.0, 134.5, 134.3, 132.8, 132.1, 131.0, 130.5, 129.4, 129.3, 129.0, 127.7, 127.4, 125.6, 114.9, 113.4. MS (EI, *m/z*): 386.2. Calculate (%) C, 87.05, H, 8.81; Found (%) C, 86.98, H, 8.79.

4-[2-ethylhexyloxy]-2,5-dimethyl-p-quaterphenyl (3c). A white crystalline was obtained following a similar method of obtaining **2a** using Bromobenzene and **3a** (yield 62%). ^{1}H NMR ($CDCl_3$, 400 MHz, ppm) δ 7.79 (m, 8H), 7.51 (m, 2H), 7.46 (m, 3H), 7.13 (s, 1H), 6.80 (s, 1H), 3.96 (d, 2H), 2.23 (s, 3H), 2.29 (s, 3H), 1.83 (m, 1H), 1.58 (m, 8H), 1.01 (m, 6H). ^{13}C ($CDCl_3$) δ 157.9, 142.4, 142.1, 141.2, 139.9, 134.9, 134.3, 134.2, 132.6, 132.0, 131.0, 130.5, 129.6, 129.5, 129.3, 129.1, 128.7, 128.1, 127.9, 127.6, 127.1, 125.5, 114.8, 113.2. MS (EI, *m/z*): 462.2. Calculate (%) C, 88.31, H, 8.22; Found (%) C, 88.34, H, 8.24.

2.3.3.3 Hybrid dots synthesis

Synthesis of hybrid material 1b. A Grignard reagent of 4-[2-ethylhexyloxy]p-xylene-1-magnesium bromide (3.2mmol) prepared from the reaction of 1g (3.20 mmol) of **1a** with 0.09g (3.80 mmol) of Mg in 8ml of dry THF, was added dropwise into a solution of **OBPP** (0.44 g, 0.27 mmol, 2.13 mmol Br) in 4ml of dry THF containing $Pd(PPh_3)_4$ (0.06 mmol) as catalyst. After refluxing for 24 hours under Argon, the reaction mixture was quenched with saturated NH_4Cl aqueous solution and extracted with ethyl acetate. The extract was washed with water two times and brine once and then dried over anhydrous MgSO4. After removal of solvent, the dark-brown liquid of mixture was subjected to purification by column chromatography on silica gel using a mixture of hexane and ethyl acetate (98:2) as eluant. A light yellowish glassy solid 0.42g (yield 60%) was obtained. ^{1}H NMR ($CDCl_3$, 400 MHz, ppm) δ 7.71 (m, 2H), 7.40 (m, 2H), 7.05 (m, 1H), 6.65 (m, 1H), 3.87 (d, 2H), 2.26 (s, 3H), 2.18 (s, 3H), 1.78 (m, 1H), 1.53 (m, 8H), 0.96 (m, 6H). ^{1}H NMR indicated eight chains have been grafted onto POSS. ^{13}C ($CDCl_3$) δ 157.9, 145.5, 142.6, 139.1, 137.5, 136.5, 134.9, 134.2, 129.6, 124.0, 114.8, 113.2. ^{29}Si NMR ($CDCl_3$) δ -78.4. GPC Mn: 2010, Mw: 2100. XRD size 2.2 nm. HPLC: 1.55 min. Calculate ($Si_8O_{20}C_{176}H_{232}$) (%) C, 73.13, H, 8.03; Found (%) C, 72.67, H, 7.54.

Synthesis of hybrid material 2b. A light yellowish glassy solid was obtained by following a similar method of obtaining **1b** using **OBPP** and **2a** (yield 51%). ^{1}H NMR ($CDCl_3$, 400 MHz, ppm) δ 8.21 - 7.33 (m, 8H), 7.10 (m, 1H), 6.78 (m, 1H), 3.94 (m, 2H), 2.28 (m, 6H), 1.81 (m, 1H), 1.59 (m, 8H), 0.99 (m, 6H). ^{1}H NMR indicated eight chains have been grafted onto POSS. ^{13}C ($CDCl_3$) δ 157.9, 142.7, 142.3, 141.7, 140.0, 137.0, 135.3, 134.9, 134.3, 134.1, 133.6, 132.6, 132.0, 131.5, 130.4, 130.0, 129.9, 128.8, 127.2, 125.452, 114.7, 113.2. ^{29}Si NMR ($CDCl_3$) δ -78.5. GPC Mn: 2220, Mw: 2293. XRD size 2.9 nm.

HPLC: 1.45min. Calculate ($Si_8O_{20}C_{224}H_{264}$) (%) C, 76.89, H, 7.55; Found (%) C, 76.52, H, 7.19.

Synthesis of hybrid material 3b. A light yellowish glassy solid was obtained by following similar method of obtaining **1b** using **OBPP** and **3a** (yield 42%). ^{1}H NMR ($CDCl_3$, 400 MHz, ppm) δ 8.21-7.37 (m, 14.5H), 7.10 (m, 1H), 6.78 (m, 1H), 3.94 (m, 2H), 2.28 (m, 6H), 1.80 (m, 1H), 1.54 (m, 8H), 0.98 (m, 6H). ^{1}H NMR indicated seven chains have been grafted onto POSS. ^{13}C ($CDCl_3$) δ 157.9, 144.3, 142.3, 141.6, 141.1, 140.8, 139.6, 137.0, 134.9, 134.4, 134.3, 134.1, 132.6, 132.0, 130.4, 129.5, 129.3, 128.6, 127.9, 127.9, 127.0, 125.5, 114.7, 113.1. ^{29}Si NMR ($CDCl_3$) δ -78.4. GPC Mn: 2620, Mw: 2714. XRD size 3.8 nm. HPLC: 1.40min. Calculate ($Si_8O_{20}C_{244}H_{263}Br$) (%) C, 77.11, H, 6.87; Found (%) C, 76.96, H, 6.59.

Synthesis of hybrid material 4b. A colorless glassy solid was obtained by following the similar method of obtaining **1b** using **OBPP** and **4a** (yield 55%). ^{1}H NMR ($CDCl_3$, 400 MHz, ppm) δ 7.98-7.03 (m, 10.6H), 2.69 (m, 2H), 2.3 (m, 6H), 1.73 (m, 1H), 1.42 (m, 8H), 1.00 (m, 6H). ^{1}H NMR indicated seven chains have been grafted onto POSS. ^{13}C ($CDCl_3$) δ 142.4, 141.7, 140.2, 133.9, 132.5, 131.0, 129.5. ^{29}Si NMR ($CDCl_3$) δ -78.6. GPC Mn: 2228, Mw: 2317. HPLC: 1.49min. Calculate ($Si_8O_{12}C_{202}H_{235}Br$) (%) C, 76.83, H, 7.44; Found (%) C, 76.77, H, 6.99.

Synthesis of hybrid material 5b. A light yellowish glassy solid was obtained following the similar method of obtaining 1b using **OBPP** and **5a** (yield 55%). ^{1}H NMR ($CDCl_3$, 400 MHz, ppm) δ 7.96 – 6.61 (m, 10H), 3.92 (m, 2H), 2.18 (m, 6H), 1.79 (m, 1H), 1.50 (m, 8H), 0.97 (m, 6H). ^{1}H NMR indicated eight chains have been grafted onto POSS. ^{13}C ($CDCl_3$) δ 159.6 141.7, 135.2, 133.8, 132.3, 130.7, 116.1, 114.56. ^{29}Si NMR ($CDCl_3$) δ -79.0. GPC Mn:

2439, Mw: 2501. HPLC: 1.45min. Calculate ($Si_8O_{20}C_{224}H_{264}$) (%) C, 76.89, H, 7.55; Found (%) C, 76.45, H, 7.51.

Synthesis of hybrid material 6b. A light yellowish glassy solid was obtained following the similar method of obtaining **1b** using **OBPP** and **6a** (yield 48%). ^{1}H NMR ($CDCl_3$, 400 MHz, ppm) δ 8.12 - 7.40 (m, 7H), 7.02 (m, 4H), 3.95 (m, 2H), 3.67 (m, 6H), 1.81 (m, 1H), 1.50 (m, 8H), 0.99 (m, 6H). ^{1}H NMR indicated six chains have been grafted onto POSS. ^{13}C ($CDCl_3$) δ 157.9, 142.7, 142.3, 141.7, 140.0, 137.0, 135.3, 134.9, 134.3, 134.1, 133.6, 132.6, 132.0, 131.5, 130.4, 130.0, 129.9, 128.8, 127.2, 125.5, 114.7, 113.2. ^{29}Si NMR ($CDCl_3$) δ -77.5. GPC Mn: 2564, Mw: 2635. HPLC: 1.41 min. Calculate ($Si_8O_{30}C_{180}H_{206}Br_2$) (%) C, 66.87, H, 6.38; Found (%) C, 66.84, H, 6.28.

2.4. Results and Discussion

2.4.1 Synthesis

Scheme 2.1. Synthesis of hybrid materials 1b – 3b

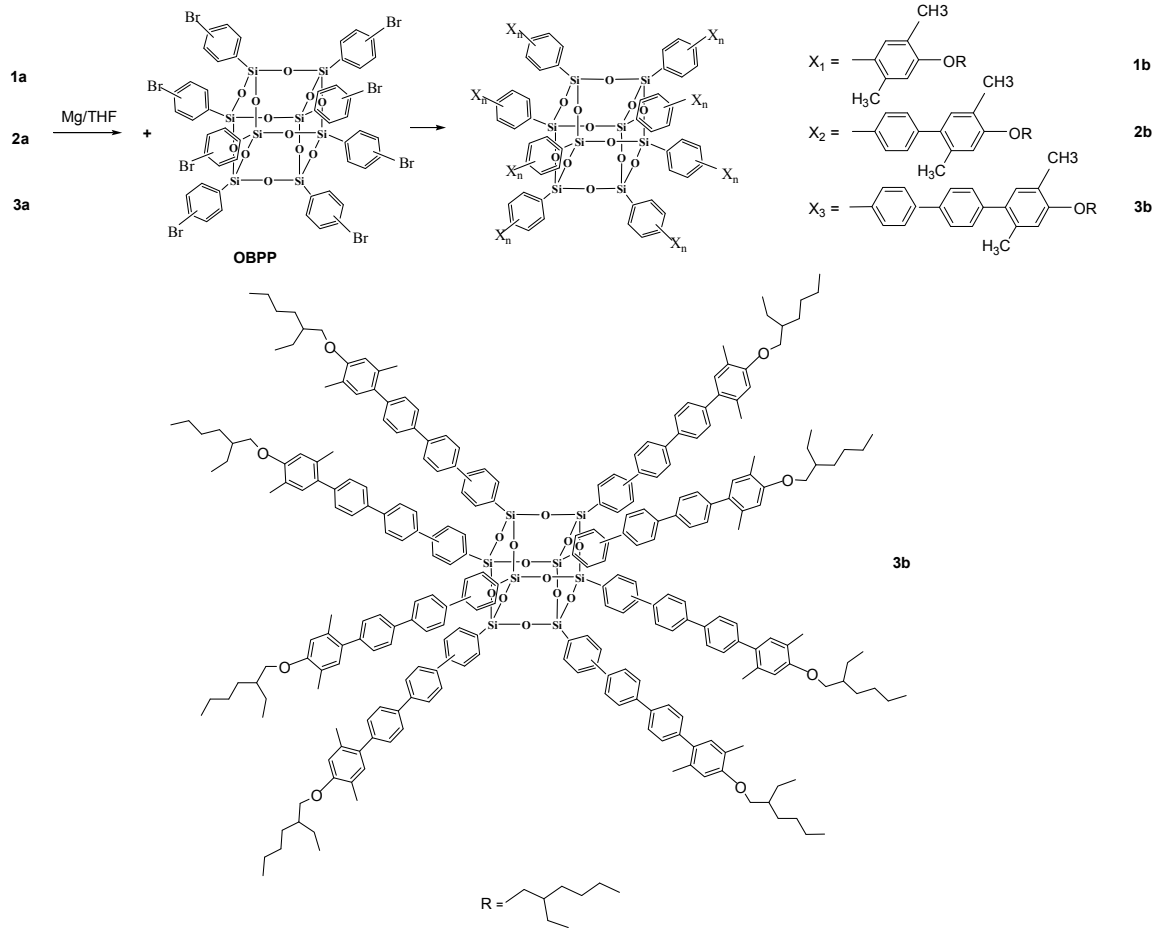

Scheme 2.2. Synthesis of corresponding organic chain 1c – 3c in hybrid materials.

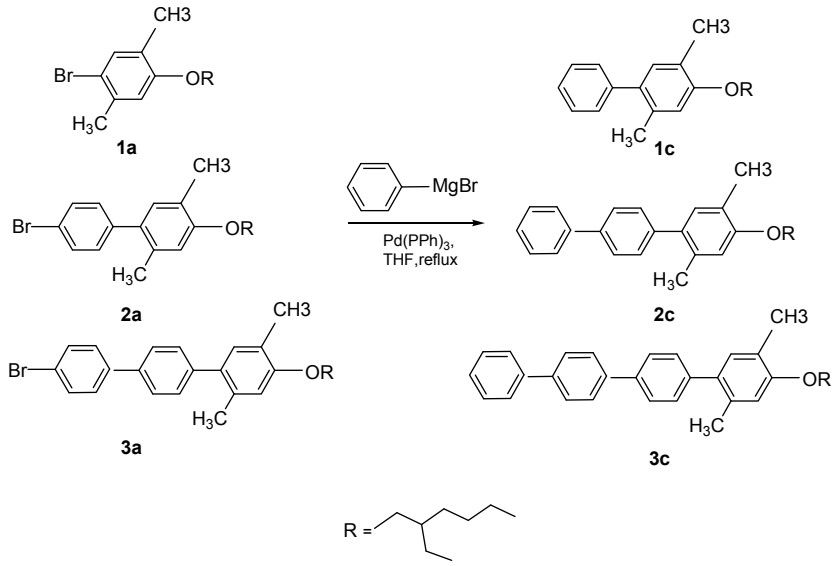

Scheme 2.3. Synthesis of hybrid materials 4b – 6b

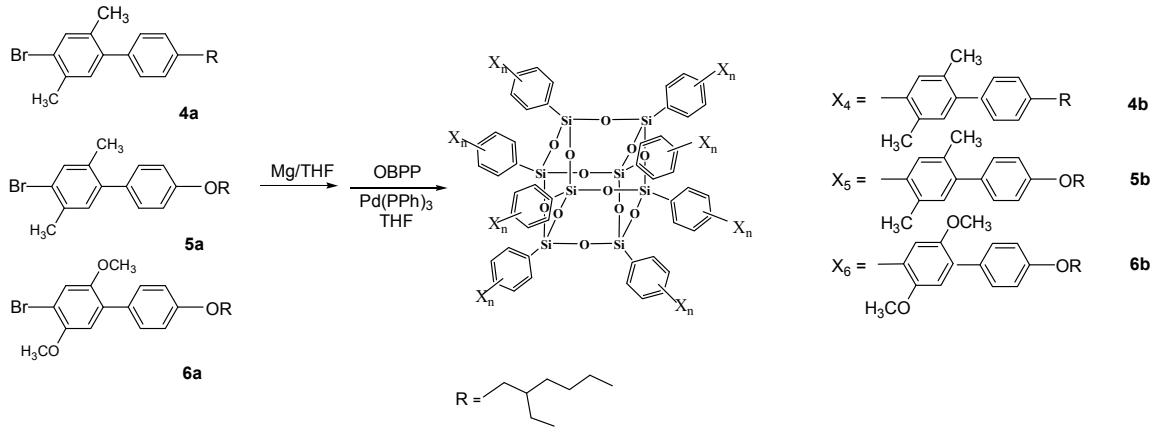

A series of hybrid materials with organic chain stretched from vertexes of POSS were obtained via Grignard coupling reaction between **OBPP** and monomers **1a – 6a**. Since eight phenyl rings in each POSS molecule are involved in the bromination, it may be thought that some phenyl rings could be double brominated while others were un-brominated in **OBPP**. However, in a previous work[23] it has been shown that the unique single peak in ^{1}H NMR at 7.38 ppm of **POSS-Ph$_8$** was totally disappeared in **OBPP**, which implies all the phenyl rings are brominated in **OBPP**. Moreover, elemental analysis indicates there were eight bromine atoms substituted on each POSS-Ph$_8$. As a result, it's reasonable to conclude that each phenyl ring has been substituted by single bromine atom.

The oligophenylene functionalized POSS with different chains length, such as two, three, and four phenyl rings denoted as **1b – 3b**, were shown in Scheme 2.1. For the purpose of comparison, identical organic chains were also synthesized (**1c – 3c)** as shown in Scheme 2.2. The hybrid materials with different side groups attached on same main chain as denoted as **4b – 6b**, were also synthesized and shown in Scheme 2.3.

2.4.2. HPLC

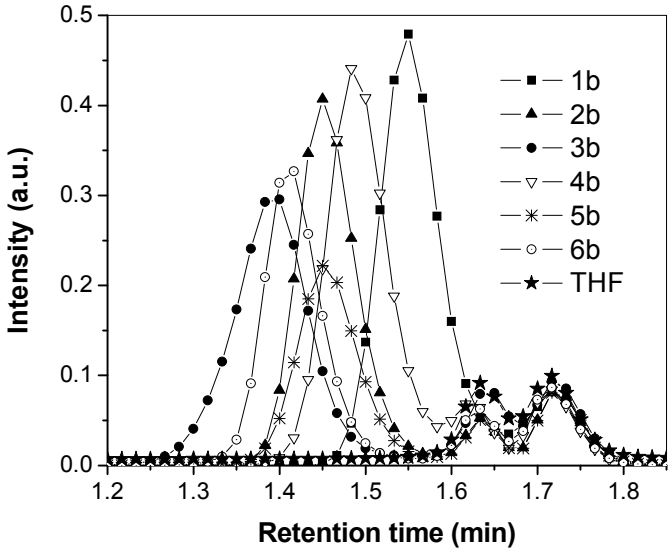

Figure 2. 1. HPLC spectrum of hybrid materials

The material components for the nano-hybrid dots were characterized using HPLC. The single sharp peak in HPLC spectrum of hybrid dots, as shown in Figure 2.1, indicated the desired hybrid molecules have been obtained. The peak for **3b** and **6b** are bit flat which might be caused by the incomplete grafting, **3b** has average seven chains substituted while **6b** has average six chains attached onto POSS as discussed in the synthesis part. The incompleteness of substitution of **3b** and **6b** might be caused by the heavier monomer of **3a** and **6a** which have less activity than **1a** or **2a**. It's well known the bigger the molecule the less activity of reaction. So the incorporation of chains to POSS is affected by the chain molecular weight.

2.4.3 FTIR

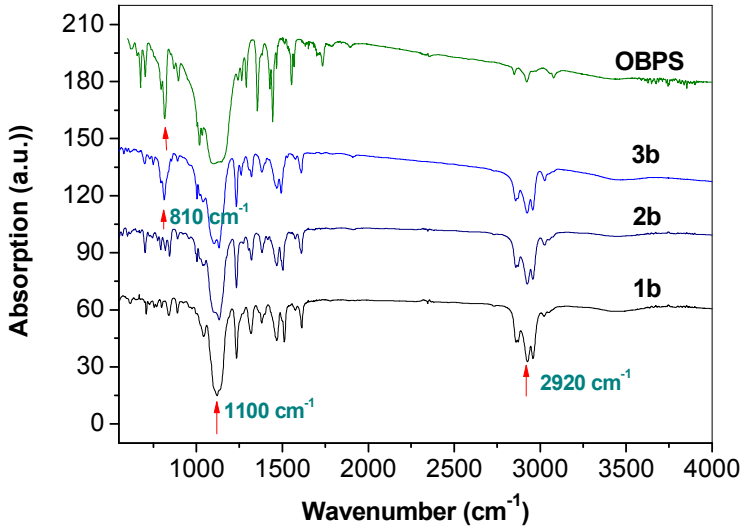

Figure 2.2. FT-IR of nano-particle 1b, 2b, 3b.

The FTIR spectra of hybrid luminescent nano-particles **1b**–**3b** are presented as Figure 2.2. The strong Si-O-Si stretching band at 1110 cm^{-1} was observed for all of three luminescent dots. This strong Si-O-Si stretching band near 1100 cm^{-1} is confirmed as cage structure of Si-O-Si bonding. This indicates that the cage structure of POSS has been maintained in the strong base environment of reaction. The other common peaks near 2920 cm^{-1} were found for **1b**-**3b** as well, which are the typical C-H stretching from alkyl or aloxy groups. Due to the column chromatography purification, the light emitting dot product is pure and identical hence, combined with FTIR spectrum, we may conclude there is no partial cage or by-product mixed up with nano-particles **1b**-**3b**. In Figure 2.2, the absorption at 810 cm^{-1} results from Br – C stretch (for aromatic compounds). This absorption disappeared in FTIR spectra of the compounds **1b** and **2b** because all of the bromo-phenyl groups in OBPS

have been substituted by conjugated chains so that there is no Br – C bond left in **1b** and **2b**. There are seven arms (in average) attached on POSS in compound **3b** so there is one Br – C bond in **3b**, and that is the reason why there is an absorption at 810 cm^{-1} in its FTIR spectrum of **3b**. This Br – C absorption is more obvious in OBPS (starting material) that has eight Br-C bonds in each molecule, as shown in Figure 2.2.

2.4.4 XRD

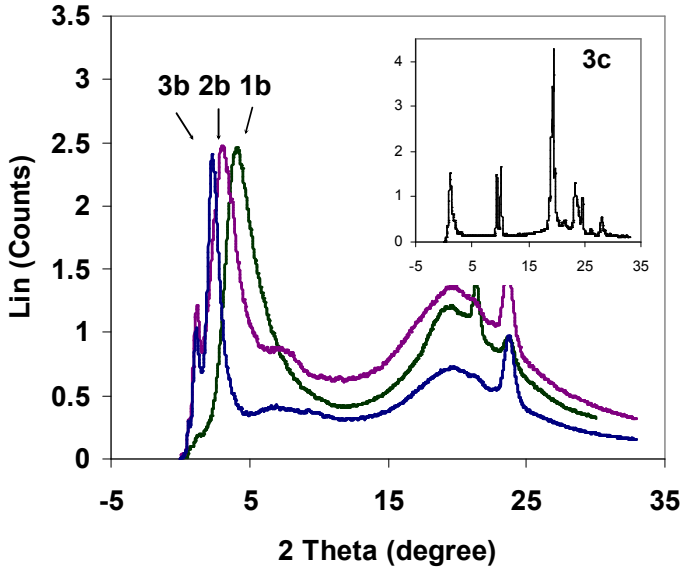

Figure 2.3. XRD spectrum of materials 1b (solid line), 2b (dotted line), 3b (dashed line), 3c (inset spectrum)

The molecular size of the nano-hybrid dots was studied using X-ray scattering method. XRD spectrum of **1b** – **3b** and chain **3c** were shown in Figure 2.3. Chain **1c** and **2c** are in liquid form while **3c** is a white crystalline material. XRD spectrum from **1b** to **3b** shows only one main peak at low angle and a broad amorphous halo appearing at about $2\theta \approx 20^{o}$. The

main peaks with *d*-spacing of 2.2 nm (in **1b)**, 2.9 nm (in **2b)** and 3.8 nm (in **3b)** correspond to the molecular size which is similar to the calculated results. The peak at low angle (2θ <2°) is caused by instrument (beam). The broad peak at $2\theta \approx 20^{o}$ corresponds to amorphous phase for three compounds. The small sharp peak at 20 - 25° (2θ) possibly corresponds to the local regular packing of alkoxy chains which are end-capped on each emissive conjugated chains. Moreover, the XRD results indicated the liquid organic material **1c** and **2c** became non-crystalline solids after incorporation of POSS. The highly crystallized organic chain **3c** also became non-crystalline after grafting onto POSS cage.

2.4.5 DSC

The DSC study also confirms the amorphous characteristics of the nano-hybrid dots. As shown in Figure 2.4 for hybrid material **3b** and organic chain **3c,** the big melting peak for **3c** at 103°C and the crystallization peak at 114°C after a fast cooling process from the highest temperature (370°C in DSC) indicating that this compound can easily form crystal structure. However, after incorporate with POSS, this highly crystallized small molecular organic compound has been transformed to amorphous hybrid material due to disruption of the packing. Moreover, no evident of glass transition was observed up to 370°C. The other two arms **1c** and **2c** are in liquid form and not subjected to testing. The other two hybrid materials **1b** and **2b** showed similar curves to that of **3b**.

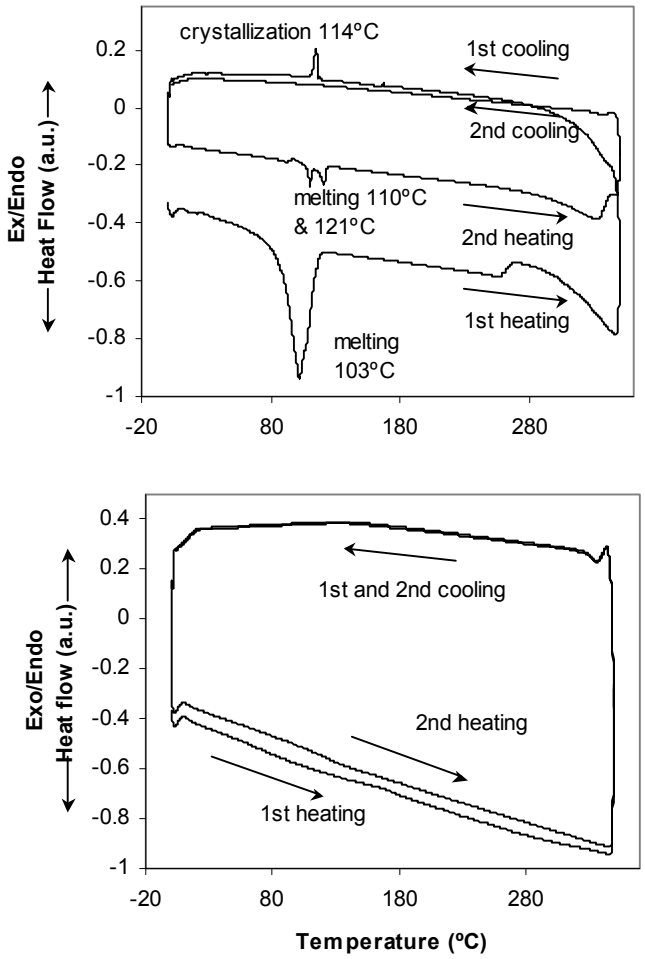

Figure 2.4. DSC curves of 3c (upper) and 3b (lower) at a heating rate of 20°C/min and cooling rate 10°C/min under nitrogen atmosphere, hold 10mins at the highest temperature before cooling and 10mins at the lowest temperature before heating.

2.4.6 Optical properties

UV absorption and PL were conducted for **1c - 3c** and **1b - 6b** in different solvents as well as in thin films. The results were shown in Figure 2.5, Figure 2.6, Figure 2.7, and summarized in Table 2.1. The chain structures in this work are different from that of our previous report[23] so the PL spectra of **1b-6b** didn't show any sharp feature since the adjacent phenyl in the chains could rotate freely due to lack of alkyl group on each α position. As a

result, the peak is broadening due to many energy levels associated with different torsion angles.

The quality of thin films of organic molecules has been dramatically improved after forming hybrid dot materials. From Figure 2.5 and Figure 2.6 we can see the UV and PL spectrum of **1b** and **2b** are much smoother than that of **1c** and **2c**, this specially true for film spectrum. **1c** and **2c** are liquid materials while **3c** is highly crystallized compound so the films formed by spin coating for **1c-3c** are very poor. As such the PLQE of these three materials are not high due to high aggregation caused by chains close packing. The hybrid luminescent dot materials **1b-3b** on the other hand could form good films with smooth and transparent surface. The thickness of films depends on concentration of solutions regardless solvent and all films can be easily made by spin coating because their amorphous and high soluble nature.

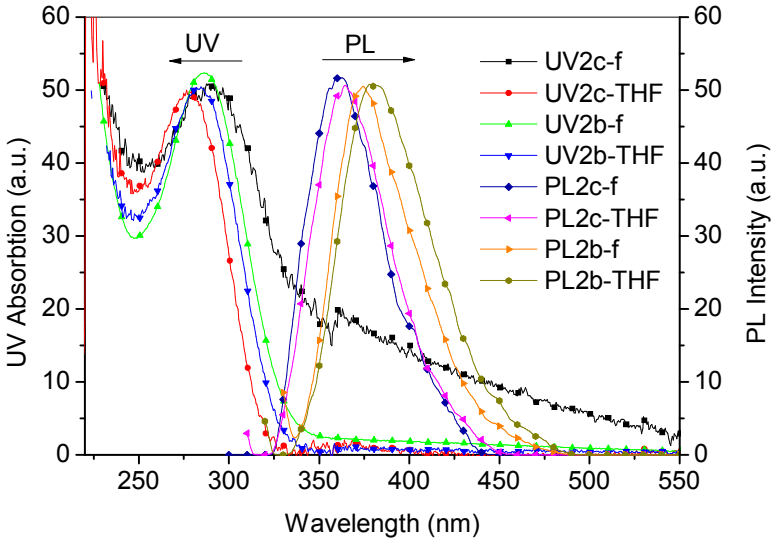

Figure 2.5. Normalized UV absorption and PL of organic chain 2c and hybrid material 2b in different solvents and in thin films.

As shown in Table 2.1, two points should be highlighted. Firstly, the PLQE for hybrid dots **1b-3b** are higher than that of corresponding linear chains **1c-3c**; secondly, PLQE of **1b-3b** in solid form are higher than that in solution form. These two typical features of hybrid POSS luminescent dots are unique and exciting. The PLQE of films have been significantly improved, i.e. from 45% (**1c**) to 66% (**1b**), 67% (**2c**) to 97% (**2b**), 59% (**3c**) to 83% (**3b**). This is due mainly to the reduction or elimination of aggregation in the oligophenylene functionalized POSS. Secondly, similar as star-like **1b** and **2b,** linear compounds **1c** and **2c** also showed high PLQE and blue-shift in condensed state. This because long bulky side chain which act as a separating layer to reduce aggregation. However, when chain length increases, i.e. **3c**, the aggregation occurred because the alkyl side group could not effective prevent aggregation and 3c even form crystalline structure, hence PLQE of **3c** in film was lower than that in solutions. The PLQE of hybrid nano-particles **1b-3b** in solutions increases from ~30%to ~70% and further to ~79% respectively. The PLQE of film samples of hybrid nano-particles, however, shows a turning point at 2**b**. The PLQE of films of hybrid nano-particles are 66% for **1b**, 97% for **2b**, and 83% for **3b** respectively. The possible explanation is when the conjugated chain extended over one limit, the aggregation in film samples became more pronounced as the conjugated chain length increasing. In dilute solution the molecules could be thought as single molecules hence the aggregation could be ignored.

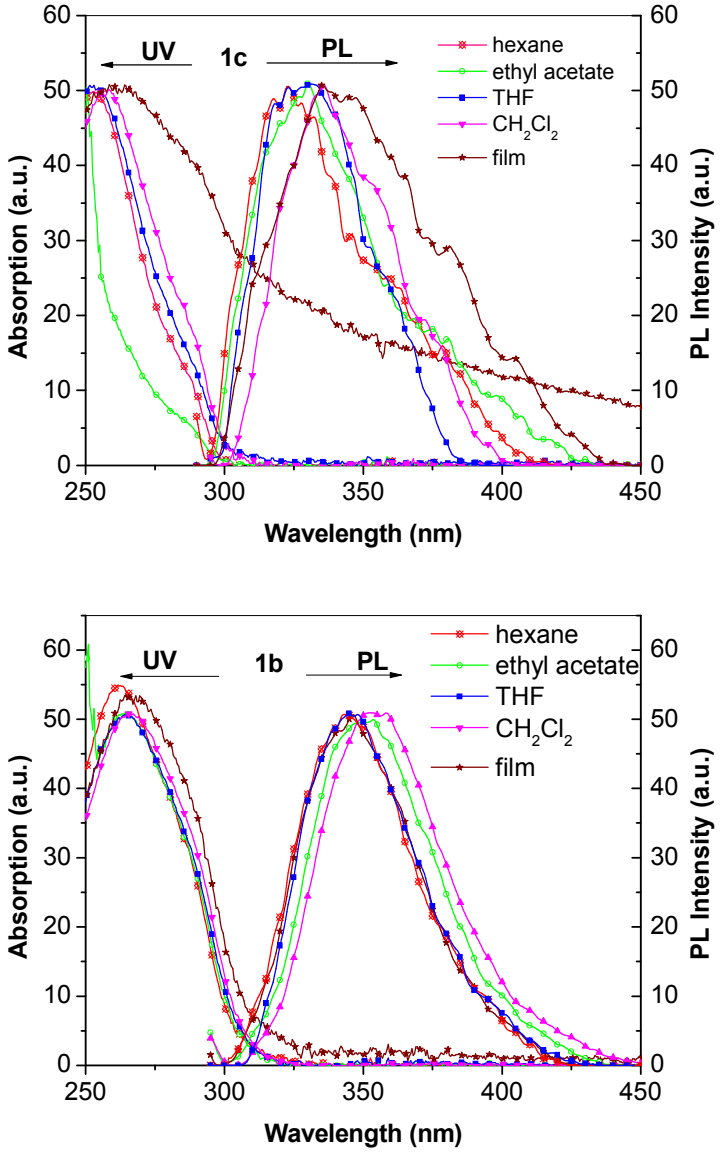

Figure 2.6. Normalized UV absorption and PL of organic chain 2c and hybrid material 2b in THF and as thin films.

Table 2.1. Optical properties of 1c - 3c and 1b - 6b. [a]

PLQE: PL quantum efficiency. [b] He: Hexane. [c] EA: eathyl acetate. [d] TF: THF. [E] DC: Dichloromethane (CH_2Cl_2). [f] Dielectric constants.

	UV on-set (nm)					**PL λ_{max} (nm)**					**Φ (PLQE) (%)[a]**				
	Bandgap (ev)														
	He[b]	EA[c]	TF[d]	DC[e]	film	He	EA	TF	DC	film	HX	EA	TF	DC	film
de[f]	1.9	6.0	7.6	9.1		1.9	6.0	7.6	9.1		1.9	6.0	7.6	9.1	
1c	296	297	300	303	312	324	331	331	336	336	18	16	14	21	45
	4.2	4.2	4.1	4.1	4.0										
1b	308	311	314	317	317	351	355	357	359	351	31	32	33	20	66
	4.0	4.0	4.0	3.9	3.9										
2c	316	322	326	328	338	352	363	365	372	361	58	57	56	60	67
	3.9	3.8	3.8	3.8	3.7										
2b	326	333	337	340	340	369	378	379	388	375	71	65	73	49	97
	3.8	3.7	3.7	3.6	3.6										
3c	336	338	343	344	354	370	379	380	388	386	69	82	85	86	59
	3.7	3.7	3.6	3.6	3.5										
3b	346	348	354	355	356	380	391	392	402	391	79	79	75	85	83
	3.6	3.6	3.5	3.5	3.5										
4b	308	309	314	314	316	353	356	356	356	359	41	43	36	37	41
	4.0	4.0	4.0	3.9	3.9										
5b	313	318	320	322	323	356	362	363	369	368	66	51	56	57	74
	4.0	3.9	3.9	3.9	3.8										
6b	356	360	361	361	366	390	395	397	404	396	39	50	41	40	99
	3.5	3.4	3.4	3.4	3.4										

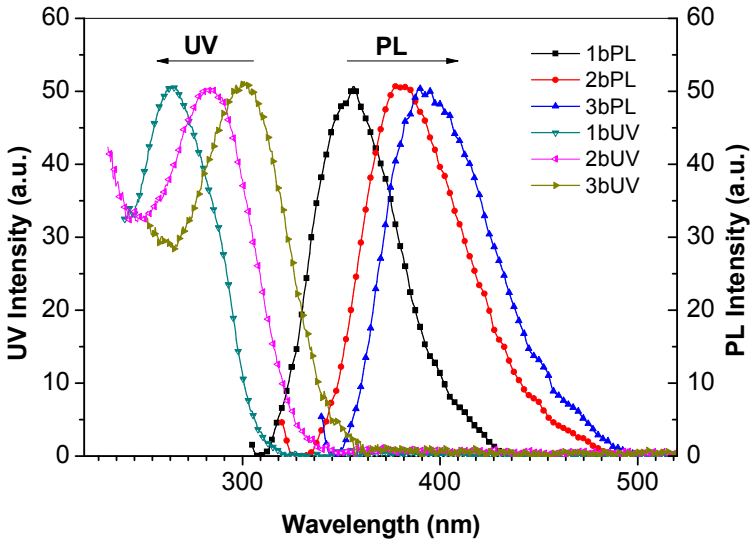

Figure 2.7. Normalized UV absorption and PL of hybrid material 1b-3b in solution THF.

Solvent effects were observed significant, as shown in Table 2.1, Figure 2.5, and Figure 2.6. UV on-set and PL curves are red shifted as solvents polarity (measured by dielectric constants) increased for all the small sized materials. The interesting phenomena is that the PL λ_{max} of **2c**, **3c**, **1b**, **2b**, **3b** in condensed states (films) are blue shifted from most of the solvents, in contrast to conjugated polymers in which PL λ_{max} in condensed state (film) is red shifted from all of the solutions due to the aggregation formed in condensed state.[26] The UV and PL of hybrid dots in solutions red shift as the polarity of solvent increases, e.g. **2b** and **3b** red shift 7nm (UV) and 10nm (PL) respectively from ethyl acetate (dielectric constant 6.0) to dichloromethane (9.1). Similar phenomenon was also found in conjugated copolymer of PPE/PPV, UV and PL λ_{max} red shift 2nm and 4nm from chlorobenzene (5.9) to dichloromethane (9.1).[26] The red shift, with increasing solvent polarity, might result from increased stabilization of the molecule in the excited state relative to that in the ground

state.[26,27] Hybrid dot red shifts more than polymer does, this could be attributed to the interaction between polar solvent and nano-hybrid dots is more profound than that between solvent and polymers.

The aggregation which was represented by red shift from solution to film is more pronounce for chain compounds **1c-2c** than for nano-particles **1b-2b,** as shown in Figure 5 and Figure 6. UV spectra for chain **1c** and **2c** red shifted from all of solutions regardless solvents. As contrast, UV and PL spectra for **1b** and **2b** blue shifted from that of most of solutions except for those solvent having small polarity such as Hexane. So the aggregation, non-preventable for linear organic luminescent materials, will be overcome by incorporation of these molecules with POSS cage structures.

The size effect is obvious, as shown in Figure 2.7. With increasing the length of chains, the UV and PL spectra of nano-hybrid dots (**1b - 3b)** red shifted no matter in solutions or in film state. For example, in hexane, the UV for **1b**, **2b**, **3b,** increases from 308nm to 326nm and further to 346nm, almost red shift 20nm for one addition phenyl unit. At the same time the PL $\boldsymbol{\lambda_{max}}$ also red shifts from 351nm to 369nm and further to 380nm respectively. This phenomenon suggests possible quantum confinement effect. From XRD we estimated the sizes of dots are 2-4nm for **1b-3b** which is near exciton Bohr radii (a_B) in bulk organic semiconductors (a_B ~ 1.2-2.0 nm). If the exciton has been localized in each arm, there should be quantum confinement effect. In contrast, when conjugated chain is long enough, i.e. bulk material, there won't be an obvious red shift on absorption and emission spectra by increasing its size. Later we will discuss modeling study of molecular orbitals from which we can see exticons have been localized on each organic arm substituted onto POSS.

The PLQE is improved by increasing molecular size from **1b** to **3b** in solution. The possible reason is in the linear π conjugated systems, an increase in π conjugation length in the excited singlet state will bring the increase in both quantum efficiency and PL wavelength[28]. Molecule **3b** has the longest conjugated chain hence it shows the largest PLQE in solution and reddest PL wavelength while **1b** has the shortest conjugated chain among **1b** – **3b** and it shows the lowest PLQE and the bluest PL wavelength. The lone pair electron on oxygen atom increases conjugation length hence the more alkoxy group the molecule has, the higher quantum yield and the redder of PL wavelength of this molecule exhibits. Molecule **6b** has three alkoxy group on each arm hence it shows the highest PLQE in film while molecule **4b** has no alkoxy chain therefore it shows the lowest PLQE in film. The solvent may quench the excitons so the PLQE in solution for all molecules are lower than that in film. The higher PLQE in film than in solution of our nano-dots are unique because all conjugated polymers show higher PLQE in solution than in film due to aggregation.

Even though these materials are not designed for OLED applications, we still could predict compound **3b,** out of six compounds in this chapter, would be the best candidate for OLED applications. The molecules **1b** - 6**b** are nano-particles with short conjugated chains and isolated by POSS and alkoxy shielding chains, which introduces interruptions to the charge transporting path and leads to much higher power to overcome the extra hopping energy of charge transportation. The charge transport process would limit the performance for these nano-particles in OLED applications so the molecule having the longest conjugated chain should be the best material in this chapter. The experiments proved this conclusion as OLED device made from **3b** shows lower turn-on voltage than the devices fabricated using **1b** and **2b**.

2.4.7 Effect of Side Groups on HOMO and LUMO of Conjugated Oligomers

The effect of the functional groups (oxygen atom) in the oligo-conjugated chains on the resulting optical properties have been studied by comparing the optical properties of three hybrid dots, **4b**, **5b** and **6b**, in which the organic main chain has same structure but with different side groups. While **4b** has three alkyl groups, **5b** possess two alkyl groups and one alkoxy chain, and **6b** has three alkoxy groups. Compared with alkyl chain, incorporating alkoxy chain onto the conjugated backbone reduced the band-gap which leads to UV and PL red shift and increased PLQE in solution and in film, as shown in Table 2.1. For **4b** and **5b,** UV on-set red shift from 308nm to 313nm in Hexane. The PLQE increased from 41% to 66% in Hexane and from 41% to 74% in films. PL and UV of **6b** red shift even more compared to that of **4b**, and the PLQE of **6b** in film increased dramatically to 99%. It was clear that the red shift and the increase of PLQE could not be explained solely by geometry of the backbone because the alkyl chain (in **4b**) and alkoxy chain (in **5b**) were substituted at the end of chain, which will not affect the torsion angle of adjacent phenyl rings. As a result, the oxygen atom must have particular contribution to the optical properties of the nano-hybrid dots. Study on alkyl and alkoxy substituted poly(p-phenylenevinylene) (PPV) derivatives indicated that the non-bonding electrons from oxygen atom in alkoxy side chain mixed with π-electrons of polymer main chain, hence the π-electron systems extended. Therefore, the effective π-conjugation length of alkoxy substituted polymer was longer than that of alkyl substituted polymer, which lead to a lower band-gap.[29] Further confirmation of the effect of 'oxygen' on the light emitting property comes from molecular modelling study.

Table 2.2. Simulation of optical properties of 4b, 5b, and 6b with comparison of that of experimental results.

[a] cal. : calculation. [b] UV onset : experimental data.

	HOMO (eV) (cal.)[a]	LUMO (eV) (cal.)	Bandgap (eV) (cal.)	Band gap (eV) UV onset (nm)[b]				
			UV onset (cal.) (nm)	Hexane	Ethyl acetate	THF	CH_2Cl_2	film
4b	-5.676	-1.794	3.9	4.0	4.0	4.0	3.9	3.9
			319	308	309	314	314	316
5b	-5.327	-1.761	3.6	4.0	3.9	3.9	3.9	3.8
			348	313	318	320	322	323
6b	-5.200	-2.079	3.1	3.5	3.4	3.4	3.4	3.4
			397	356	360	361	361	366

To illustrate this phenomenon, simulation was conducted for **4b** - **6b**, as was shown in Figure 2.8. The results are summarized in Table 2.2. By comparing the HOMO and LUMO of **4b** with **5b,** it was noted that oxygen atom was only involved in the formation of HOMO but not in the formation of energy levels of LUMO. With the oxygen joining in the HOMO, the energy level was increased from -5.676eV (**4b**) to -5.327eV (**5b**). This increment accounts for the bandgap reducing from 3.9 eV (**4b**) to 3.6 eV (**5b**) and the correspondence red shift of UV and PL, because the LUMO of **4b** (-1.79 eV) and that of **5b** (-1.76 eV) are similar.

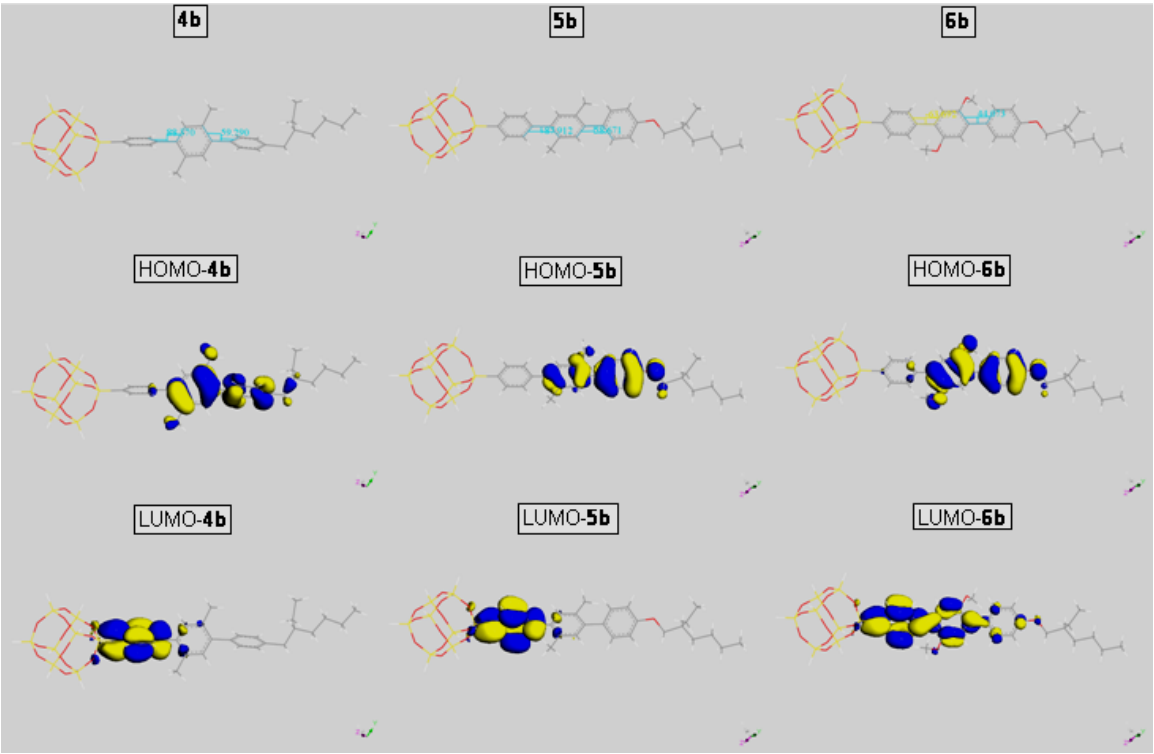

Figure 2.8. Simulation of molecular orbital of materials 4b, 5b, 6b. For simplifying situation, only one organic arm instead of eight arms was presented. The line in red color represents "O" atom.

When more alkoxy groups were grafted onto the phenyl ring such as in **6b,** the high concentration of alkoxy groups not only affect the energy levels due to more oxygen atom involved in the formation of HOMO, but also changed the conformation of the backbone because the torsion angle in **6b** was 63° instead of 89° for both **4b** and **5b**. As a result, the 'effective conjugated length' for **6b** is longer than that of **4b** and **5b** and hence the PL and UV of **6b** are more red shift.

In Table 2.2, the band gaps derived from UV-Vis measurement actually are larger than the bad gap values calculated for **4b**, **5b**, and **6b**. This is possibly due to the assumption based on which the calculation was conducted. The assumption is there is no difference

between mono- and octa-substituted POSS-oligophenylene. Therefore in simulation only one arm substituted POSS was studied to save time. The organic chain's structure and the dihedral angles between adjacent phenyl rings have been optimized, under single chain situation, to reach the lowest energy level for the whole molecule. In a real molecule, however, eight organic chains were substituted on each vertex of POSS cage and there are un-avoidable interactions between eight chains. So the ideal dihedral angles between adjacent phenyl rings may not be able to be maintained due to inter-chain reactions. As more alkoxy chains attached onto chain for **6b**, the calculated dihedral angles of 6b are small in single arm situation. The ideal planner structure of single arm could be twisted easily in crowded eight -chain substituted molecule of **6b** which results in higher band gap from UV measurement compare to calculation.

The influence of side group on the PL characteristics of conjugated polymers was also reported elsewhere.[30] It was found that big bulky alkoxy side groups grafted on the backbone could improve the PLQE in solutions, but in condensed state (films) the PLQE were much lower than that in solutions due to the aggregation which is unavoidable in conjugated polymers. In contrast, in our nano-hybrid system, the hybrid dot **6b** has much higher PLQE in condensed state (film) than in solution, which demonstrated once again the non-aggregation features of oligophenylene functionalized POSS due to the unique structures of hybrid materials.

2.4.8 Effect of POSS on HOMO and LUMO of Conjugated Oligomers

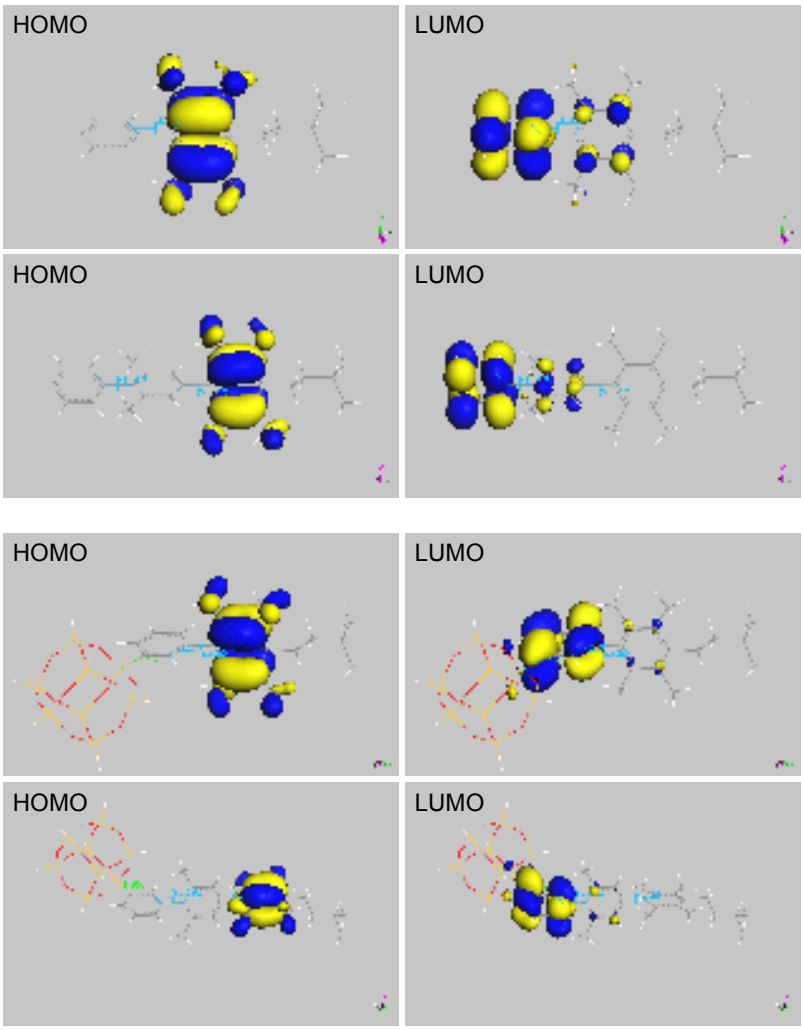

Figure 2.9. Molecular orbital modeling for alkyl chains substituted bi-phenyl and tri-phenyl (top group) and corresponding POSS substituted bi-phenyl and tri-phenyl (bottom group)

To address the basic question whether POSS cage contributed to the formation of frontier molecular orbital HOMO and LUMO, simulation was conducted to molecules bi-phenyl and

tri-phenyl substituted POSS molecules. To simplify calculation, only one-arm-model was used. Figures 2.9 displayed the HOMO and LUMO orbitals obtained by calculation for molecules of alkyl chain encapsulated bi-phenyl and tri-phenyl substituted POSS compounds. It was found that π and π* orbital contributed solo by phenyl rings, same as our previous results, these orbitals are localized on each arm[31]. It is clear that HOMO and LUMO of chains and hybrid materials are exactly same regardless two phenyl or three phenyl rings in the arm structure.[32] The POSS substituted tri-phenyl molecule in the ground state has a total of 104 occupied (208 electrons) orbitals. Both HOMO and continuously followed five orbitals, and LUMO and continuously followed five orbitals are all contributed by organic arm which means POSS does not involve in the frontier molecular orbital formation. The POSS cage involved orbital of **3b**, for example, is the 6th lowest unoccupied molecular orbital (LUMO+6), i.e. LUMO + 1.335 eV**,** which would cause a higher band gap of 1.335 eV compared to the band gap of organic chains. The experimental results support the conclusion as the wavelength of UV on-set shows similar band gap to the calculated results. Therefore POSS cage is not involved in the charge transfer under photo-luminescent process for all compounds discussed in this work.

2.4.9 Film Formation Property

The morphology of thin films from **3b** and **3c** were studied by SEM and AFM, as shown in Figure 2.10. Film of **3b** and **3c** were cast on glass substrates using an ethyl acetate solution. It is shown that **3c** could not form homogeneous film because **3c is** hightly crystalline materials, while star-like material **3b** is an non-crystalline materials and can easily form a thin film with a smooth surface. To reduce crystallinity of light-emitting materials is

a major driving force of modification of conventional material structures to increase the PL and EL efficiency. It is well accepted that crystallized structure increases the inter-molecular interaction, e.g. π-π stacking between conjugated molecules, which reduce the radiation efficiency. The reason of increased PL efficiency of hybrid dot materials compared to linear conjugated polymers /oligomers is mainly because the incorporation of POSS largely eliminate the crystallinity.of the resulting light emitting dots.

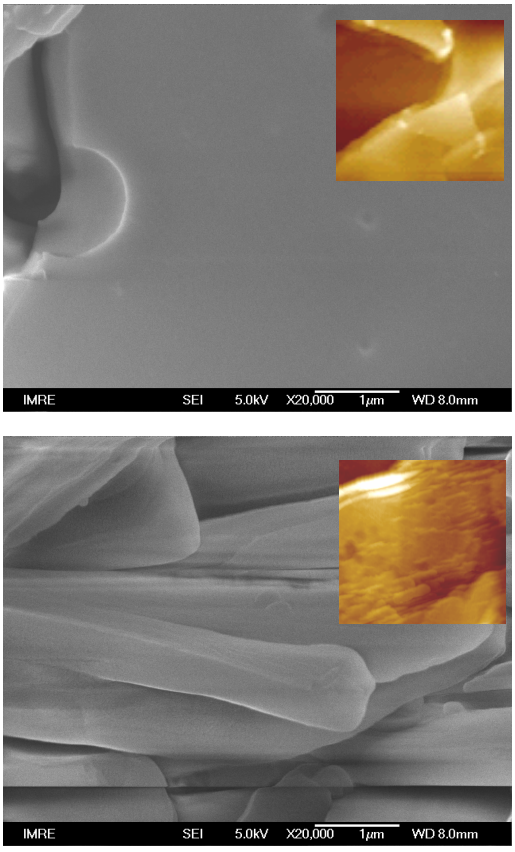

Figure 2.10. SEM and AFM (inset) images of hybrid material 3b (upper) and organic chain 3c (lower). AFM scale unit is same with SEM.

2.4.10 Time resolved PL Study

Time-resolved fluorescence studies can provide direct information on various underlying physical processes on a molecular scale. The molecule relaxes from the vibrational excited state S_n^* to the lowest level of the singlet state S_1 through vibrational relaxation at a rate of k_{relax}. The fluorescence rate is a measure of radiative and non-radiative processes. The constant k_R is the radiative decay rate. Various other non-emission channels denoted as non-radiative decay processes are described by the rate k_{NR}. These non-radiative decay processes may occur due to collision by diffusion, exciton quenching by another species, etc. The fluorescence decay rate is given as $k_F = k_R + k_{NR}$ where the fluorescence lifetime $\tau_F = (k_F)^{-1}$, $\tau_R = (k_R)^{-1}$, $\tau_{NR} = (k_{NR})^{-1}$. The fluorescence decay curves appear to contain more than one component of fluorescence lifetime, for example, if there are two time-resolved fluorescence profiles were tested for a concentrated sample solution, one profile is fast (denoted as f) and the other component is slow (denoted as s), the PL intensity can be expressed as $I(t) = a_s \exp(-t/\tau s) + a_f \exp(-t/\tau_f)$.[33]

Time-resolved PL studies which reveal the exciton decay for nano-particle **1b**, **2b**, and **3b** have been conducted in THF solution, as shown in Figure 2.11. The time resolved PL spectrum can be well fitted using a single exponential function, $I = I_0\exp(-t/\tau)$, suggesting that the recombination is dominated by single-process exciton recombination, reflecting no obvious nonradiative decay channels. The exciton decay time (τ) is 840 ps for **1b**, 940 ps for **2b** and 1000 ps for **3b,** as shown in Figure 2.11. We still remember excitons are located on each arm of conjugated chains, as discussed previously. The increase of decay time with molecular size, together with the increase of emission wavelength, indicates the presence of quantum confinement effects. Normally in a quantum confined system, the excitons are localized in an area which is smaller than the Bohr radii, and when the size of localization

increases, a red shift of emission wavelength and longer decay time typically occurs.[22] If there are aggregation or inter molecular interactions occurred, the PL decay curves will contain more than one components so the PL intensity will be described as, e.g. $I(t) = a_s \exp(-t/\tau s) + a_f \exp(-t/\tau_f)$.

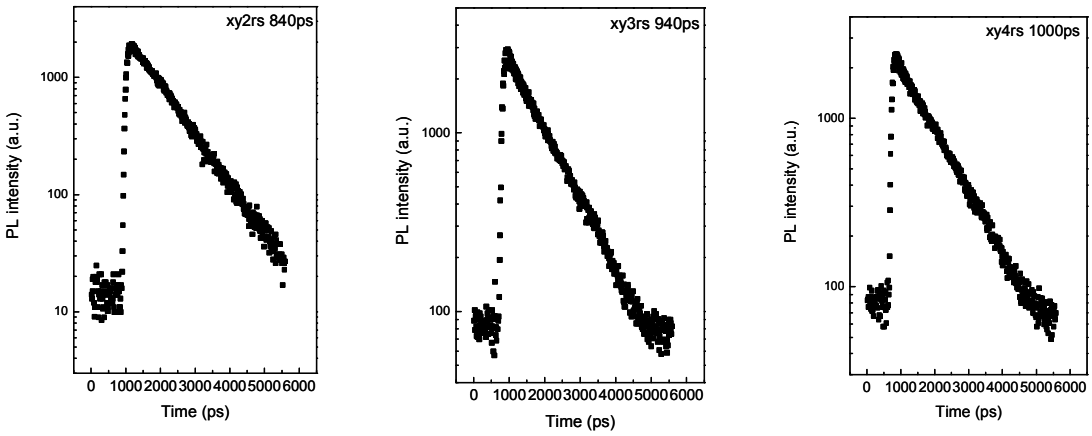

Figure 2.11. Time-resolved PL study of 1b (xy2rs 840ps), 2b (xy3rs 940ps), and 3b (xy4rs 1000ps) in THF solution.

2.5 Conclusion

A series of nano-hybrid light emitting dots with diameter range from 2nm to 4nm were synthesized through grafting organic conjugated chains directly onto an inorganic rigid cage polyhedral oligomeric silsesquioxanes (POSS). The effect of chain length, side groups, polarity of solvents on the property of light emitting dots were studied using FTIR, XRD, DSC, UV, PL, AFM and SEM. The unique structure of these nano-hybrid dots renders them with excellent PL properties which are much different from bulk organic molecules or conjugated polymers. Furthermore, the incorporation of POSS greatly improve the processibility of oligo- conjugated chains by transforming them from a crystalline materials to a non-crystalline solid with molecular weight of a few thousands and soluble in most of

conventional organic solvents. The PLQE (PL quantum efficiency) of the oligo-conjugated arms in condensed state increases significantly after grafting onto POSS. The light emitting dots are very sensitive to the polarity of organic solvents due to their nano-scaled size. PL spectrum of the nano-hybrid dots in solid film was blue shift from that in most of organic solvents. POSS as a spacer could separate the organic chains from overlapping while the outer layer of alkyl and alkoxy chains grafted on organic chains reduced the inter-molecular interaction. This unique structure improves PLQE of the light emitting materials significantly either in solution or in condensed states. This opens a new approach to achieve novel light emitting materials with uniform nano-scaled size and much improved properties such as thermal stability, PLQE, processibility, absorption and emission, etc.

2.6 References

1. Huynh, W. U., Dittmer, J. J., & Alivisatos, A. P. (2002). Hybrid nanorod-polymer solar cells. *Science,* 295, 2425-2427.
2. Gur, I., Fromer, N. A., Geier, M. L., & Alivisatos, A. P. (2005). Air-stable all-inorganic nanocrystal solar cells processed from solution. *Science,* 310, 462-465.
3. Steckel, J. S., Snee, P., Coe-Sullivan, S., Zimmer, J. R., Halpert, J. E., Anikeeva, P., Kim, L. A., Bulovic, V., & Bawendi, M. G., (2006). Color-saturated green-emitting QD-LEDs. *Angewandte Chemie-International Edition,* 45, 5796-5799.
4. Yang, W. J., Trau, D., Renneberg, R., Yu, N. T., & Caruso, F. (2001). Layer-by-layer construction of novel biofunctional fluorescent microparticles for immunoassay applications. *Journal of Colloid and Interface Science,* 234, 356-362.

5. Chan, C. P.-Y., Bruemmel, Y., Seydack, M., Sin, K.-K., Wong, L.-W., Merisko-Liversidge, E., Trau, D., & Renneberg, R. (2004). Nanocrystal biolabels with releasable fluorophores for immunoassays. *Analytical Chemistry,* 76, 3638-3645.
6. Bruemmel, Y., Chan, C. P.-Y., Renneberg, R., Thuenemann, A., & Seydack, M., (2004). On the influence of different surfaces in nano- and submicrometer particle based fluorescence immunoassays. *Langmuir,* 20, 9371-9379.
7. Jeon, J., Lim, D. K., & Nam, J. M. (2009). Functional nanomaterial-based amplified bio-detection strategies. *Journal of Materials Chemistry*, 19, 2099-2117.
8. Yan, M., Rothberg, L. J., Papadimitrakopoulos, F., Galvin, M. E., & Miller, T. M. (1994). Defect quenching of conjugated polymer luminescence. *Physical Review Letters*, 73, 744-747.
9. Samuel, I. D. W., Rumbles, G., & Collison, C. J. (1995). Efficient interchain photoluminescence in a high-electron-affinity conjugated polymer. *Physical Review B,* 52, 11573-11576.
10. Sariciftci, N. S., Smilowitz, L., Heeger, A. J., & Wudl, F. (1992). Photoinduced electron-transfer from a conducting polymer to buckminsterfullerene. *Science,* 258, 1474-1476.
11. Son, S., Dodabalapur, A., Lovinger, A. J., & Galvin, M. E. (1995). Luminescence enhancement by the introduction of disorder into poly(p-phenylene vinylene). *Science*, 269, 376-378.
12. Yan, M., Rothberg, L. J., Kwock, E. W., & Miller, T. M. (1995). Interchain excitations in conjugated polymers. *Physical Review Letters,* 75, 1992-1995.

13. Bellete^te, M., Bouchard, J., Leclerc, M., & Durocher, G. (2005). Photophysics and solvent-induced aggregation of 2,7-carbazole-based conjugated polymers. *Macromolecules,* 38, 880-887.
14. Xiao, S., Nguyen, M., Gong, X., Cao, Y., Wu, H. B., Moses, D., & Heeger, A. J. (2003). Stabilization of semiconducting polymers with silsesquioxane. *Advanced Functional Materials,* 13, 25-29.
15. Lee, J., Cho, H. J., Jung, B. J., Cho, N. S., & Shim, H. K. (2004). Stabilized blue luminescent polyfluorenes: Introducing polyhedral oligomeric silsesquioxane. *Macromolecules,* 37, 8523-8529.
16. Chou, C. H., Hsu, S. L., Dinakaran, K., Chiu, M. Y., & Wei, K. H., (2005). Synthesis and characterization of luminescent polyfluorenes incorporating side-chain-tethered polyhedral oligomeric silsesquioxane units *Macromolecules 38*, 745-751.
17. Chou, C. H., Hsu, S. L., Yeh, S. W., Wang, H. S., & Wei, K. H. (2005). Enhanced luminance and thermal properties of poly(phenylenevinylene) copolymer presenting side-chain-tethered silsesquioxane units. *Macromolecules* 38, 9117-9123.
18. Kang, J. M., Cho, H. J., Lee, J., Lee, J. I., Lee, S. K., Cho, N. S., Hwang, D. H., & Shim, H. K., (2006). Highly bright and efficient electroluminescence of new PPV derivatives containing polyhedral oligomeric silsesquioxanes (POSSs) and their blends. *Macromolecules* 39, 4999-5008.
19. Lee, J., Cho, H. J., Cho, N. S., Hwang, D. H., Kang, J. M., Lim, E., Lee, J. I., & Shim, H. K. Enhanced efficiency of polyfluorene derivatives: Organic-inorganic hybrid polymer light-emitting diodes. *Journal of Polymer Science Part A-Polymer Chemistry*, 44, 2943-2954.

20. Cho, H. J., Hwang, D. H., Lee, J. I., Jung, Y. K., Park, J. H., Lee, J., Lee, S. K., and Shim, H. K., (2006). *Chem. Mater*. 18, 3780.
21. Lin, W. J., Chen, W. C., Wu, W. C., Niu, Y. H., & Jen, A. K. Y. (2004). Synthesis and optoelectronic properties of starlike polyfluorenes with a silsesquioxane core. *Macromolecules 37*, 2335-2341.
22. Yoffe, A. D., (2002). Low-dimensional systems: quantum size effects and electronic properties of semiconductor microcrystallites (zero-dimensional systems) and some quasi-two-dimensional systems. *Advances in Physics*, 51, 799-890.
23. He, C. B., Xiao, Y., Huang, J. C., Lin, T. T., Mya, K. Y., & Zhang, X. H. (2004). Highly efficient luminescent organic clusters with quantum dot-like properties. *Journal of the American Chemical Society*, 126, 7792-7793.
24. Joshi, H. S., Jamshidi, R., & Tor, Y. (1999). Conjugated 1,10-phenanthrolines as tunable fluorophores. *Angewandte Chemie-International Edition*, 38, 2722-2725.
25. Tonzola, C. J., Alam, M. M., Bean, B. A., & Jenekhe, S. A. (2004). New soluble n-type conjugated polymers for use as electron transport materials in light-emitting diodes. *Macromolecules*, 37, 3554-3563.
26. Ding, L. M., Egbe, D. A. M., & Karasz, F. E. (2004). Photophysical and optoelectronic properties of green-emitting alkoxy-substituted PE/PV hybrid conjugated polymers. *Macromolecules*, 37, 6124-6131.
27. Reichardt, C. (1994). Solvatochromic dyes as solvent polarity indicators. *Chemical Reviews,* 94, 2319-2358.

28. Yamaguchi, Y., Matsubara, Y., Ochi, T., Wakamiya, T., Yoshida, Z. I. (2008). How the pi conjugation length affects the fluorescence emission efficiency. *Journal of The American Chemical Society*, 130, 13867-13869.

29. Onoda, M., & Tada, K. (2002). A consideration of thermochromic behavior in poly (p-phenylene vinylene) derivatives. *Thin Solid Films,* 438, 187-194.

30. Egbe, D. A. M., Roll, C. P., Birckner, E., Grummt, U. W., Stockmann, R., & Klemm, E. (2002). Side chain effects in hybrid PPV/PPE polymers. *Macromolecules*, 35, 3825-3837.

31. Lin, T. T., He, C. B., & Xiao, Y. (2003). Theoretical studies of monosubstituted and higher phenyl-substituted octahydrosilsesquioxanes. *Journal Of Physical Chemistry B,* 107, 13788-13792.

32. Xiao, Y., Tripathy, S., Lin, T. T., & He, C. B. (2006). Absorption and Raman study for POSS-oligophenylene nanohybrid molecules. *Journal of Nanoscience and Nanotechnology*, 6, 3882-3887.

33.Das, B. B., Liu, F., & Alfano, R. R. (1997). Time-resolved fluorescence and photon migration studies in biomedical and model random media. *Reports on Progress in Physics,* 60, 227-292.

Chapter Three

Quantum confined light emitting dots

3.1. Introduction

It has been demonstrated in chapter 2 and other studies that incorporation of a bulky polyhedral oligomeric silsesquioxane (POSS) into conjugated chains could greatly improve the performance of light emitting materials by reducing aggregations.[1-9] The brightness and quantum efficiency as well as thermal stability of linear conjugated materials could be greatly improved by incorporating POSS cage either onto chain end or as core to form star-like oligomers or polymers. Furthermore, POSS as a cage-like cubic structure provides an excellent building block for developing novel nano-particles. The synthesis of fully functionalized POSS via attaching identical groups onto eight vertexes of the cage has attracted much attention recently.[10-12]

Nano-particles with diameter in a range of 2-4 nm are very useful for application in bio-detection and bio-imaging. The light emitting dots investigated in Chapter 2 mainly emit blue light. In Chapter 3, green light emitting dot based on POSS-oligo-thiophene will be synthesized and investigated. Furthermore, water soluble green light emitting dots will be prepared. The characteristic of the light emitting dots will be investigated in detail and time-resolved PL study will be conducted to gain better understanding of the exciton decay time of the light emitting dot in dilute solution, condensed state, or blended with other polymers. The exciton recombination mechanism and the confinement effect due to the small size of the dots and the unique structure of the molecules will be investigated.

In synthesis of POSS light emitting dots, octa(bromophenyl) silsesquioxane (OBPS) is one of the representative key starting materials. The precise control of the number and the position of the bromination on such nanometer-sized molecules present however, substantial challenge for macromolecules like POSS[1,2,13,14] and fullerene.[15] OBPS reported in literatures so far is a mixture of *ortho*-(*o*), *meta*-(*m*), and *para*-(*p*) substituted compounds. As a result, the conjugated oligomers are randomly grafted onto *meta*- and *para*-positions of the phenyl rings in the octophenyl-POSS.

A question may arise as how such random grafting of light emitting oligomers could affect the characteristics of light emitting dot? In order to address this issue, a highly regioselective bromination of octaphenyl-POSS is required. In this chapter, the bromination of octaphenyl-POSS will be optimized to synthesize meta-bromo- octaphenyl-POSS. POSS light emitting dot based on this structure will be synthesized and compared with that without a highly regioselective bromination of octaphenyl-POSS.

3.2. Experimental section

3.2.1. Materials

2-ethylhexyl bromide (95%), magnesium turnings (99.9+%), tetrakis(triphenylphosphine)-palladium(0) $Pd(PPh_3)_4$ (99%), anhydrous zinc chlorid ($ZnCl_2$) (98+%), iodine chips (I_2) (99+%), octaphenylsilsesquioxane (OPS) were purchased from Aldrich Chemical Co. and were used as received. Acetic acid glacial (J. T. Baker), ether anhydrous (J. T. Baker), ethyl acetate (TEDIA), dichloromethane (TEDIA) were used as received. Tetrahydrofuran (THF) (99.8%, TEDIA) was distilled from sodium/benzophenone.

3.2.2. Characterization

^{1}H, ^{13}C, ^{29}Si nuclear magnetic resonance (NMR) data were obtained by Bruker Avance 400 spectrometer with chloroform-*d* as the solvent. Matrix-assisted laser desorption/ionization time-of-flight (MALDI-TOF) mass spectra were obtained on a Bruker Autoflex TOF/TOF instrument using dithranol as a matrix and silver trifluoroacetate as an ionizing salt. Elemental micro-analysis was carried out by the Microanalysis Laboratory of the National University of Singapore. XRD was recorded on a Bruker GADDS under a voltage of 40 kV and a current of 40 mA using CuK_α radiation (λ = 0.15nm). Gel permeation chromatography (GPC) analysis was carried out with a Shimadzu SCL-10A and LC-8A system equipped with two Phenogel 5μ 50 and 1000Å columns in series and a refractive detector, using THF as a eluent at a flow rate of 0.3ml/min at 40ºC. Monodispersed poly(ethylene glycol) were used as standards. UV-Vis spectra were recorded on a Shimadzu 3101 spectrophotometer. Fluorescence (PL) measurement was carried out on a Perkin-Elmer LS 50B luminescence spectrometer with a xenon lamp as a light source. The concentration of polymers for UV and PL analysis is less than 1 x 10^{-3} g/ml. The relative photoluminescence quantum efficiency (PLQE) of the materials in film form were recorded by using 9,10-diphenylanthracene dispersed in PMMA film at a concentration lower than 1 x 10^{-3} M as the standard and assuming that the PLQE of the standard is 83%. The polymer thin films were cast on a quartz plate using a spin coater and all of thin films are uniform and transparent. The morphology of *m*-OBPS was examined by field emission scanning electron microscopy (SEM) (JEOL JMS 6700, JAPAN). TEM sections were collected in a Philips CM300 – FEG operating at an accelerating voltage of 200 kV on carbon coated Copper grids. The time-resolved PL measurements were conducted with the excitation of the frequency doubled output of a Ti:sapphire femosecond laser (Sunami, Spectra Physics). The pulses were

centered at 400 nm with pulse duration of 100 fs and pulse repetition rate of 82 MHz. The time evolution of the luminescence was recorded using a streak scope (Hamamatsu, C4334) with the time resolution of 15 ps. The samples were kept in vacuum and the experiments were conducted at room temperature. Power of excitation is 12 W/ cm^2.

3.2.3. Synthesis

Z1 I0

To a 150ml two-net RBF, OPS (2.58g, phenyl 20mmol) and CH_2Cl_2 (50ml) were added under stirring. Five minutes later Bromine (1ml, 20mmol) was added into the suspension. Then anhydrous $ZnCl_2$ (0.30g) was added under stirring. The reaction mixture was stirred at room temperature. The reaction was monitored by NMR spectrum study. Br_2 (0.5ml) was added to the reaction system if there is no change in NMR spectrum after 24-hour stirring. After 10 days stirring, there was no sign of reaction. Then stop stirring, Na_2CO_3 (50ml, 2M) was added to absorb remaining Br_2. Work up the organic phase, remove the solvent to obtain white crude powder product. The product was used to characterization directly. ^{1}H NMR: 7.78 (d, 2H), 7.45(t, 1H), δ 7.38 (d, 2H). ^{13}C NMR: δ 134.3, 131.1, 128.4. ^{29}Si NMR: δ -78.6. This compound is proved to be OPS, starting material.

Z2 I0

The similar procedure of synthesis of **Z1 I0** was followed except using $ZnCl_2$ (1.0g). The crude product was used to characterization directly. ^{1}H NMR: δ 8.0 – 6.5 (broad) ^{13}C NMR: δ 136.4, 136.2, 131.2, 127.4, 124.9, 124.8. ^{29}Si NMR: δ -78.6, -81.7.

Z3 I0

The similar procedure of synthesis of **Z1 I0** was followed except using $ZnCl_2$ (1.5g). The crude product was used to characterization directly. ^{1}H NMR: δ 7.78 (m), 7.65(m), 7.45(m), 7.38 (m). ^{13}C NMR: δ 137.1, 135.8, 134.4, 132.7, 131.7, 130.2, 129.3, 126.6, 123.3. ^{29}Si NMR: δ -78.7, -81.7.

Z0 I1

The similar procedure of synthesis of **Z1 I0** was followed except using I_2 (0.05g). The crude product was used to characterization directly. ^{1}H NMR: δ 7.78 (m), 7.65(m), 7.45(m), 7.38 (m). ^{13}C NMR: δ 138.2, 134.3, 133.3, 131.2, 129.1, 128.1, 127.0, 125.7. ^{29}Si NMR: δ -78.6, -80.2, -81.7, -83.2.

Z1 I1 (*m*-OBPS)

To a 150ml two-net RBF, 2.58g OPS (phenyl 20mmol) and CH_2Cl_2 (50ml) were added under stirring. Five minutes later Bromine (1ml, 20mmol) was added into the suspension. Then anhydrous $ZnCl_2$ (0.30g) and I_2 (0.05g) was added respectively under stirring. The reaction mixture was stirred at room temperature. The reaction was monitored by NMR spectrum study. Br_2 (0.5ml) was added to the reaction system if there is no change in NMR spectrum. Upon reaction completion, stop stirring, Na_2CO_3 (50ml, 2M) was added to absorb remaining Br_2. Work out the organic phase, remove the solvent to obtain white crude powder product. The white powder is subjected for two times self-assembling in ethyl acetate. The final yield is 50%. ^{1}H NMR: δ 7.84 (m, 2H), 7.59(d, 1H), 7.33(m, 1H). ^{13}C NMR: δ 138.1,

136.6, 132.9, 131.5, 129.4, 126.7. ^{29}Si NMR: δ -81.8. MALDI-TOF: m/z (Ag+ adduct) 1772.06. GPC Mn: 1141, Mw: 1143, PDI: 1.00. XRD size: 1.05nm. Calculate (%) C, 34.61, H, 1.92; Found (%) C, 34.42, H, 2.03.

Z2 I1

The similar procedure of synthesis of **Z1 I1** was followed except using $ZnCl_2$ (1.00g) and I_2 (0.05g). The crude product was used to characterization directly. ^{1}H NMR: δ 7.88(m), 7.64(m), 7.46(m), 7.42 (m). ^{13}C NMR: δ 138.0, 134.3, 133.8, 133.6, 133.2, 129.1, 127.0, 125.5. ^{29}Si NMR: δ -78.5, -80.2, -81.7.

Z3 I1

The similar procedure of synthesis of **Z1 I1** was followed except using $ZnCl_2$ (1.50g) and I_2 (0.05g). The crude product was used to characterization directly. ^{1}H NMR: δ 7.78(m), 7.63(m), 7.45(m), 7.42(m). ^{13}C NMR: δ 138.2, 134.8, 134.0, 133.3, 133.8, 130.1, 127.2, 125.6. ^{29}Si NMR: δ -78.5, -80.2, -81.7, -83.2.

ZO I2

The similar procedure of synthesis of **Z1 I1** was followed except using $ZnCl_2$ (0.30g) and I_2 (0.30g). The crude product was used to characterization directly. ^{1}H NMR: δ 7.78 (m), 7.65(m), 7.45(m), 7.38 (m). ^{13}C NMR: δ 138.3, 134.4, 133.4, 131.1, 129.1, 128.1, 127.0, 125.8. ^{29}Si NMR: δ -78.6, -80.2, -81.7, -83.2.

Z1 I2

The similar procedure of synthesis of **Z1 I1** was followed except using $ZnCl_2$ (0.30g) and I_2 (0.30g). The crude product was used to characterization directly. ^{1}H NMR: δ 7.78 (m), 7.65(m), 7.45(m), 7.38 (m). ^{13}C NMR: δ 138.0, 134.1, 133.1, 131.2, 129.2, 128.1, 127.0, 125.4. ^{29}Si NMR: δ -78.6, -80.2, -81.7, -83.2.

Z2 I2

The similar procedure of synthesis of **Z1 I1** was followed except using $ZnCl_2$ (1.00g) and I_2 (0.30g). The crude product was used to characterization directly. ^{1}H NMR: δ 7.78 (m), 7.65(m), 7.45(m), 7.38 (m). ^{13}C NMR: δ 138.2, 134.3, 133.3, 131.1, 129.1, 128.1, 127.0, 125.7. ^{29}Si NMR: δ -78.6, -80.2, -81.7, -83.2.

Z3 I2

The similar procedure of synthesis of **Z1 I1** was followed except using $ZnCl_2$ (1.50g) and I_2 (0.30g). The crude product was used to characterization directly. ^{1}H NMR: δ 7.78 (m), 7.65(m), 7.45(m), 7.38 (m). ^{13}C NMR: δ 138.1, 134.5, 133.5, 131.5, 129.7, 128.0, 127.4, 125.4. ^{29}Si NMR: δ -78.4, -80.6, -81.9, -83.4.

ZO I3

The similar procedure of synthesis of **Z1 I1** was followed except using $ZnCl_2$ (0.00g) and I_2 (0.60g). The crude product was used to characterization directly. ^{1}H NMR: δ 7.78 (m), 7.65(m), 7.45(m), 7.38 (m). ^{13}C NMR: δ 138.3, 134.4, 133.4, 131.1, 129.1, 128.1, 127.0, 125.8. ^{29}Si NMR: δ -78.6, -80.2, -81.7, -83.2.

Z1 I3

The similar procedure of synthesis of **Z1 I1** was followed except using $ZnCl_2$ (0.30g) and I_2 (0.60g). The crude product was used to characterization directly. ^{1}H NMR: δ 7.78 (m), 7.65(m), 7.45(m), 7.38 (m). ^{13}C NMR: δ 139.0, 134.6, 133.4, 131.2, 129.2, 128.6, 127.2, 125.9. ^{29}Si NMR: δ -78.6, -80.2, -81.7, -83.2.

Z2 I3

The similar procedure of synthesis of **Z1 I1** was followed except using $ZnCl_2$ (1.00g) and I_2 (0.60g). The crude product was used to characterization directly. ^{1}H NMR: δ δ 7.78 (m),

7.65(m), 7.45(m), 7.38 (m). ^{13}C NMR: δ 139.4, 134.2, 133.8, 131.5, 129.1, 128.0, 127.4, 125.5. ^{29}Si NMR: δ -78.5, -80.6, -81.9, -83.3.

Z3 I3

The similar procedure of synthesis of **Z1 I0** was followed except using $ZnCl_2$ (1.50g) and I_2 (0.60g). The crude product was used to characterization directly. ^{1}H NMR: δ δ 7.78 (m), 7.65(m), 7.45(m), 7.38 (m). ^{13}C NMR: δ 139.4, 134.1, 133.8, 131.4, 129.2, 128.1, 127.0, 125.6. . ^{29}Si NMR: δ -78.1, -80.5, -81.4, -83.6.

2,3,3'-Tri-ethylhexyl-5,5'-bithiophene

A Grignard reagent of 2-Ethylhexyl-magnesium (32mmol) made from the reaction of 2-Ethylhexyl-bromide (6.2g, 32mmol) with Mg (0.9g, 38mmol) in ether (80ml), was added dropwise into a solution of 2-bromo-3,3'-bis-ethylhexyl-5,5'-bithiophene (9.38g, 20mmol) in 20ml of ether containing $Pd(PPh_3)_4$ (0.6mmol) as catalyst at -10-0°C and raised to room temperature 4hr later. After stirring 24 hours under Argon, the reaction mixture was quenched with saturated NH_4Cl aqueous solution and extracted with ethyl acetate. The extract was washed with water twice and brine once and then dried over anhydrous MgSO4. After removal of solvent, the dark-brown liquid of mixture was obtained and subjected to purification by column chromatography on silica gel using hexane as eluant. A color-less liquid (6.2g, yield 61%) was obtained. ^{1}H NMR: δ 7. 270 (d, 1H, *J*=5.2), 6.942 (d, 1H, *J*=5.2), 6.626 (S, 1H), 2.758 (d, 2H, *J*=6.4), 2.498 (d, 2H, *J*=6.8), 2.418 (d, 2H, *J*=7.2). ^{13}C NMR: δ 144.219, 141.485, 141.340, 130.545, 129.360, 127.545, 127.142, 125.002. MALDI-TOF: m/z (Ag+ adduct) 502.156. Calculate ($C_{32}H_{54}S_2$) (%) C, 76.49, H, 10.75, S, 12.75; Found (%) C, 76.12, H, 10.42, S, 12.70.

2-Bromo-3,2',3'-tri-ethylhexyl-5,5'-bithiophene (monomer A in Scheme 2)

Bromine (1.92g, 12mmol) solution in HOAc (12ml) was added drop wise into another solution containing of 2,3,3'-tri-ethylhexyl-5,5'-bithiophene (6g, 12mmol) in HOAc (16ml) at -10°C - 0°C. Then water (30ml) and ethyl acetate (20ml) were added into this solution subsequently. The organic phase was washed with water twice and brine once and then dried over anhydrous MgSO4. After removal of solvent, the light yellowish liquid was obtained and subjected to purification by column chromatography on silica gel using hexane as eluant. A light yellowish liquid (6.62g, yield 95%) was obtained. ^{1}H NMR: δ 6.868(s, 1H), 6.559(s, 1H), 2.701 (d, 2H, *J*=6.8), 2.378 (d, 2H, *J*=7.2), 2.329 (d, 2H, *J*=7.2). ^{13}C NMR: δ 144.958, 142.415, 142.049, 132.246, 132.071, 127.560, 125.868, 112.367. MALDI-TOF: m/z (Ag+ adduct) 582.435. Calculate ($C_{32}H_{53}S_2Br$) (%) C, 66.09, H, 9.12, S, 11.01; Found (%) C, 66.06, H, 9.02, S, 10.94.

Octa[2,3,3'-ethylhexyl-5,5'-dithiophene-2'-phenyl-3'']-POSS (PDTP)

A Grignard reagent of 3,2',3'-tri-ethylhexyl-5,5'-bithiophene-2-magnesium bromide (3.2mmol) prepared from the reaction of **A (**1.7g, 3.2mmol) with Mg (0.09g, 3.8mmol) in dry THF (8ml), was added drop wise into a solution of *m*-OBPS (0.44g, 0.27mmol, 2.13mmol Br) in dry THF (4ml) containing $Pd(PPh_3)_4$ (0.06mmol) as catalyst. After refluxing for 24 hours under Argon, the reaction mixture was quenched with saturated NH_4Cl aqueous solution and extracted with ethyl acetate. The extract was washed with water two times and brine once and then dried over anhydrous MgSO4. After removal of solvent, the dark-brown liquid of mixture was subjected to purification by column chromatography on

silica gel using hexane as eluant. A light yellowish glassy solid 0.42g (yield 60%) was obtained. ^{1}H NMR: δ 7.82 - 7.23 (m, 5.6H), 2.89 – 2.36 (m, 2.4H), ^{1}H NMR indicated in average there are 5.6 chains (**B**) have been grafted onto POSS. ^{29}Si NMR: δ -78.592, -81.745. GPC Mn: 2942, Mw: 3001, PDI 1.02. XRD size: 2.0nm. Calculate $Si_8O_{20}[C_{38}H_{57}S_2]_{5.6}[C_6H_4Br]_{2.4}$ (%) C, 67.79, H, 8.18; Found (%) C, 67.70, H, 8.38.

Octa[3,3'-ethylhexyl-5,5'-dithiophene-2-phenyl]-POSS (**M**).

A Gignard regent prepared from 2-Bromo-3,3'-di-(2-ethylhexyl)-5,5'-bithiophene(4.7g, 10mmol) and Mg turning (0.29g, 12mmol)in 50ml THF was added dropwise to a solution of Octa-Bromophenyl substituted POSS[10,15](1.672g, 1mmol) and $Pd(PPh_3)_4$ in 20ml THF at room temperature, and then reflux for 24 hours. saturated NH_4Cl aqueous solution and extracted with ethyl acetate. The product was obtained after the mixture was passed through a silica gel column as a viscose liquid with yield of 55%. ^{1}H NMR δ 8.120(m, 1H), 7.618(m, 1H), 7.551(m, 1H), 7.402(m, 1H), 7.325(m, 1H), 6.964 (m, 2H), 2.444(m, 4H,), 1.538(m, 2H), 1.188(m, 16H), 0.914(m, 12H). ^{13}C NMR δ 143.8, 143.3, 142.9, 142.8, 135.3, 133.9, 131,1, 130.7, 129.4, 128.8, 127.4, 125.8, 125.8. ^{29}Si NMR δ -78.8. GPC: Mw 4200, Mn 4090. FTIR: 2938, 2917, 2850 (υ-C-H), 1452, 1374 (υ=C-H), 1108 (υ-Si-O-Si), 813 (υ=C-H)

Quaternized POSS-(phenyl-bithiophene-PDMAEMA)$_8$ (W)

General procedures is: 10mmol n-BuLi (1.6M solution in Hexane, 6.25ml) was added into a solution of **M** (4.14g, 1mmol) in dry THF 40ml at -78°C under stirring. After two hours stirring under -78°C a CO2 was flowed into the mixture from dry ice. Allow the flowing continue overnight and gradually warmed to room temperature, then the mixture was

poured into a cooled 1M HCl solution (with ice). The aqueous solution was extracted twice with Chloroform. The combined extracts were washed with water and dried over anhydrous Mg SO4. The 3,3'-di-ethylhexyl-5-carboxy-2,2'-bithiophene substituted POSS-phenyl (**M-COOH**) was obtained with yield 80% after going through a silica column from the mixture. The obtained carboxy ended **M-COOH** (3.8g ,0.85mmol) in a solution of 20ml ether was added drop wise into LiAlH4 (15mmol, 0.57g) solution of ether 70ml under refluxing and remain stirring at this temperature for four hours. The reaction mixture was added a cool 0.1M HCl 30ml (with ice), the organic phase was separated and washed by water and then remove the solvent by distillation. The hydroxyl ended **M-OH** was obtained with yield 75% after going through a silica column from the mixture. From **M-OH** to the final product is followed the procedures of Lu's work.[40] The solution of **M-OH** (0.5g, 0.117mmol) and triethylamine (4.4ml, 31mmol) in dry CH_2Cl_2 (40ml) was added drop wise by 2-bromoisobutyryl bromide (BiBB) (3.6ml, 26mmol) at 0°C under Ar atmosphere, then the mixture was stirred at room temperature over night. Work out the organic phase and pass it through a short silica column using toluene as eluent. The Microinitiator (**N**) was obtained with yield 25%. In a glass tube charged with 0.07g (0.0125mmol) of **N** and 0.01g of CuCl (0.1mmol) was sealed and degassed and filled with Ar. *o*-dichlorobenzene (1.2ml) and 1,1,4,7,10,10-hexamethyltriethylenetetramine (HMTETA) (0.0268ml, 0.1mmol) were added with syringes. The glass reactor was immersed in an oil bath at 90°C, and a clear solution with light green color formed within a few seconds. Upon dissolution, 2.21ml of 2-(dimethylamino)ethyl methacrylate (DMAEMA) (13.26mmol) was quickly injected into the tube to carry out the polymerization. Two hours later the polymer was going through a silica column to remove the catalysts and precipitated into excess of hexane and dried in a vacuum

at 40°C. The light yellow product was dissolved in 50ml dry THF, and methyl iodide (methyl iodide/DMAEMA as 2:1) was added and stirred for overnight at room temperature. The light yellow precipitate was collected and washed with THF. The sample was dried and a light yellow crystalline **W** was obtained (yield > 90%). **W** was only soluble in water. ^{1}H NMR (D_2O, ppm) 4.5(s, O-CH_2-), 3.8(s, N-CH_2-), 3.26[s, N-$(CH_3)_4$], 1.8[s, CH_2-$C(CH_3)$], 1.0(s, C-CH_3). Calculation for **W** (**M**-[$C_5H_8O_2$-$(C_9H_{18}O_2NI)_{132}$]$_8$) (according to feed ratio) Mw 320688 (M=4144). C, 36.6; H, 6.1; N, 4.6, Found, C, 35.3; H, 6.3; N, 4.7. The Light-scarrtering studies indicate hydrophilic compound **W** is a spherical molecule with uniform size of 33 nm.

3.3. Results and Discussion

3.3.1 Bromination of OBPS

The electron-withdrawing feature of POSS cage decides only *meta*-position substitution can occur. The synthesis of *m*-OBPS is shown in Scheme 3.1. We have proven that the bromination of OPS by molecular bromine at room temperature in the presence of iodine and $ZnCl_2$ in CH_2Cl_2 is an effective way for the synthesis of *m*-OBPS. The MALDI-TOF and ^{29}Si NMR spectra of the product are shown in Figure 3.1 and Figure 3.2 respectively. The calculated molecular mass for *m*-OBPS ($AgSi_8O_{12}C_{48}H_{32}Br_8$) is 1772.67, which is close to the experimental value of 1772.07. A single ^{29}Si NMR peak corresponding to *m*-OPBS appears at δ-81.78 ppm. The ^{13}C NMR (with six peaks) and ^{1}H NMR spectra (with three peaks), as shown in Figure 3.3, confirm that the bromination is at *meta* position because *para* substitution would lead to two double peaks on proton spectrum and four peaks on ^{13}C spectrum. The proton spectrum displayed a broad multiplet peak at δ 7.5 corresponding to chemical shift of α proton due to the electron withdrawing feature of POSS cage. The

integration ratio of α proton over β looks smaller than expected in proton spectrum possibly due to the POSS cage blocking effect.

Scheme 3.1. Synthesis of *m*-OBPS

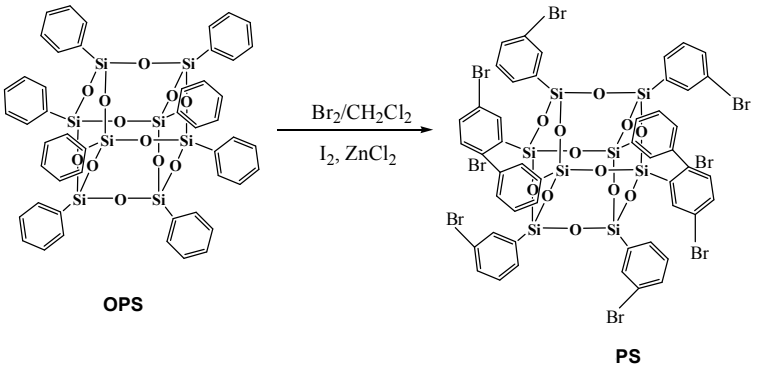

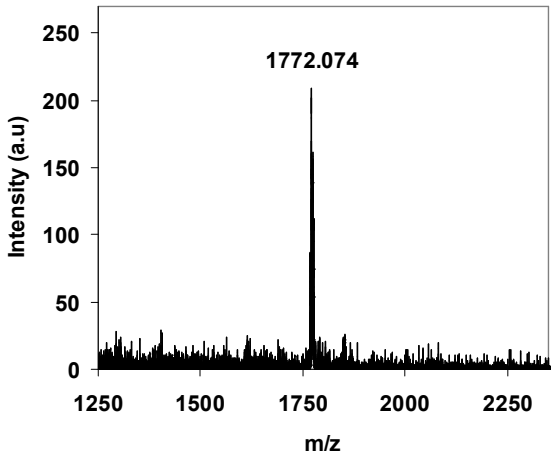

Figure 3.1. MALDI-TOF of *m*-OBPS with matrix and Ag+.

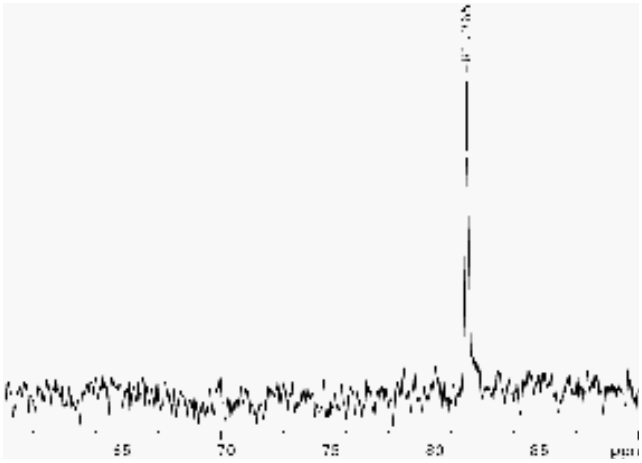

Figure 3.2. ^{29}Si NMR spectrum of *m*-OBPS.

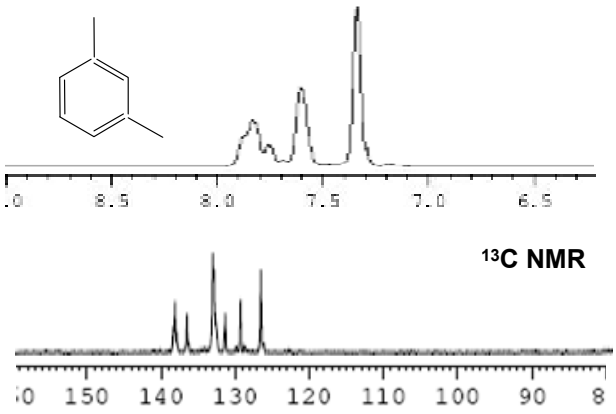

Figure 3.3. ^{1}HNMR (top) and ^{13}C NMR (bottom) spectra of *m*-OBPS.

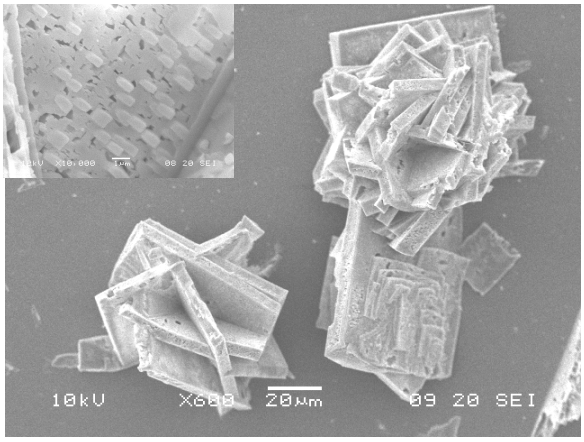

Figure 3.4. SEM image of *m*-OBPS. (inset is an enlarged image of single plate of crystal-like aggregate).

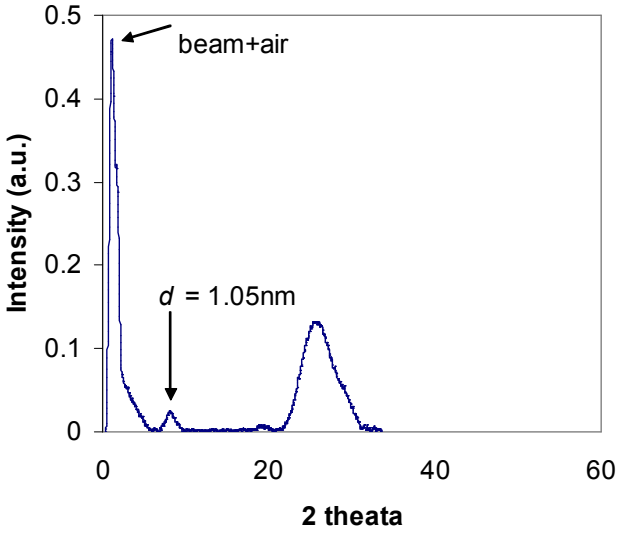

Figure 3.5: XRD pattern of *m*-OBPS. The sharp peak (2θ<5°) is caused by the instrument. The broad peak at 25° is caused by glass tube which was used as sample holder, the blank glass tube show same peak.

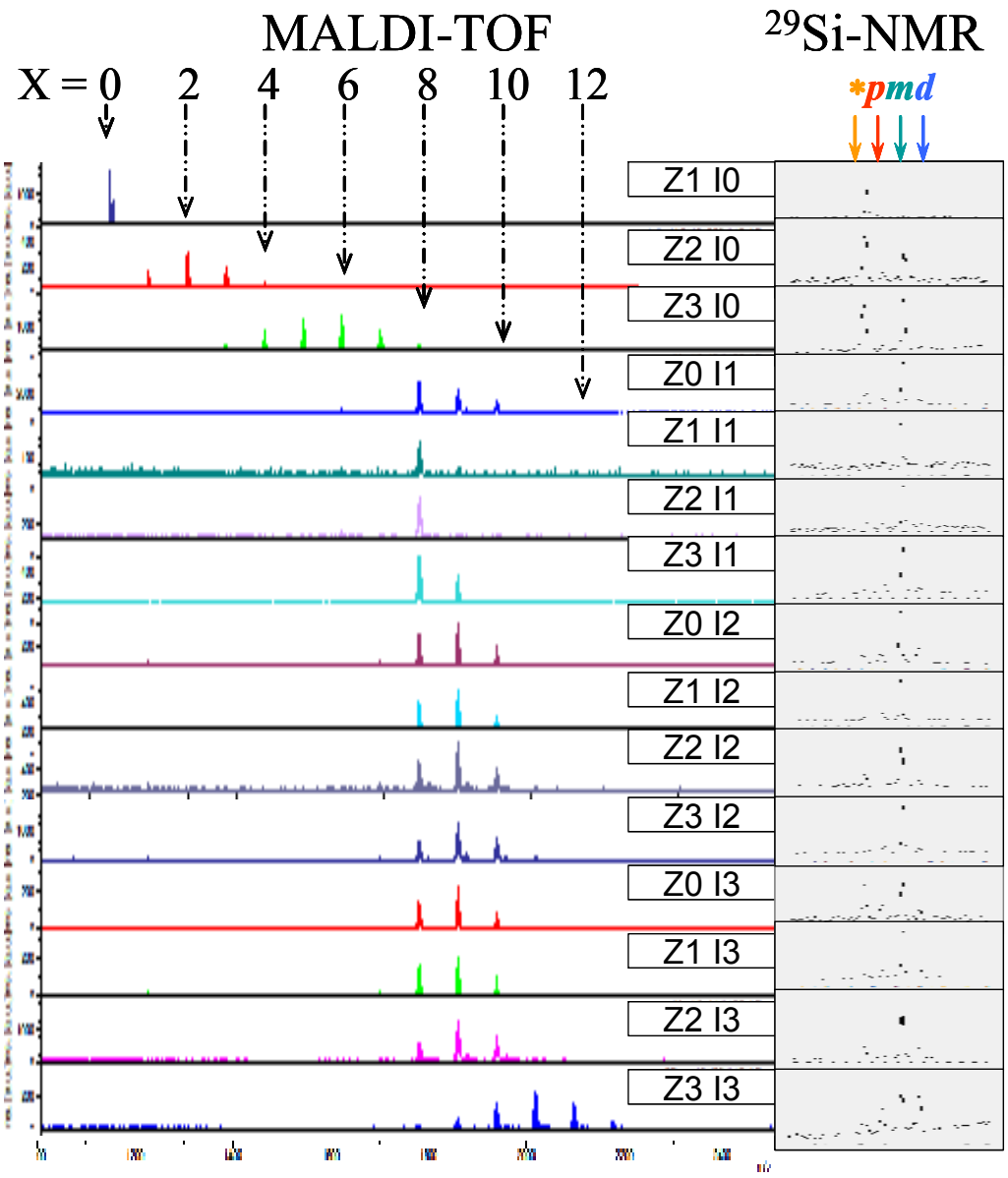

Figure 3.6. (left) MALDI-TOF and (right) ^{29}Si NMR of OPS-Brx. Z and I represents the amount of $ZnCl_2$ and I_2. The amount of OPS (2.58g, 20 mmol phenyl on OPS), Br_2 (1ml), and solvent CH_2Cl_2 (50ml) are fixed. The amount of $ZnCl_2$ is denoted as Z0 (0g), Z1 (2.20mmol), Z2 (7.35mmol), Z3 (11.03mmol). The amount of I_2 is I0 (0g), I1 (0.20mmol), I2 (1.18mmol), I3 (2.36mmol). ^{29}Si NMR,*, *p*, *m*, *d* represents *non*, *para*-, *meta*-, and *di*-bromo-substitution.

The SEM image, as shown in Figure 3.4, is interesting to see that *m*-OPBS can form crystal-like aggregate, which implies that the packing structure of the material is somewhat regular. However, in the wide-angle x-ray diffraction (WAXD) pattern of *m*-OBPS there is only one peak with d-spacing of 1.05 nm, which corresponds to its calculated molecular size, as shown in Figure 3.5.

Table 3.1. Different ratio of ZnCl2 and Iodine

(g) (mmol)	$ZnCl_2$ (0.00g) (0.00mmol)	$ZnCl_2$ (0.30g) (2.20mmol)	$ZnCl_2$ (1.00g) (7.35mmol)	$ZnCl_2$ (1.50g) (11.03mmol)
I_2 (0.00g) (0.00mmol)	**Z0 I0**[a]	**Z1 I0**	**Z2 I0**	**Z3 I0**
I_2 (0.05g) (0.20mmol)	**Z0 I1**	**Z1 I1**	**Z2 I1**	**Z3 I1**
I_2 (0.30g) (1.18mmol)	**Z0 I2**	**Z1 I2**	**Z2 I2**	**Z3 I2**
I_2 (0.60g) (2.36mmol)	**Z0 I3**	**Z1 I3**	**Z2 I3**	**Z3 I3**

[a] the reaction has not started yet.

To obtain *m*-OPBS, the amounts of I_2 and $ZnCl_2$ have to be carefully controlled. The optimal feed molar ratio of phenyl : I_2 : $ZnCl_2$ was found to be 100 : 1 : 10. To demonstrate the influences of the catalysts on the substitution, the MALDI-TOF and ^{29}Si NMR spectra of the products obtained under different bromination conditions are shown in Table 3.1 and Figure 3.6. At the top of the MALDI-TOF spectra in Figure 3.6, X indicates the number of the bromo group on an OBPS molecule. In the ^{29}Si NMR spectra, there are four peaks at δ -

78.0, -81.0, -81.8 and -83.6 ppm corresponding to *non*-substitution, *p*-bromo- substitution, *m*-bromo-substitution and *di*-bromo-substitution, respectively. The amount of I_2 and $ZnCl_2$ for 20 mmol phenyl (on OPS) varied across four scales respectively, which are denoted as I0 (0g), I1 (0.20mmol), I2 (1.18mmol), I3 (2.36mmol) for I_2 and Z0 (0g), Z1 (2.20mmol), Z2 (7.35mmol), Z3 (11.03mmol) for $ZnCl_2$, as shown in Table 1. By increasing $ZnCl_2$ concentration without adding any I_2, i.e. from Z1 I0 to Z3 I0, the distribution of molecular weight is broadened but the regioselectivity remains high. ^{29}Si NMR indicates that almost only *meta* substitution occurred. On the other hand, the position of the substituents became random when a relatively high amount of iodine was introduced into the reaction. For example, the products for Z3 I0 and Z3 I3 are fairly different. The former is a mixture of *non*-substituted and *meta*-substituted products while the latter has a full range of products with *non*-, *m*-, *p*-, and *di*-substitution. In short, using zinc chloride as the catalyst, at current level, without the addition of iodine, only *meta*-substituted bromination was observed. However, when sufficient amount of iodine was introduced, products with both *meta* and *para* substitution were obtained. Moreover, *di*-bromo substitution was also obtained at high iodine concentration. It seems that zinc chloride controls the substitution position while iodine accelerates the reaction and reduces the regioselectity. It is also interesting to note that at low level of zinc chloride without iodine, e.g. Z1 I0, no bromination occured. On the other hand, only using iodine as the catalyst, e.g. from Z0 I1 to Z0 I3, bromination gave fully substituted products with low regioselectivity. Another thing needs to be noted is that when a big amount (far more than Z3) of zinc chloride was used, even without iodine, the full substituted products will be obtained.

The bromination of electron-deficient aromatic compounds in the presence of combined iodine and zinc chloride catalyst has not been reported. It's common to accelerate a halogenation reaction by adding halogen carriers such as iodine, iron, zinc, aluminum, or the anhydrous halides of these metals, or pyridine. The order of catalytic activity of halogen carriers for the bromination of acetanilide is IBr > ZnCl2 > FeCl3.[18] The electrophilic substitution of aromatic compounds, including bromination, is well known having a two-step mechanism.[19] The role of the catalyst, as believed, is to polarize the bromine molecule and to remove Br^- in the rate-determining step.[20] Iodine is more favourable than $ZnCl_2$ in the second step of removing Br^- as IBr^-. This explains why adding I_2 could accelerate the whole bromiantion process of OPS. For electrophilic aromatic substitution, in exothermic fast reaction with low position selectivity the transition state of highest energy is of a π-complex nature,[21] while in the slow reaction with high position selectivity the transition state of highest energy is of a σ-complex nature.[22] In our experiment, it is reasonable to assume that $ZnCl_2$ involves an σ-complex with high position selectivity as the transition state. In contrast to $ZnCl_2$, it seems that I_2 involves a π-complex as the transition state because in I_2 rich system the bromination of OPS is faster and with lower position selectivity than the reaction which only uses $ZnCl_2$ as catalyst.

3.3.2. Synthesis and morphology of Light Emitting Dot

Scheme 3.2. Synthesis route for PDTP

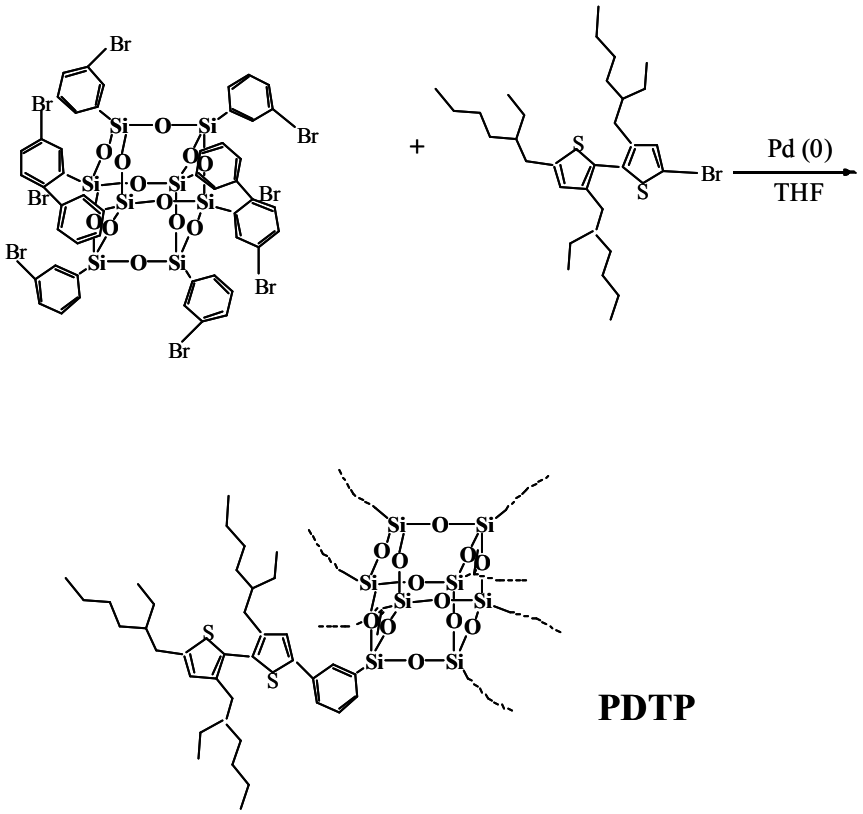

After the successful synthesis of *m*-OBPS, 2,3,3'-tri[ethylhexyl]-5,5'-dithiophene was attached onto *m*-OBPS via Grignard coupling to obtain a hybrid molecule, PDTP, with well-defined structure as shown in Scheme 3.2. The light emitting dot has a three layer structure. The core is the octa-phenyl silsesquioxane. The middle layer is the light emitting layer and the outer-layer consists of alkyl chains which are designed for preventing inter-molecular aggregation. In the WAXD pattern of PDTP as shown in Figure 3.7, one scattering peak with *d*-spacing of 2.1 nm, which is similar to the calculated molecular size, and an amorphous halo at 22° are observed, which indicates that PDTP is an amorphous material. Figure 3.8 displays TEM image of PDTP which indicates the spherical molecules with size around 3nm.

The molecular size of **PTDP** taken from TEM is only a rough estimation due to the poor contrast of the image. Ten particles were measured to derive the value, and this coincides with the XRD result. The molecular size taken from TEM picture (~3 nm) is larger than that measured using XRD (2.04 nm) in this work. There are two possible reasons for the discrepancy. Firstly, the sample preparation methods are different. The sample for XRD analysis is a chunk of bulk material, in which molecules could be closely packed. The end-capped alkyl/alkoxy chains from different molecules may form interdigitated structure so that the average inter-molecular distant are shorter than the size of an individual molecule. The molecular size taken from TEM may corresponds to the size of an individual molecule because the sample for TEM technique was obtained by dropping very dilute suspension of sample in alcohol (under ultra-sonication) on copper grid. In addition, the X-ray diffraction peak corresponding to the molecular size is broad (the higher end of *d*-spacing is about 3.2 nm), which implies there is a distribution of inter-molecular distance caused by in-perfect packing of molecules.

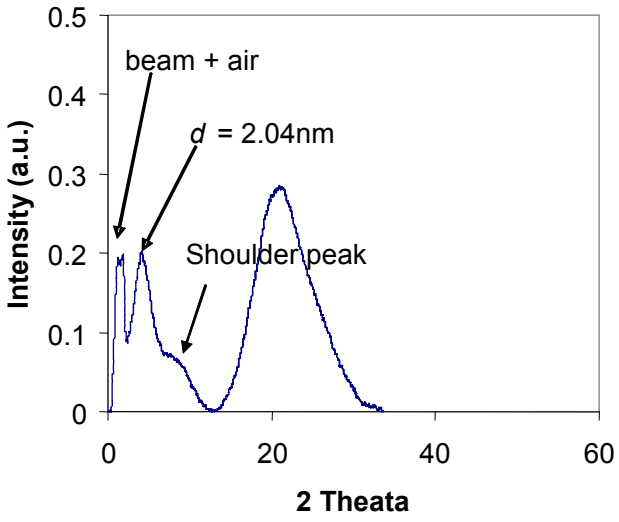

Figure 3.7. XRD pattern of PDTP. The sharp peak (2θ<5°) is caused by the instrument. The shoulder peak is because in average there are only 5.6 chains have been grafted onto POSS cage hence the size of incompletely grafted molecule of PDTP is slightly smaller compare to those eight-arm grafted molecules. The broad peak at 22° is caused by amorphous halo from sample which is a piece of free standing bulk solid without any glass tube holder.

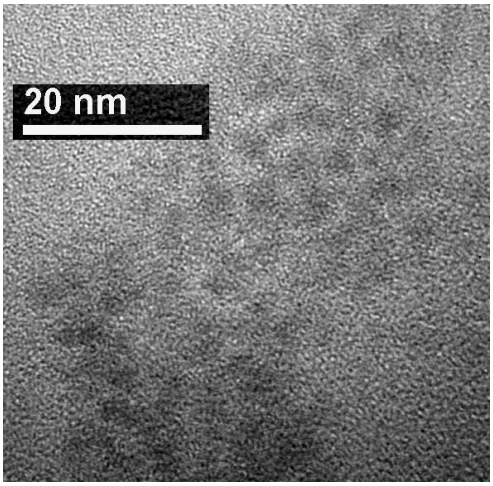

Figure 3.8. TEM image of PDTP. The molecular size from TEM is estimated as 3nm.

3.3.3. Optical Property of Light Emitting Dot

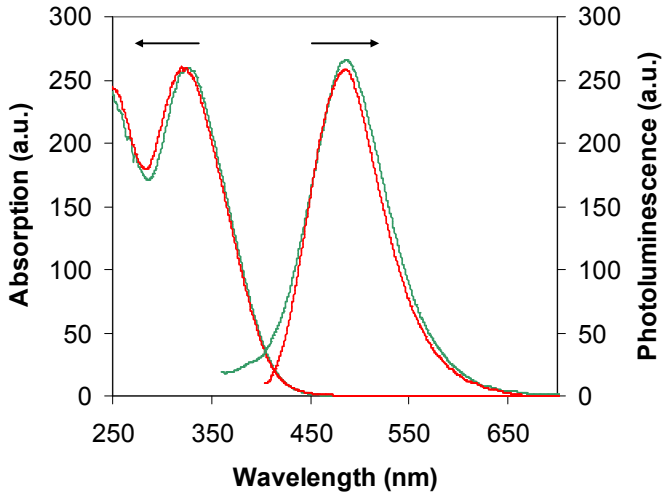

Figure 3.9. Normalized UV-vis absorption and photoluminescent (PL) spectra of PDTP in thin film form (red) and in THF solution (green).

The normalized UV-vis absorption and photoluminescent (PL) spectra of PDTP in THF solution and in thin film are shown in Figure 3.9. In contrast to conventional light-emitting polymers and oligomers, the spectra of PDTP thin film show no red-shift from that of the solution. Furthermore, the spectrum of PDTP thin film is narrower than the spectrum of PDTP in solution. The results illustrate that the unique molecular structure of PDTP can effectively prevent both intra- and inter- molecular aggregation due to the rigid frame and the outer shielding layer made of branched alkyl chains.

To further study whether aggregation occurs in the condensed state of PDTP, PDTP was blended with a blue emissive polymer Hi-bg,[23] which structure is shown in Figure 3.10, at various weight ratios to form solid solutions because the blended materials would perform differently if there is aggregation in neat polymer with lower band gap.[24] By varying concentration of PDTP in the polymer, PL spectrum of PDTP would shift accordingly if

there is intra- or inter-molecular aggregation. For a homogeneous blend, the aggregation of PDTP could be reduced while the energy transfer between PDTP and the polymer matrix could occur. The interplay between these two factors could lead to a change in the PL spectra of PDTP and the polymer matrix. The PL spectra of the blends are shown in Figure 3.10. It can be seen that the position of the peak corresponding to PDTP are not influenced by Hi-bg : PDTP ratio, implying that there is no intra- or inter-molecular interaction between PDTP molecules.

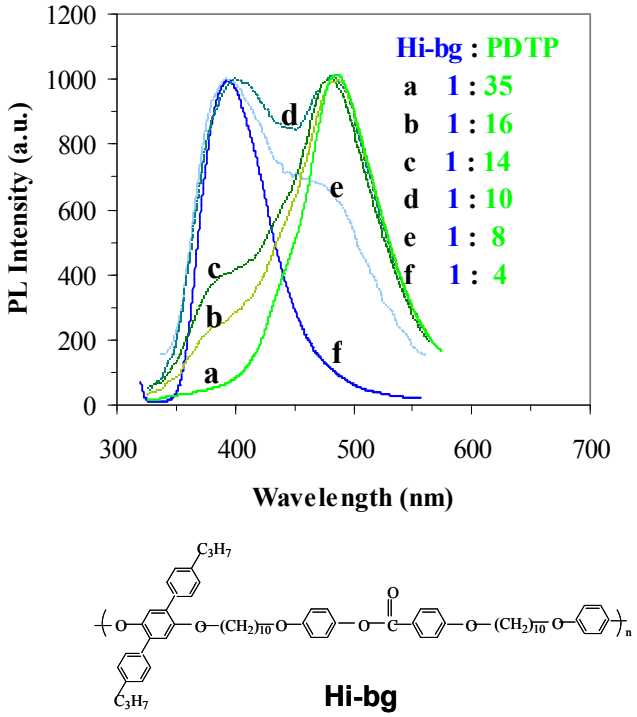

Figure 3.10. PL spectra of the blends of PDTP and Hi-bg. The weight ratio of Hi-bg to PDTP was a 1:35; b 1:16; c 1:14; d 1:10; e 1:8; f 1:4.

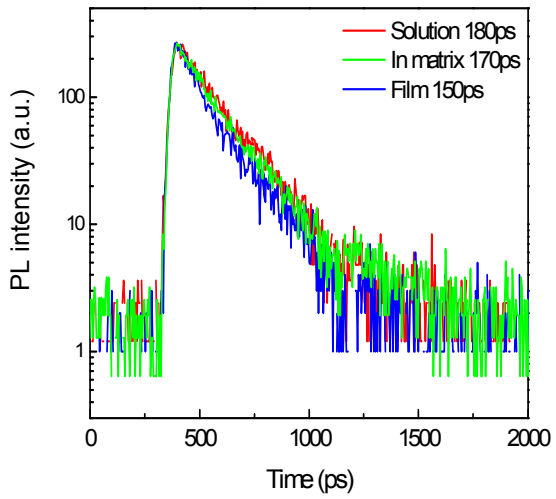

Figure 3.11. Time-resolved PL decay spectra of PDTP as solid thin film (blue), in THF solution (red) and in solid solution (green).

Further confirmation regarding the unique optical property of the light emitting dot comes from Time-resolved PL study. Figure 3.11 shows time-resolved PL decay curves PDTP in dilute solution (THF), solid film, and film blend with Hi-bg. The three decay curves reveals that the exciton decay for PDTP, regardless in solution, condensed state or in solid solution, can be well fitted using a single exponential function, $I = I_0\exp(-t/\tau)$, suggesting that the recombination in these three state are all dominated by single-process exciton recombination. The similar decay times (τ) in condensed state, i.e. thin film (150 ps), dilute solution in THF (180 ps), and blend with polymer Hi-bg (170 ps), as listed in Figure 3.11, imply that the excitons recombination in three states, are all dominated by single-process exciton recombination, reflecting no obvious nonradiative decay channels. It is interesting to compare this result with conventional conjugated polymers e.g. MEH-PPV which shows

much different decay time in solution (330 ps) and in solid state (580 ps).[25] The longer decay time in the conjugated polymer film than in the solution for MEH-PPV has been attributed to exciton three-dimensional inter- and intra-chain migration.[25,26] If there are aggregation or inter molecular interactions occurred, the PL decay curves will contain more than one components so the PL intensity will be described as, e.g. as $I(t) = a_s \exp(-t/\tau s) + a_f \exp(-t/\tau_f)$. Normally the fast decay comes from unaffected emissive units and the slow component comes from aggregated chains.[27] The study on partially conjugated polymer system confirmed the existence of two emission species contributed by isolated conjugated chains and the aggregated chains. The longer decay time, corresponding to the red shifted PL spectrum part, was attributed to the aggregated chains formed because of the higher concentration of polymer in solution. The unaffected decay time by varying concentration of polymer solution, at blue part of PL spectrum, was attributed to the isolated conjugated chins.[28] Based on the work reported by other people we may conclude there is nearly no aggregation in the condensed state of **PDTP** and the reason is due to the unique structure of hybrid dots in which conjugated chains confined by POSS cage and alkyl chain shielding layers.

The shorter decay time of PDTP has three advantages over longer decay time of MEH-PPV. Firstly, the shorter intrinsic decay time of PDTP indicates more overlapping of electron wave function and hole wave function so there are more chances for radiative recombination of electron and hole so that higher quantum yield can be expected. Secondly, the shorter intrinsic decay time of PTDP than MEHPPV means there are less chances for excitons to be trapped by defect sites or undergoing other non-radiative process hence higher quantum yield will be expected. Thirdly, similar decay times of film and solution of **PDTP** imply the

emission species in both states are same, i.e. there is no aggregation in film state. The much longer decay time of MEHPPV in film than that of the solution implies the existence of two emission species contributed by isolated conjugated chains and the aggregated chains in film state. The fast decay comes from unaffected emissive units and the slow component comes from aggregated chains.

3.3.4 Water soluble nano-particles

To demonstrate the potential bio-applications, hydrophilic green emissive nano-particles have been made, as shown in Scheme 3.3. In this synthesis, the starting material OPBS was obtained from previous work[1,2] which has both *m*- and *p*- substituted positions.

Hybrid water soluble nano-particle **W** was synthesized by using **M** as starting monomer and subsequently following all the water-solublizing reactions described in the reference paper reported by Lu and co-workers.[29] The Light-scarrtering studies indicate hydrophilic compound **W** is a spherical molecule with uniform size of 33 nm. So the novel hydrophilic hybrid nano-particle **W** is obtained. The thickness of water-soluble layer, and thus the size of the light emitting dots could be easily controlled by feed ratio of starting materials. Compound **M** has only one sharp peak in ^{29}Si NMR at–78.8, which means all of eight vertexes of POSS have been grafted with dithiophene chains.

Absorption and Photoluminescance studies of **W** in water are shown in Figure 3.12. The emission wavelength of **W** is similar with monomer **M**. It is worth to mention **W** is highly soluble in water, just like conventional inorganic salts e.g. NaCl. The application of this compound as biosensor materials will be conducted in near future. The PL spectra of monomer **M** in solution and solid form are also studied and compared with that of **W** in

water solution. The maximum PL position of **M** and **W** are identical, as expected, due to the identical active emissive unit. The PL curve of **W** is broader than that of **M** possibly due to the stretching by long hydrophilic chains to molecule **W** which generated more torsion conformations for dithiophene unit than that in monomer **M**. The PL spectrum of **M** in film state is not red shifted from that in solution of THF.

Scheme 3.3. synthesis of water soluble nano-particle W

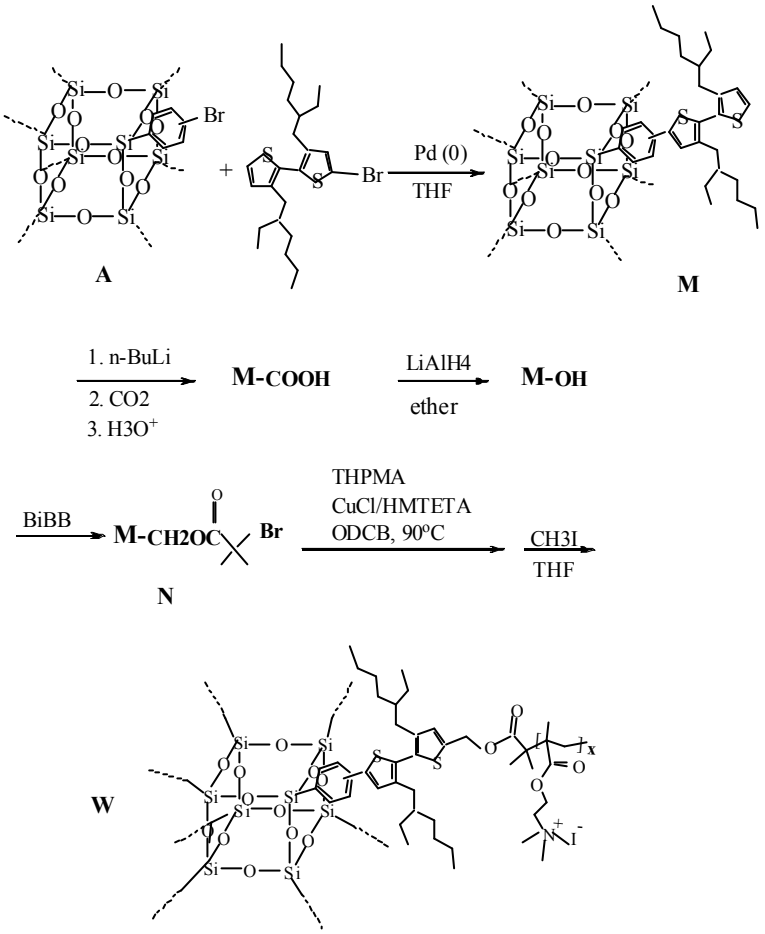

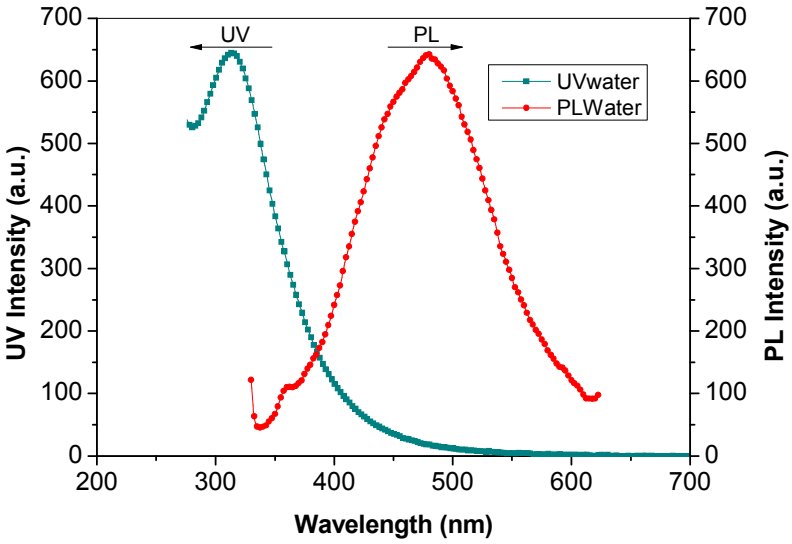

Figure 3.12. UV absorption and PL spectrum of hydrophilic nano-particle W in water solution.

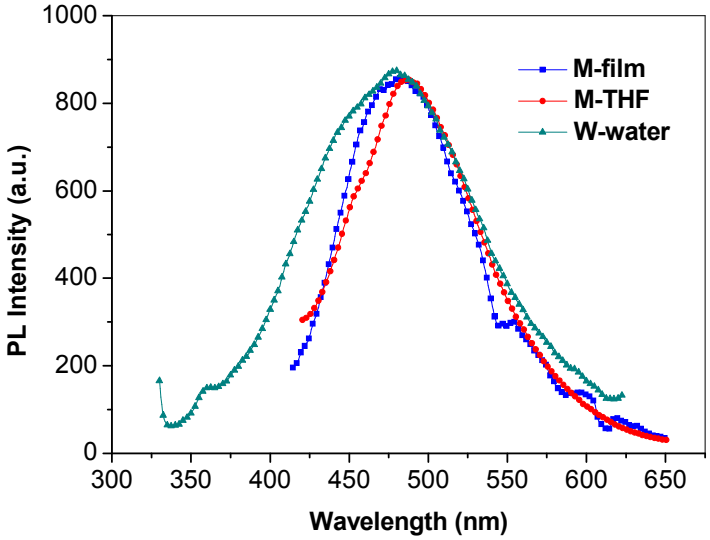

Figure 3.13. comparison the PL spectrum of monomer M in THF solution and in solid film form with PL spectrum of hydrophilic nano-particle W in water solution.

3.3.5 Effect of Regioselective Bromination of OBPS on the Characteristic of PL

The effect of regioselective bromination of **OBPS** on the characteristic of photoluminesecne can be studied by comparing the PL spectra of **PDTD** and that of **M**. It can be seen, from Figure 3.13, the PL spectrum of M in film blue shifted from that in solution of THF, the phenomenon same with that of PDTD, as shown in Figure 3.9. The substitution position in OBPS is not significantly affecting the optical properties of the materials M and PDTD, not only the wavelength of emission, but more importantly the aggregation free property in both materials. This is possibly due to the fact that the light emitting components in both materials are same which is dithiophene-Ph and the *m* or *p* grafting of dithiophene to Ph does not alter the conjugated length of the light emitting component. Even though there are two alkyl chains on dithiophene in molecule **M**, the PL spectrum doesn't shift from solution to film which demonstrated the effectiveness of branchy alkyl chains in protecting conjugated chains from aggregation. As a result, random bromination of OBPS, which is easier to synthesize could be used for future preparation of green light emitting dots for bio-detection.

3.4. Conclusions

In summary, An unique approach to the synthesis of pure *m*-octa(bromophenyl) silsesquioxane (*m*-OBPS) is reported. The highly regioselective bromination of octaphenylsilsesquioxane is achieved by using combined catalyst of iodine and zinc chloride at room temperature in dichloromethane. From *m*-OBPS a novel hybrid luminescent nano-particle with well-defined chemical structure is synthesized via coupling conjugated short chains with *m*-OBPS. UV absorption and PL spectra of this light emitting dot remain same in

dilute solution, condensed state, and solid solutions. The exciton decay time of the nano-particle remains similar regardless it is in dilute solution or condensed state, suggesting that the charge carriers are well confined by the silsesquioxane cage and shielding alkyl chains attached on the conjugated short chains. The conjugated chains confined by the cage and alkyl chains, which are considered as two barriers with higher band gap, can thus be treated as isolated chromophores as both intra- and inter-molecular aggregation of the chains are prohibited. The materials can potentially be used as light emitting dots for OLED or bio-sensor. Further to the luminescent nano-particle, a highly water soluble nano-particle with same emissive structure has been synthesized to demonstrate the potential bio-applications of this kind of materials.

3.5 References

1. He, C. B., Xiao, Y., Huang, J. C., Lin, T. T., Mya, K. Y., & Zhang, X. H. (2004). Highly efficient luminescent organic clusters with quantum dot-like properties. *Journal of the American Chemical Society*, 126, 7792-7793.
2. Xiao, Y., Liu, L., He, C. B., Chin, W. S., Lin, T. T., Mya, K. Y., Huang, J. C., & Lu, X. H. (2006). Nano-hybrid luminescent dot: synthesis, characterization and optical properties. *Journal Of Materials Chemistry,* 16, 829-836.
3. Xiao, S. Nguyen, M. Gong, X., Cao, Y., Wu, H. B., Moses, D., & Heeger, A. J. (2003). Stabilization of semiconducting polymers with silsesquioxane. *Advanced Functional Materials.* 13, 25-29.

4. Lee, J., Cho, H. J., Jung, B. J., Cho, N. S., & Shim, H. K. (2004). Stabilized blue luminescent polyfluorenes: Introducing polyhedral oligomeric silsesquioxane. *Macromolecules,* 37, 8523-8529.
5. Lin, W. J., Chen, W. C., Wu, W. C., Niu, Y. H., & Jen, A. K. Y. (2004). Synthesis and optoelectronic properties of starlike polyfluorenes with a silsesquioxane core. *Macromolecules* 37, 2335-2341.
6. Chou, C. H., Hsu, S. L., Dinakaran, K., Chiu, M. Y., & Wei, K. H., (2005). Synthesis and characterization of luminescent polyfluorenes incorporating side-chain-tethered polyhedral oligomeric silsesquioxane units *Macromolecules 38*, 745-751.
7. Chou, C. H., Hsu, S. L., Yeh, S. W., Wang, H. S., & Wei, K. H. (2005). Enhanced luminance and thermal properties of poly(phenylenevinylene) copolymer presenting side-chain-tethered silsesquioxane units. *Macromolecules*, 38, 9117-9123.
8. Kang, J. M., Cho, H. J., Lee, J., Lee, J. I., Lee, S. K., Cho, N. S., Hwang, D. H., & Shim, H. K., (2006). Highly bright and efficient electroluminescence of new PPV derivatives containing polyhedral oligomeric silsesquioxanes (POSSs) and their blends. *Macromolecules,* 39, 4999-5008.
9. Cho, H. J., Hwang, D. H., Lee, J. I., Jung, Y. K., Park, J. H., Lee, J., Lee, S. K., & Shim, H. K. (2006). Electroluminescent polyhedral oligomeric silsesquioxane-based nanoparticle. *Chemistry of Materials*, 3780-3787.
10. Lickiss, P. D., & Rataboul, F. (2008). Fully condensed polyhedral oligosilsesquioxanes(POSS): From synthesis to application. *Advances In Organometallic Chemistry*, 57, 1-116.

11. Choi, J., Harcup, J., Yee, A. F., Zhu, Q., & Laine, R. M. (201). Organic/inorganic hybrid composites from cubic silsesquioxanes. *Journal of the American Chemical Society*, 123, 11420-11430.
12. Xiong, S. X., Xiao, Y., Ma, J., Zhang, L. Y., & Lu, X. H. (2007). Enhancement of electrochromic contrast by tethering conjugated polymer chains onto polyhedral oligomeric silsesquioxane nanocages. *Macromolecular Rapid Communications*, 28, 281-285.
13. Tamaki, R., Tanaka, Y., Asuncion, M. Z., Choi, J. W., & Laine, R. M. (2001). Octa(aminophenyl)silsesquioxane as a nanoconstruction site. *Journal of the American Chemical Society*, 123, 12416-12417.
14. Brick, C. M., Tamaki, R., Kim, S. G., Asuncion, M. Z., Roll, M., Nemoto, T., Ouchi, Y., Chujo, Y., & Laine, R. A. (2005). Spherical, polyfunctional molecules using poly(bromophenylsilsesquioxane)s as nanoconstruction sites. *Macromolecules*, 38, 655-4660.
15. Olah, G. A., Bucsi, I., Lambert, C., Aniszfeld, R., Trivedi, N. J., Sensharma, D. K., & Prakash, G. K. S. (1991). Considered polycarbon supercage chemistry .2. chlorination and bromination of fullerenes - nucleophilic methoxylation of polychlorofullerenes and their aluminum trichloride catalyzed friedel-crafts reaction with aromatics to polyarylfullerenes. *Journal of the American Chemical Society*, 113, 9385-9387.
16. Joshi, H. S., Jamshidi, R., & Tor, Y. (1999). Conjugated 1,10-phenanthrolines as tunable fluorophores. *Angewandte Chemie-International Edition*, 38, 2722-2725.

17. Tonzola, C. J., Alam, M. M., Bean, B. A., & Jenekhe, S. A. (2004). New soluble n-type conjugated polymers for use as electron transport materials in light-emitting diodes. *Macromolecules*, 37, 3554-3563.
18. Gnanapragasam, N. S., Ramanujam, R., Srinivasan, & S. P. (1976). Bromination of acetanilide catalyzed by anhydrous ferric-chloride, anhydrous zinc-chloride and iodine bromide. *Current Science*, 45, 862-863.
19. Olah, G. A. (1971). Aromatic substitution .28. mechanism of electrophilic aromatic substitutions. *Accounts of Chemical Research*, 4, 240-&.
20. Yeddanapalli, L. M., & Gnanapragasam, N. S. (1956). kinetics and mechanism of bromination of phenol with bromine and iodine bromide in glacial acetic acid and carbon tetrachloride. *Journal of the Chemical Society,* Dec. 4934-4943.
21. Dewar, M. J. S. (1946). The mechanism of benzidine-type rearrangements, and the role of pi-electrons in organic chemistry. *Journal of the Chemical Society,* 406-408.
22. Brown, H. C., Pearsall, H. W. (1952). The action of the catalyst couple aluminum chloride-hydrogen chloride on toluene at low temperatures - the nature of friedel-crafts complexes. *Journal of the American Chemical Society,* 74, 191-195.
23. Lu, X. H., He, C. B., Liu, P. W., & Griffin, A. C. (2005). Structures and properties of liquid-crystalline polymers based on laterally attached oligo p-phenylenes. *Journal of Polymer Science Part A-Polymer Chemistry,* 43, 3394-3402.
24. Liu, J., Shi, Y. J., & Yang, Y. (2001). Improving the performance of polymer light-emitting diodes using polymer solid solutions. *Applied Physics Letters,* 79, 578-580.

25. Samuel, I. D. W., Rumbles, G., Collison, C. J., Friend, R. H., Moratti ,S. C., & Holmes, A. B. (1997). Picosecond time-resolved photoluminescence of PPV derivatives. *Synthetic Metals*. 84, 497-500.

26. Daniel, C., Makereel, F., Herz, L. M., Hoeben, F. J. M., Jonkheijm, P., Schenning, A. P. H. J., Meijer, E. W., Friend, R. H., & Silva, C. (2005). The effects of supramolecular assembly on exciton decay rates in organic semiconductors. *Journal of Chemical Physics,* 123, Article Number: 084902.

27. Das, B. B., Liu, F., & Alfano, R. R. 91997). Time-resolved fluorescence and photon migration studies in biomedical and model random media. *Reports on Progress in Physics,* 60, 227-292

28. Fakis, M., Polyzos, I., Tsigaridas, G., Giannetas, V., & Persephonis, P. (2004). Excited state dynamics of a partially conjugated polymer studied by feratosecond fluorescence upconversion spectroscopy. *Chemical Physics Letters*, 394, 372-376.

29. Lu, S., Fan, Q. L., Chua, S. J., & Huang, W. (2003). Synthesis of conjugated - Ionic block copolymers by controlled radical polymerization. *Macromolecules,* 36, 304-310.

Chapter Four

Red hyper-branched polymer containing POSS

4.1 Introduction

Having understood the effect of incorporating of POSS on the property of light emitting dots, in chapter 2 and 3, the research will be extended to applications of POSS in conjugated polymers. Since the bulky structure of POSS cage significantly reduces the potential intra- and inter-chain interactions, and hence reduced the chances of non-radiative combination of excitons, higher luminescent efficiency will be expected in POSS-polymer system. Hyper-branched emissive polymer based on POSS will be synthesized and used to demonstrate the effectiveness of POSS cage in improvement of luminescent efficiency for a series of red conjugated polymers. Through this investigation, the effect of POSS, either via chemical bond to or physically blended with conjugated polymer on the PL quantum efficiency and device performance will be studied.

As well known, conjugated polymers have been used in many applications such as large-area flat-panel LED (light-emitting diodes) displays,[1-4] solar cells,[5,6] field-effect transistors[7,8] and bio-detections.[9] The development of full-color LED devices greatly depends on the performance of primary RGB (red, green, and blue) light-emitting materials. A wide range of conjugated polymers, such as poly(p-phenylenevinylene) (PPV) and its derivatives,[10-12] polyfluorenes[13,14] and polythiophenes,[15,16] have been developed and extensively studied to achieve stable and highly efficient RGB electroluminescent materials. Compared with green and blue electroluminescent materials, the development of red emissive materials however falls far behind in terms of both color purity and light emitting efficiency.[17] The most widely

used red emissive polymers have either planar backbone such as CN-PPV[3] or aromatic heterocycles such as thiophene[16] and benzothiadiazole.[18-21] With narrower band gap and planar backbone structure compared with blue and green conjugated polymers, red luminescent polymers are susceptible to aggregation in condensed state due to intra- and inter-molecular π-π stacking. They are therefore highly prone to exciton quenching that renders the materials either weakly emissive or even not emissive at all in condensed sate. To overcome the strong inter- and intra-molecular interactions that are inherent in red emissive polymers, several strategies have been used. One approach is to blend red emissive polymers with suitable host to reduce the aggregations.[22-24] This process effectively utilizes the Förster resonance energy transfer from the host. Another approach is to incorporate rare earth metal europium (Eu) as an emitter into suitable ligands and Eu (3+) will give typical red emission.[25,26] This process also relies on the Förster resonance energy transfer from the ligands to Eu (3+) which, however, normally causes high turn-on voltages. There were also reports on using alternative copolymers containing fluorene and 4,7-dithienyl-2,1,3-benzothiadiazole or its derivatives to achieve red-light emission in a range of 640-670 nm with improved efficiencies.[27-30]

Recent studies have shown that incorporation of bulky polyhedral oligomeric silsesquioxane (POSS) cages into conjugated polymers could greatly improve the performance of light emitting polymers by reducing aggregations.[31-40] The brightness and quantum efficiency as well as thermal stability of linear conjugated polymers could be greatly improved by incorporating POSS cages either onto chain end or as core to form star-like polymers. In this chapter, POSS cage was incorporated into red luminescent polymers for the first time to enhance the light emitting characteristic of the polymers. We will report the

synthesis of soluble hyperbranched conjugated polymers via $FeCl_3$-oxiditive polymerization of octa(3-ethylhexyl-2-thienyl-phenyl)POSS and 4,7-bis(3-ethylhexyl-2-thienyl)-2,1,3-benzothiadiazole. Our results show that by incorporating suitable percentage of POSS cage, the hyperbranched red luminescent polymers exhibit much less aggregation in solid state, much higher photoluminescence (PL) quantum efficiencies and EL brightness as well as narrower electroluminescent emission widths than their linear counterpart.

4.2 Experimental section

4.2.1 Materials

Tetrahydrofuran (THF) (99.8%, TEDIA) was distilled from sodium/benzophenone. $CHCl_3$ (98%, TEDIA) was used as received. 3-Bromothiophene (97%), 2-ethylhexyl bromide (95%), tetrakis(triphenylphosphine)-palladium(0) $Pd(PPh_3)_4$ (99%), 4,7-dibromo-2,1,3-benzothiadiazole (95%), magnesium turnings (99.9+%), iron(III) chloride anhydrous (98%), bromine (99.99%) and [1,3-bis(diphenylphosphino)propane]dichloronickel(II) [Ni(dppp)Cl_2] (99%) were purchased from Aldrich Chemical Co. and used as received. SiliaFlash P60 (particle size distribution 40-63 nm, 230-400 mesh, pore size 60A from Alpha Analytical) was used as received. Octa(bromophenyl)silsesquioxane (OBPS) was synthesized according to our previous reports.[39,40]

4.2.2 Characterization

^{1}H, ^{13}C, ^{29}Si nuclear magnetic resonance (NMR) data were obtained using a Bruker Avance 400 spectrometer. Elemental micro-analysis was carried out by the Microanalysis

Laboratory of the National University of Singapore. Gel permeation chromatography (GPC) analysis was carried out with a Shimadzu SCL-10A and LC-8A system equipped with two Phenogel 5μ 50 and 1000Å columns in series and a refractive detector, using THF as the eluent at a flow rate of 0.3ml/min at 40ºC. Monodispersed poly(ethylene glycol) were used as standards. Thermogravimetric analyses (TGA) was conducted on a Perkin-Elmer thermogravimetric analyzer TGA 7 under a heating rate of 15 °C/min and a nitrogen flow rate of 40 cm^3/min. Differential scanning calorimetry (DSC) measurements were performed under nitrogen flow of 10 ml/min on a TA Instruments 2920 differential scanning calorimeter equipped with a cooling accessory. All the samples were heated to 110 °C and cooled down to room temperature at 5 °C/min under nitrogen flow to remove moisture, and then heated to 280 °C at 5 °C/min. Modulated DSC was conducted from room temperature to 280 °C at 3 °C/min with a heating–cooling modulation cycle time of 60 s and amplitude of ±0.477 °C. X-ray diffraction (XRD) patterns were recorded on a Bruker GADDS under a voltage of 40 kV and current of 40 mA using CuK_α radiation (λ = 0.15418nm). Film samples for DSC and XRD studies were prepared by solution casting of polymers on glass substrates. UV-Vis spectra were recorded on a Shimadzu 3101 spectrophotometer. Photoluminescence (PL) measurement was carried out on a Perkin-Elmer LS 50B luminescence spectrometer with a xenon lamp as a light source. PL quantum efficiency (Φ_{PL}) of the materials in solution was recorded by using a diluted quinoline solution in 0.1 N H_2SO_4 as the standard and assuming that its Φ_{PL} is 55%. The concentration of polymers for UV and PL analysis is less than 1 x 10^{-3} g/ml. $\Phi_{PL\text{-}f}$ of the materials in film form was recorded by using 9,10-diphenylanthracene dispersed in PMMA films at a concentration lower than 1 x 10^{-3} M as the standard and

assuming that the $\Phi_{PL\text{-}f}$ of the standard is 83%. The polymer thin films were cast on a quartz plate using a spin coater.

4.2.3 Synthesis of polymers

4,7-bis(3-ethylhexyl-2-thienyl)-2,1,3-benzothiadiazole (A): Magnesium (1.23g, 51.2mmol) was added into a 250ml three-necked round-bottomed flask (RBF) and heated to 120°C for one hour under argon atmosphere and then cooled down to room temperature. A solution containing of 2-bromo-3-ethylhexyl-thiophene (11.80g, 42.9mmol) and dry THF (100ml) was added drop-wisely into the RBF. The mixture was refluxed for three hours to yield the corresponding Grignard reagent. The Grignard reagent was transferred to a solution containing 4,7-dibromo-2,1,3-benzothiadiazole (5.00g, 17.0mmol) and tetrakis(triphenylphosphine)-palladium(0) $Pd(PPh_3)_4$ (1.00g, 0.9mmol) and dry THF (40 ml) under argon atmosphere. The mixture was reacted overnight under reflux and cooled down to room temperature. The reaction was quenched with 1N NH_4Cl aqueous solution. The mixture was added into ethyl acetate (50ml) and water (50ml). The organic phase was washed with water twice and brine once and then dried over anhydrous $MgSO_4$. After removal of solvent, the mixture was subjected to purification by column chromatography on silica gel using hexane as eluent. Yield: 70%. ^{1}H NMR: δ 7.95(s, 2H), 7.83 (s, 2H), 7.02(s, 2H), 2.64(d, 4H, *J*=6.8 Hz). ^{13}C NMR: δ 153.1 143.4, 139.2, 129.9, 126.4, 125.8, 122.8, 40.8, 35.1, 33.0, 30.1, 29.3, 26.1, 23.5, 14.5, 11.3. MS (EI, *m/z*): 524.3. Calculated ($C_{30}H_{40}N_2S_3$) (%): C, 68.70; H, 7.63; N, 5.34; S, 18.32; Found (%): C, 68.85; H, 7.54; N, 5.02; S, 17.17.

Octa(3-ethylhexyl-2-thienyl-phenyl)POSS (B) Magnesium (0.30g, 12.5 mmol), 2-bromo-3-ethylhexyl-thiophene (2.35g, 8.5 mmol) and octa(bromophenyl)silsesquioxane (OBPS) (0.87g, 0.5 mmol) were reacted following the method for synthesis of monomer **A**. A light yellowish glassy solid 0.68g (yield 50%) was obtained. ^{1}H NMR: δ 8.2-6.2 (m, 6H), 2.83 (s, 2H). ^{13}C NMR: δ 149.5, 143.6, 140.7, 138.9, 137.8, 136.0, 132.4, 130.0, 128.3, 124.1, 122.6, 41.1, 33.1, 29.2, 26.3, 23.4, 14.1, 11.2. ^{29}Si NMR: δ -81.0, 82.3. GPC Mn: 2.0 x 10^3, Mw: 3.1 x 10^3. Polydispersity index (PDI): 1.1. Calculated ($Si_8O_{20}C_{144}H_{184}S_8$) (%): C, 66.87; H, 7.12; S, 9.90. Found (%): C, 66.94; H, 7.02; S, 8.65.

P1: monomer **A** (0.52g, 1.0 mmol) and **B** (0.16g, 0.1 mmol) were dissolved in $CHCl_3$ (30ml) and cooled to 0°C. A slurry of $FeCl_3$ (0.98g, 6.0 mmol) in $CHCl_3$ (70ml) was carfully added. The reaction mixture was purged and stirred for 8 hours at 0°C. The mixture was then warmed to room temperture and stirred for another 15 hours. When reaction completed, the mixture was poured into methanol. The solid material precipitated was filted and successively washed with water and methanol. The polymer was then purified using ammonia hydroxide to remove $FeCl_3$ residues.[42-44] Despite exhaustive cleaning, it's difficult to completely remove the ferric chloride salts from the polymers because the salts strongly bind with thiophene moieties. The resulting solid material was therefore further purified by stirring with aqueous ammonia (125ml, 25%) for 3 hours at room temperture. The red polymer was filted and washed successively with water, methanol and acetone. The polymer was re-dissolved in $CHCl_3$, filtered, and precipitated in methanol. Yield: 38% (0.25g). ^{1}H NMR: δ 8.08 (s, 2H), 7.89 (s, 2H), 7.82-7.50 (m, 0.64H) 2.64 (s, 4H); ^{13}C NMR: 153.1, 143.2, 139.4, 131.5, 130.3, 126.1, 125.8, 40.8, 34.0, 33.2, 29.3, 26.4, 23.4, 14.5, 11.3. ^{29}Si NMR: -81.3. ^{1}H NMR indicates that there are six repeat units on each arm in average (see

supporting information). Calculated for ($C_{1584}H_{2008}N_{96}S_{152}Si_8O_{12,}$ Mn 27640) (%): C, 68.77; H, 7.26; N, 4.86; S, 17.59. Found (%): C, 68.45; H,7.46; N, 4.62; S, 16.77. GPC: Mn: 2.74 x 10^4. PDI: 1.6.

P2: monomer **A** (0.26g, 0.5mmol) and **B** (0.16g, 0.1 mmol) were used and the procedure used for the synthesis of **P1** was followed. Yield: 25% (0.98g). ^{1}H NMR: δ 8.08 (s, 2H), 7.89 (2, 2H), 7.8-7.5 (m, 1H), 2.64 (s, 4H); ^{13}C NMR: 153.1, 143.2, 139.3, 131.5, 130.3, 126.1, 125.8, 40.8, 33.9, 33.2, 29.2, 26.3, 23.5, 14.5, 11.3. ^{29}Si NMR: -81.0. ^{1}H NMR indicates that there are four repeat units on each arm in average (see supporting information). Calculated for ($C_{1104}H_{1400}N_{64}S_{104}Si_8O_{12,}$ Mn 19288) (%): C, 68.68; H, 7.26; N, 4.64; S, 17.25. Found (%): C, 68.53; H,7.35; N, 4.67; S, 16.70. GPC: Mn: 1.54 x 10^4. PDI: 1.5.

Polymer (PM): compound **A** (0.30g, 1.0mmol) was used and the procedure used for the synthesis of **P1** was followed. Yield 65% (0.25g). ^{1}H NMR: δ 8.08(s, 2H), 7.88 (s, 2H), 2.64(s, 4H,). ^{13}C NMR: δ 153.1 143.2, 139.4, 131.5, 130.3, 126.1, 125.8, 40.8, 34.0, 33.2, 30.7, 29.8, 26.3, 23.5, 14.5, 11.3. Calculated for ($C_{30}H_{38}N_2S_3$) (%): C, 68.96; H, 7.28; N, 5.36; S, 18.39. Found (%): C, 68.86; H, 7.47; N, 5.06; S, 17.96. GPC: Mn: 2.47 x 10^4. PDI: 1.6.

4.3 Results and discussion

4.3.1 Synthesis and characterization

Scheme 4.1. Synthesis of polymers P1 and P2.

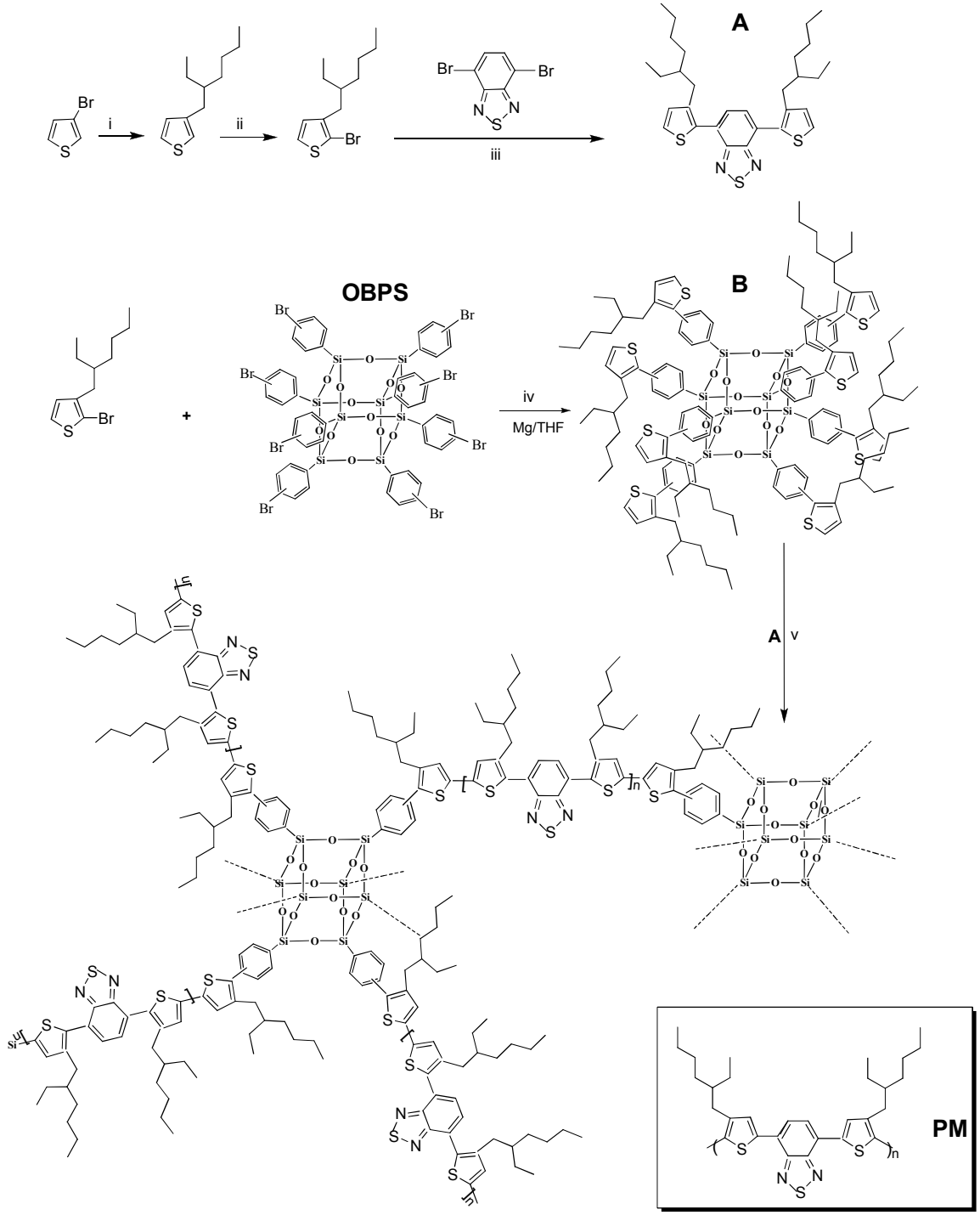

[a] Reaction and conditions: (i) BrC_8H_{17}, ether, $Ni(dppp)_2Cl_2$; (ii) NBS, AcOH; (iii) Mg, THF, $Pd(PPh_3)_4$; (iv) Mg, THF, $Pd(PPh_3)_4$; (v) $FeCl_3$, $CHCl_3$.

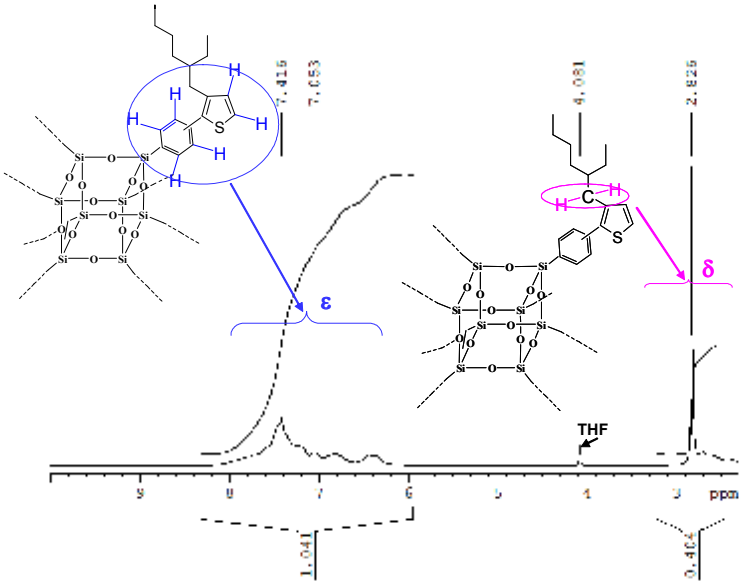

Figure 4.1. ^{1}H NMR of monomer B. The number ratio of "H" (aromatic) to "H" (alkyl) is 6: 2 (=3) by calculation based on the molecular formula. The actual ratio is 1 : 0.4 (=2.5) meaning that eight arms on POSS have been substituted with thiophene moieties. Normally the integrals of protons on alkyl chain appear slightly larger than that of aromatic protons.

The general synthetic methods for the monomers and polymers are outlined in Scheme 4.1. Compound 2-Bromo-3-ethylhexyl-thiophene was obtained via a two-step reaction. In the first step, 3-ethylhexyl-thiophene was obtained via Grignard coupling reaction between 3-bromo-thiophene and 2-ethylhexyl bromide. The second step was bromination of 3-ethylhexyl-thiophene by NBS in AcOH at 0°C to yield mono-brominated compound. Monomer A was synthesized via Grignard coupling reaction between 4,7-dibromo-2,1,3-benzothiadiazole and 2-bromo-3-ethylhexyl-thiophene with a moderate yield. Monomer B was obtained through Grignard coupling reaction between OBPS and 2-bromo-3-ethylhexyl-

thiophene. OBPS was obtained from our previous work in which bromine atom was attached on phenyl group of octaphenylsilsesquioxane (OPS). The bromine atom on phenyl in OBPS could be at *para*- or *meta*- position. The ^{1}H NMR of monomer **B** indicates that all the eight phenyl groups have been grafted with alkyl chain substituted thiophene, as shown in Figure 4.1 The carbon NMR was shown in Figure 4.2. Elemental analysis result provides a further confirmation. The low steric hindrance of monomer **A** and **B** enables successful polymerization between **A** and **B.**

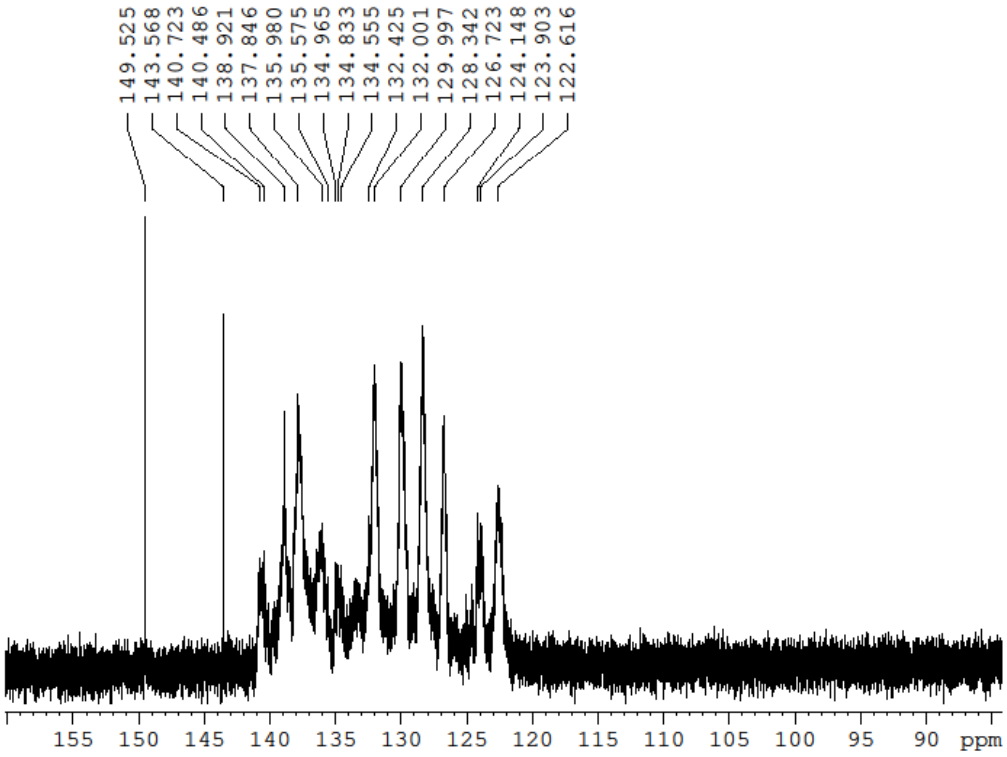

Figure 4.2. ^{13}C NMR of monomer B. There are ten major peaks corresponding to the 10 "C" in monomer B. The minor peaks may be due to the different substitution position of "Br" on phenyl in OBPS.

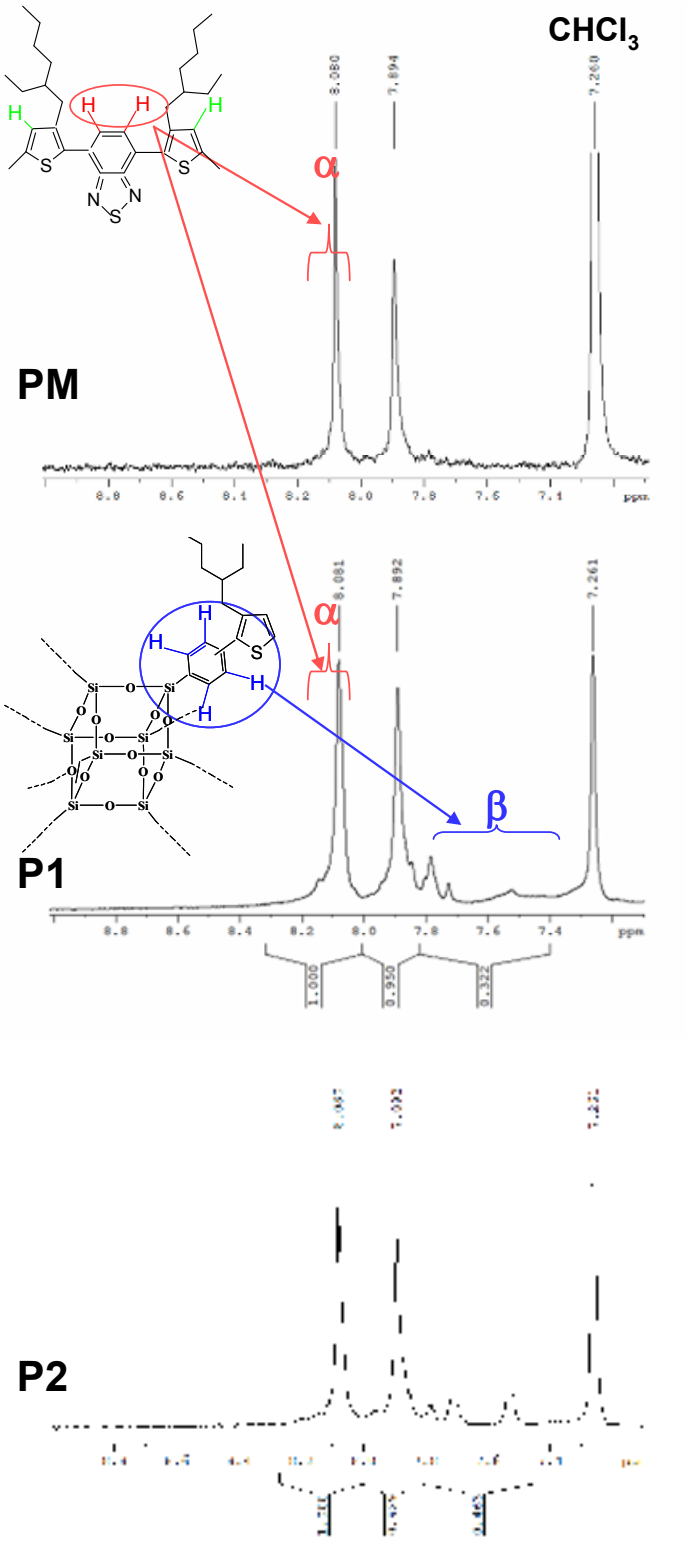

Figure 4.3. ^{1}H NMR of monomer A, polymers P1 and P2. The area ratio of $2\alpha/\beta$ ($\frac{\alpha}{2} \div \frac{\beta}{4}$)represents the number of repeat units on each arm of POSS.

The yield for polymer synthesis is about 25-40% depending on the concentration of monomer **B**. High concentration of monomer **B** leads to a low yield, which is due to the formation of highly cross-linked structure that is insoluble in organic solvents and precipitated out during the polymerization process. This is also the reason that the yield of **P2** (25%) is lower than that of **P1** (37%). The weight-average molecular weights, Mw, of the polymers are in the range of 2.37 x 10^4 – 4.41 x 10^4 g/mol. Table 4.1 is a summary of the composition, molecular weight and molecular weight distribution of the polymers synthesized. The average number of repeat unit on each arm of **P1** and **P2** estimated by ^{1}H NMR is six and four respectively, as shown in Figure 4.3. It is worthy mention that this number may be overestimated because **P1** and **P2** may also contain some linear homopolymer and hence the number of repeat unit on each arm of POSS in **P1** and **P2** maybe smaller than six and four.

Table 4.1 Polymer synthesis and characterization

Polymers	Feed ratio[a]	Content ratio[b]	wt% benzothiadiazole[c] (%)	wt% POSS[c] (%)	Yield (%)	M_n	M_w g/mol	PDI
PM		1 : 0			65	24719	41817	1.6
P1	16 : 1	6 : 1	23	1.5	38	27446	44073	1.6
P2	8 : 1	4 : 1	22	2.1	25	15443	23665	1.5

[a] Feed ratio is the feed molar ratio of monomer A to B.

[b] Content ratio is defined as the average number of repeat units (A) on each arm of POSS in the final polymer products measured by 1H NMR.

[c] wt% is the weight percentage of benzothiadiazole (C_6N_2S) and POSS (Si_8O_{12}) in polymer.

4.3.2 Thermal properties

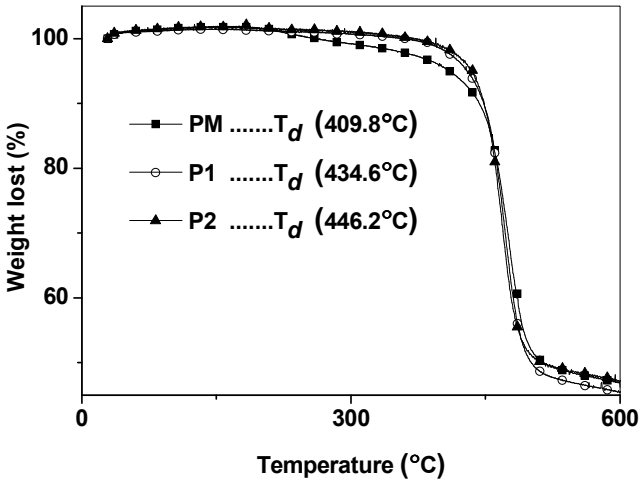

Figure 4.4. TGA curves of PM, P1, P2 under nitrogen.

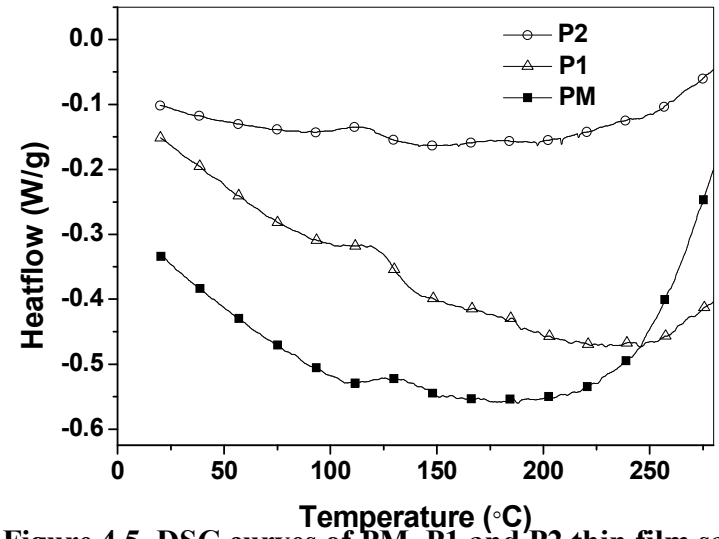

Figure 4.5. DSC curves of PM, P1 and P2 thin film samples.

Thermal properties of linear polymer PM, hyperbranched polymers P1 and P2 are characterized by TGA and DSC. TGA curves of PM, P1 and P2 are shown in Figure 4.4. The decomposition temperature T_d (defined as the temperature at 5% loss of original weight) of

PM is 409.8°C which is much lower than that of P1 (434.6°C) and P2 (446.2°C). It can be concluded that the incorporation of POSS in P1 and P2 has led to significant improvements in the thermal stability of the conjugated polymer.

DSC curves of the polymers are shown in Figure 4.5. It clearly shows that for all the three polymers there is an obvious peak at a temperature slightly higher than 100°C on heating. This peak was confirmed as a non-reversible process by modulated DSC and thus is likely to be associated with the re-crystallization process although the melting peak could not be observed up to 280°C. The shifting of this re-crystallization process towards high temperature from **P2** to **PM** is due possibly to the looser packing of polymer chains in the hyberbranched polymers. It is reasonable to conclude that the incorporation of POSS cage effectively disrupt the dense packing of the conjugated polymers.

4.3.3 Morphology

X-ray diffraction (XRD) patterns obtained from monomers **A** and **B** and polymers **PM, P1** and **P2** are shown in Figure 4.6. Monomer **A** is a highly crystalline compound that exhibits multi sharp diffraction peaks. Monomer **B** has a strong peak at $2\theta \approx 6^{o}$ corresponding to a *d* spacing of 1.47 nm, which is correspondent to the calculated molecular size of **B**. The scattering from monomer **B** is relative weak and broad indicating that this semi-liquid compound possesses a slightly ordered packing structure. For polymers **PM, P1** and **P2**, the normalized XRD patterns (normalized based on the height of the broad amorphous peak at $2\theta = 20^{o}$) show a clear trend that a higher feed ratio of POSS monomer (**B**) to linear monomer (**A**) leads to a lower crystallinity of the polymer. This could be

attributed to the fact that the more conjugated chains are connected to POSS cage, the less chance for close packing of polymer chains.

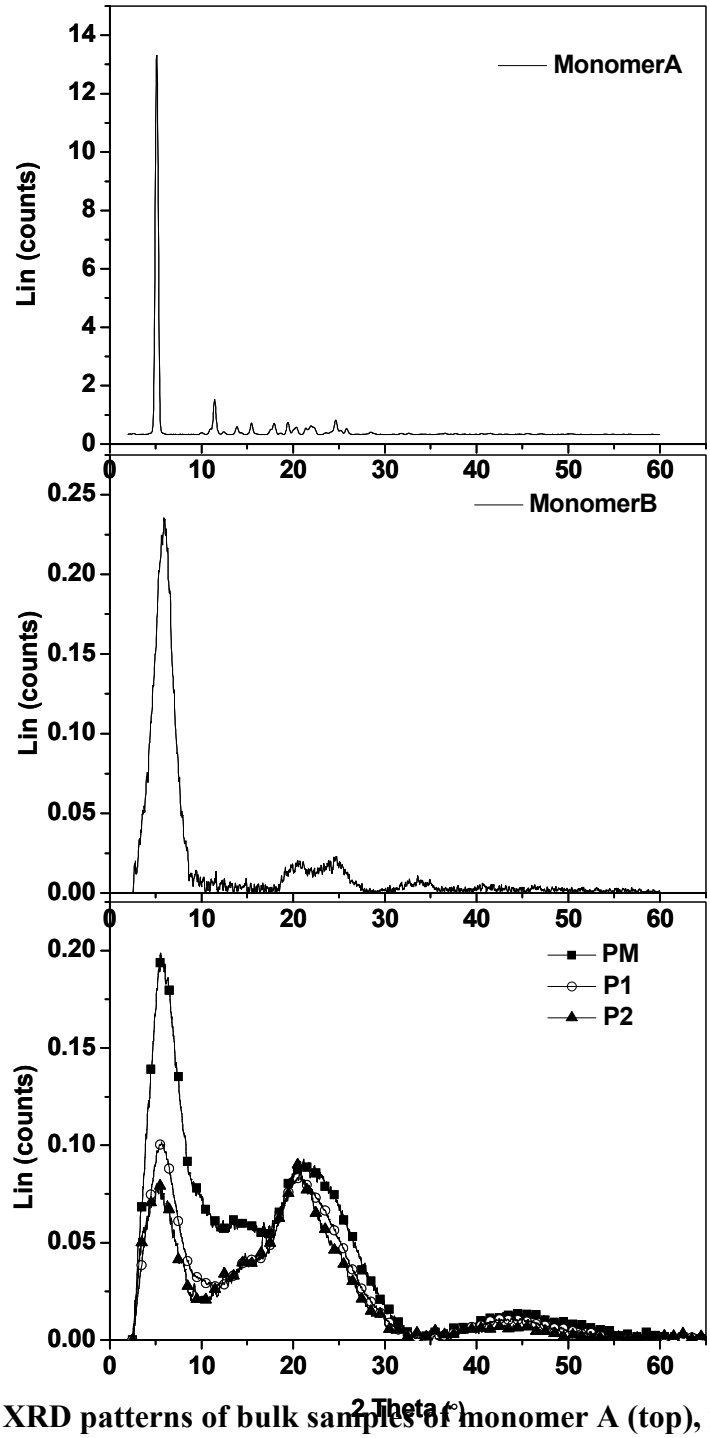

Figure 4.6. XRD patterns of bulk samples of monomer A (top), monomer B (middle), and polymer PM, P1, P2 (bottom) thin films.

4.3.4 Optical properties

UV absorption of **PM**, **P1**, and **P2** were measured in dilute solution of THF as well as in solid thin films. The normalized spectra are shown in Figure 4.7 and the data summarized in Table 4.2. The maximum absorption wavelengths of three polymers are similar in dilute solution, which indicates that the active absorption components in these **U**V absorption of **PM**, **P1**, and **P2** were measured in dilute solution of THF as well as in solid thin films. The normalized spectra are shown in Figure 4.7 and the data summarized in Table 4.2. The maximum absorption wavelengths of three polymers are similar in dilute solution, which indicates that the active absorption components in these **U**V absorption of **PM**, **P1**, and **P2** were measured in dilute solution of THF as well as in solid thin films. The normalized spectra are shown in Figure 4.7 and the data summarized in Table 4.2. The maximum absorption wavelengths of three polymers are similar in dilute solution, which indicates that the active absorption components in these three polymers are similar. The UV absorption of three polymers in different solvents, e.g. $CHCl_3$, THF and ethyl acetate, were measured. The on-set and maximum of the absorption peaks of the three red polymers do not shift by changing solvents. This result is different from our previous work on nanometer-sized hybrid light-emitting dot materials in which the absorption peak shifts with the polarity of solvent.[40] The results imply that the nanometer-sized chromophores are more sensitive to the polarity of solvent than the chromophores of larger size, e.g. hyper-branched polymers. The on-set of the absorption peaks for **PM**, **P1**, **P2** in condensed state are slightly red-shifted compared with that in solution. The maximum PL emission for **PM**, **P1**, **P2** in condensed state is however blue shifted compared with that of the solution. This could be due to the change in torsion

angle of polymer chains in condensed state, which leads to higher band gap compared with that in dilute solution.

Table 4.2. Optical properties of polymers

Polymers	λmax (UV, nm)		λmax (PL, nm)		$\Phi_{PL\text{-}f}$	$\Phi_{PL\text{-}f}$ (blend)			
	Solution	film	Solution	film	film	Content ratio[a]	wt% Ben[b]	wt% POSS[b]	$\Phi_{PL\text{-}f}$
PM	326, 511	333, 520	660	617	10	1 : 0			10
P1	328, 514	337, 525	660	620	18	6 : 1	23	1.5	13
P2	330, 514	340, 533	660	620	50	4 : 1	22	2.1	26

[a] Content ratio is the molar ratio of the repeat units of **PM** to monomer **B** in the blends, which is same as the content ratio in Table 1.

[b] wt% is the weight percentage of benzothiadiazole (C_6N_2S)and POSS (Si_8O_{12}) in blends, which is same as that in Table 1.

The relative PL quantum efficiencies ($\Phi_{PL\text{-}f}$) of **PM**, **P1** and **P2** in film were determined and also summarized in Table 4.2. $\Phi_{PL\text{-}f}$ of film **P2** is about 50% which is much higher than that of **PM** (10%) and **P1** (18%). The significant increase in quantum efficiency of **P2** can be attributed to the high concentration of POSS which effectively reduces the degree of aggregation. For comparison, polymer **PM** was blended with monomer **B** at the same POSS molar concentration as that of polymers **P1** and **P2,** respectively, and the PL quantum efficiencies of the blends were also tested and the results are listed in Table 2.2. It is interesting to see that by simply blending polymer **PM** with monomer **B**, the quantum efficiency of the resulting polymer blend is also higher than that of **PM**. This could be attributed to the disruption of packing of **PM** by the POSS molecules. On the other hand, the

quantum efficiencies of polymer blends (13% and 26%) are lower than those of their corresponding polymers (18% for **P1** and 50% for **P2**). This demonstrates that the covalent bonding of conjugated polymers onto POSS is more effective than simply blending POSS moieties with polymers in reducing aggregation.

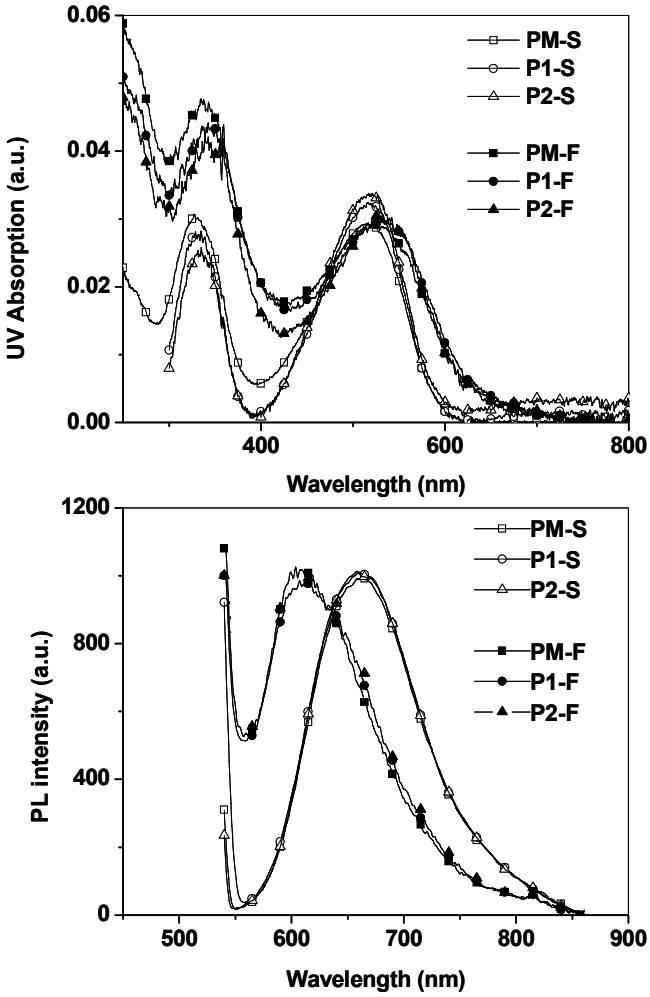

Figure 4.7. UV absorption (upper) and Photoluminescence (PL) spectra (lower) of PM, P1, P2 in solution THF (S) and thin film (F).

4.3.5 Electroluminescence properties.

Electroluminescence (EL) properties of the three red emissive polymers were studied by fabricating LED devices using **PM**, **P1**, and **P2** as emissive layer. The configuration of double-layer light-emitting device is (indium tin oxide) ITO/(poly(3,4-ethylenedioxythiophene) PEDOT (30 nm)/emissive polymer (60 nm)/LiF (0.5 nm)/Ca (20 nm)/Ag (100 nm). PEDOT doped with poly(styrenesulfonic acid) (PPS) was used as the hole injection/transporting layer. The active area of the device was about 4.0 mm^2. The EL spectrum of **PM** and **P1** are shown in Figure 4.8. The EL spectrum of **P1** is narrower than that of **PM**. The full width at half maximum (FWHM) for **PM** is 128 nm while for **P1** it is 93 nm. Incorporating of POSS cage narrowed the EL spectrum of **PM** by 34%. The narrowness of EL spectrum has been found in polyfluorene (PF)-POSS polymers. The cage reduces the undesired green emission, which was caused by aggregation in PF, and naturally narrowed down the EL spectrum of PF.[32,34] The narrowness of EL spectrum of PF-POSS is normally accompanied by blue shifting of EL spectrum compared to that of PF.[32,34] This is however not observed in **P1**.

The I-V-L (current-voltage-luminescence) spectra of PM and P1 are shown in Figure 4.9. It is interesting to see that the turn-on voltage of P1 (4.7 V) is slightly lower than that of PM (5.3V), although P1 is a hyperbranched polymer with polymer chains interrupted by POSS. The lower turn-on voltage is possibly due to the improved adhesion to ITO glass substrate.31 Investigation of LED device reveals that hybrid material P1 has higher EL brightness than that of PM at the same voltage. At 9.2 V, the electroluminescence of P1 is 5 x 10^2 cd/m2 while that of **PM** is only about 1 x 10^2 cd/m^2. The brightness of **P1** is 500% of that of **PM**. The wavelengths at maximum electroluminescence, $\lambda_{EL\text{-}max,}$ for **PM** and **P1** are similar to

their wavelengths at maximum photoluminescence, $\lambda_{PL\text{-}max}$, in solution. The color of LED device fabricated using **P1** as the emissive layer is pure red with CIE coordinates of x = 0.52, y = 0.32. The maximum current efficiency Φ_{EL}-max for a device using **P1** as the emissive layer is 0.43 (cd/A) at 7.7V, which is more than 7-times of that of **PM** (0.06 cd/A).

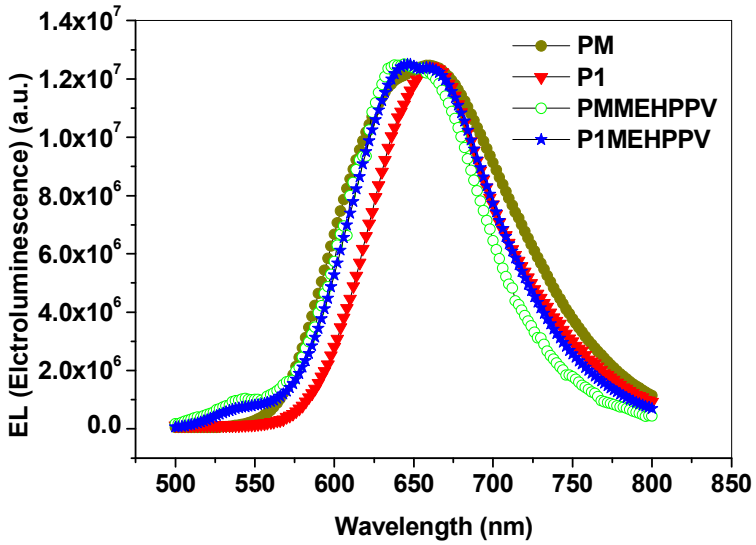

Figure 4.8. Normalized Electroluminescence spectra of PM, P1, PM-MEH-PPV, and P1-MEH-PPV.

When **PM** and **P1** were blended with poly[2-methoxy-5-(2'-ethylhexyloxy)-1,4-phenylenevinylene] (MEH-PPV) at weight ratio of **PM** (or **P1**) : MEH-PPV = 2 : 1, the device performance is enhanced significantly as shown in table 3. The EL spectra of **P1**-MEH-PPV and **PM**-MEH-PPV, as shown in Figure 4.8, are narrower than that of **PM** but still broader than that of **P1**. The narrowness of EL spectrum of blended polymers is due to the reduction of aggregation, both J-aggregation and H-aggregation[45] because MEH-PPV penetrated into the closely packed **PM** chains. The full width at half maximum (FWHM) of

PM-MEHPPV is 97 nm while for **P1**-MEHPPV it is 104nm. Even though the maximum of emission for blends shifted a bit but the whole spectra of blends are similar with that of PM and P1 which implies the emission of blended polymers come from PM and P1 instead of MEH-PPV due to Förster resonance energy transfer. The *I-V-L* spectrum of PM-MEH-PPV and P1-MEH-PPV are shown in Figure 4.10. The maximum brightness of device fabricated using P1-MEH-PPV is 2.6 x 10^3 cd/m^2 at 17V with a maximum current efficiency of 1.46 cd/A at 14V, which are much higher than those of PM-MEH-PPV (1.1 x 10^3 cd/m^2 at 16.8 V and 0.34 cd/A at 12.8V). It is worth noting that there is an optimal POSS concentration in terms of LED performance. For example, **P2** that has a higher POSS concentration shows a much higher turn-on voltage (~18V) than that of linear polymer **PM** because the POSS cage interrupted the conjugation. The emission of blended polymers come from **PM** and **P1** instead of MEH-PPV because the EL of device is 660nm instead of 570nm of MEHPPV. The *I-V-L* spectrum of **PM-**MEH-PPV and **P1-**MEH-PPV are shown in Figure 4.11. The maximum brightness of device fabricated using **P1-MEH-PPV** is 2.6 x 10^3 cd/m^2 at 17V with a maximum current efficiency of 1.46 cd/A at 14V, which are much higher than those of **PM-**MEH-PPV (1.1 x 10^3 cd/m^2 at 16.8 V and 0.34 cd/A at 12.8V).

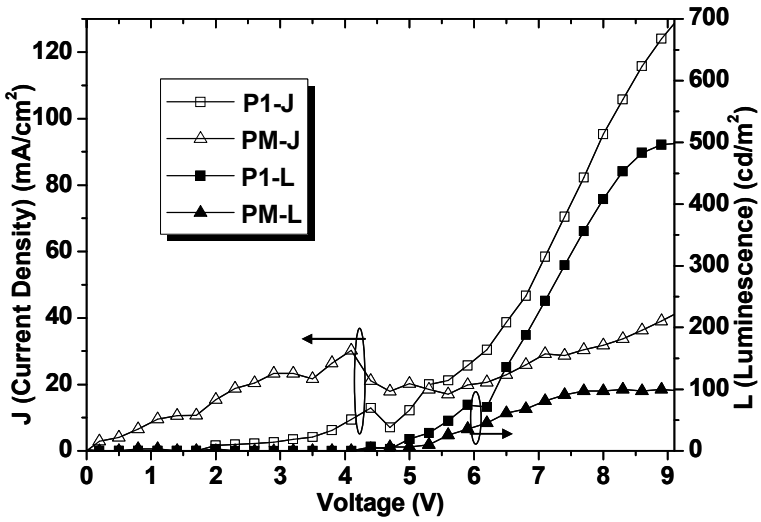

Figure 4.9. *I-V-L* spectra of PM and P1.

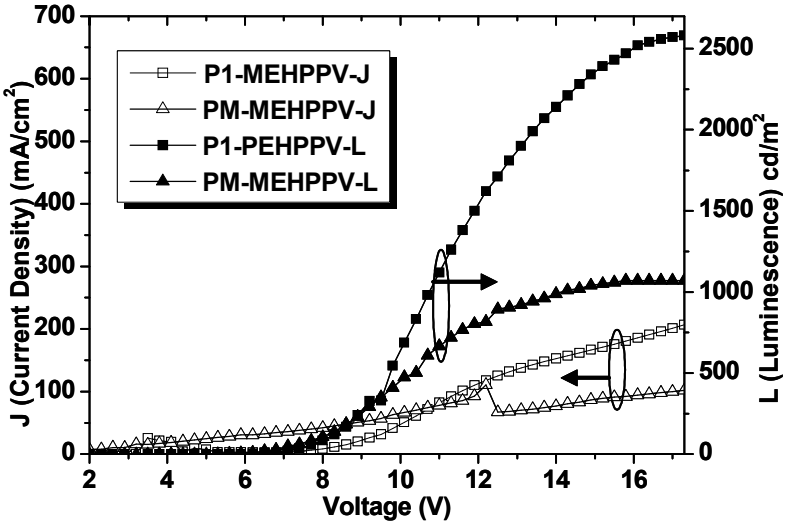

Figure 4.10. I-V-L spectra of blended PM and P1 with MEH-PPV.

Table 4.3. Elctroluminescent properties of polymers

polymers	Turn-on Voltage (V)	Max. brightness (cd/m^2)	Max Current density (mA/cm^2)	Max Current efficiency (cd/A)	λ_{EL-max} (nm)	FWHM (EL) (nm)
PM	4.7	100 (at 9.2V)	879	0.06 (at 7.7V)	660	128
P1	3.6	500 (at 9.2V)	718	0.43 (at 7.7V)	660	93
P2	18.0	96	590	0.02		
PM+ MEHPPV	6.0	1070 (at 16.8V)	523	0.34 (at 12.8V)	644	104
P1 + MEHPPV	6.0	2600 (at 17.0V)	235	1.46 (at 14.0V)	648	104
P2 + MEHPPV	20.0	970	1900	0.05		

4.4 Conclusion

Novel red emissive hyperbranched polymers that consist of inorganic POSS cage tethered with red emissive conjugated linear polymer chains were synthesized. The new red electroluminescence materials show higher PL quantum efficiency, improved thermal stability and lower crystallinity compared with that of their linear counterpart. The electroluminescent spectra of the hyperbranched polymers have emission λ_{max} at 660 nm which falls in the pure red range. Moreover, the hyperbranched polymer shows much narrower EL spectrum than that of linear polymer. The LED device fabricated using the new hyperbranched polymer **P1** as the emissive layer shows that the polymer has much higher electroluminescence brightness than that of the corresponding linear polymer at same voltage and film thickness and with the same device structure. The brightness of the hyperbranched polymer is 500% of that of the liner polymer at same voltage. It is also found that with low POSS incorporation, the turn-on voltage of the device is hardly changed, i.e. the device made of **PM** and **P1** have similar turn-on voltage. The much improved performance of the hyperbranched polymer over that of the linear polymer is due to the unique structure of this new hybrid material, in which the aggregation of polymer chains resulted from π - π stacking is greatly reduced. The new material could be used as an effective red electroluminescent material for LED applications.

4.5 Reference

1. Chiang, C. K., Fincher, C. R., Park, Y. W., Heeger, A. J., Shirakawa, H., Louis, E. J., Gau, S. C., & Macdiarmid, A. G.(2005). Electrical-conductivity in doped polyacetylene. *Physical Review Letters*, 39, 1098-1101.

2. Burroughes, J. H., Bradley, D. D. C., Brown, A. R., Marks, R. N.,, Mackay, K., Friend, R. H.,, Burns, P. L., & Holmes, A. B. (1990). Light-Emitting-Diodes Based on Conjugated Polymers. *Nature,* 347, 539-541.

3. Friend, R. H., Gymer, R. W., Holmes, A. B., Burroughes, J. H., Marks, R. N., Taliani, C., Bradley, D. D. C., Dos Santos, D. A., Bredas, J. L., Logdlund, M., & Salaneck, W. R. (1999). Electroluminescence in conjugated polymers. *Nature*, 397, 121-128.

4. Kraft, A.; Grimsdale, A. C.; & Holmes, A. B. (1998). Electroluminescent conjugated polymers - Seeing polymers in a new light. *Angewandte Chemie-International Edition*, 37, 402-428.

5. Xin, H., Ren, G. Q., Kim, F. S., & Jenekhe, S. A. (2008). Bulk heterojunction solar cells from poly(3-butylthiophene)/fullerene blends: in situ self-assembly of nanowires, morphology, charge transport, and photovoltaic properties. *Chemistry of Materials*, 20, 6199-6207.

6. Xin, H., Kim, F. S., & Jenekhe, S. A. (2008). Highly efficient solar cells based on poly(3-butylthiophene) nanowires. *Journal of the American Chemical Society,* 130, 5424-5425.

7. Dimitrakopoulos, C. D., & Malenfant, P. R. L. (2002). Organic thin film transistors for large area electronics. *Advanced Materials*, 14, 99-117.

8. Balk, P. (1995). Dielectrics for Field-Effect Technology. *Advanced Materials,* 7, 703-710.

9. Englebienne, P. Synthetic materials capable of reporting biomolecular recognition events by chromic transition. *Journal Of Materials Chemistry,* 9, 1043-1054.

10. Greenham, N. C.; Moratti, S. C.; Bradley, D. D. C; Friend, R. H.; & Holmes, A. B. (1993**).** Efficient light-emitting-diodes based on polymers with high electron-affinities. *Nature,* 365. 628-630.

11. Xiao, Y., Yu, W. L., Chua, S. J., & Huang, W. (2000). A novel series of copolymers containing 2,5-dicyano-1,4-phenylene-vinylene - Synthetic tuning of the HOMO and LUMO energy levels of conjugated polymers. *Chemistry-A European Journal,* 6, 1318-1321.

12. Xiao, Y., Yu, W. L., Pei, J., Chen, Z. K., Huang, W., & Heeger, A. J. (1999). Conjugated copolymers of 2-methoxy-5-2 '-ethyl-hexyloxy-1,4-phenylenevinylene and 2,5-dicyano-1,4-phenylenevinylene as materials for polymer light-emitting diodes. *Synthetic Metals*, 106, 165-170.

13. Fukuda, M.; Sawada, K.; Yoshino, K. J Polym Sci Part A: Polym Chem 1993, 31, 2465-2471.

14. Liu, B., Yu, W.-L.;, Lai, Y.-H.; Huang, W. Chem Mater 2001, 13, 1984-1991.

15. Pei, J.; Yu, W.-L.; Ni, J.; Lai, Y.-H.; Huang, W.; Heeger, A. J. Macromolecules 2001, 34, 7241-7248.

16. Moratti, S. C.; Cervini, R.; Holmes, A. B.; Baigent, D. R.; Friend, R. H.; Greenham, N. C.; Gruner, J.; Hamer, P. J. Synth Met 1995, 71, 2117-2120.

17. Chen, C.-T. Chem Mater 2004, 16, 4389-4400.

18. Yang, R. Q.; Tian, R. Y.; Yan, J. G.; Zhang, Y.; Yang, J.; Hou, Q.; Yang, W.; Zhang, C.; Cao, Y. Macromolecules 2005, 38, 244-253.

19. Hou, Q.; Zhou, Q. M.; Zhang, Y.; Yang, W.; Yang, R. Q.; Cao, Y. Macromolecules 2004, 37, 6299-6305.

20. Park, M. J.; Lee, J.; Jung, I. H.; Park, J. H.; Hwang, D. H.; Shim, H. K. Macromolecules 2008, 41, 9643-9649.

21. Huang, J.; Niu, Y.-H.; Yang, W.; Mo, Y.-Q.; Yuan, M.; Cao, Y. Macromolecules 2002, 35, 6080-6082.

22. Niu, Y. H.; Huang, J.; Cao, Y. Adv Mater 2003, 15, 807-811.

23. Kim, Y.; Bradley, D. D. C. Cur. Appl Phy 2005, 5, 222-226.

24. Peng, K. Y.; Chen, S. A. Synth Met 2006, 156, 219-223.

25. Pei, J.; Liu, X.-L.; Yu, W.-L.; Lai, Y.-H.; Niu, Y.-H.; Cao, Y. Macromolecules 2002, 35, 7274-7280.

26. Yang, M.-J.; Ling, Q.-D.; Hiller, M.; Fun, X.-Z.; Liu, X.; Wang, L.-H.; Zhang, W.-G. .J Polym Sci Part A: Polym Chem 2000, 38, 3405-3411.

27. Hou, Q.; Xu, Y.-S.; Yang, W.; Yuan, M.; Peng, J.-B.; Cao, Y. J Mater Chem 2002, 12, 2887-2892.

28. Wu, F. I.; Shih, P. I.; Tseng, Y. H.; Shu, C. F.; Tung, Y. L.; Chi,Y. J. Mater Chem 2007, 17, 167-173.

29. Jespersen, K. G.; Beenken, W. J. D.; Zaushitsyn, Y.; Yartsev, A.; Andersson, M.; Pullerits, T.; Sundstrom, V. J Chem Phys 2004, 121, 12613-12617.

30. Xia, R. D.; Heliotis, G.; Bradley, D. D. C. Synth Met 2004, 140, 117-120.

31. Xiao, S.; Nguyen, M.; Gong, X.; Cao, Y.; Wu, H.-B.; Moses, D.; Heeger, A. J. Adv Funct Mater 2003, 13, 25-29.

32. Lee, J.; Cho, H.-J.; Jung, B.-J.; Cho, N.-S.; Shim, H.-K. Macromolecules 2004, 37, 8523-8529.

33. Lin, W.-J.; Chen, W.-C.; Wu, W.-C.; Niu, Y.-H.; Jen, A. K. Y. J. Macromolecules 2004, 37, 2335-2341.

34. Chou, C.-H.; Hsu, S.-L.; Dinakaran, K.; Chiu, M.-Y.; Wei, K.-H. Macromolecules 2005, 38, 745-751.

35. Chou, C.-H.; Hsu, S.-L.; Yeh, S.-W.; Wang, H.-S.; Wei, K.-H. Macromolecules 2005, 38, 9117-9123.

36. Lickiss, P. D.; Rataboul, F. Adv Organomet Chem 2008, 57, 1-116.

37. Kang, J.-M.; Cho, H.-J.; Lee, J.; Lee, J.-I.; Lee, S.-K.; Cho, N.-S.; Hwang, D.-H.; Shim, H.-K. Macromolecules 2006, 39, 4999-5008.

38. Cho, H.-J.; Hwang, D.-H.; Lee, J.-I.; Jung, Y.-K.; Park, J.-H.; Lee, J.; Lee, S.-K.; Shim, H.-K.; Chem Mater 2006, 18, 3780-3787.

39. He, C.-B.; Xiao, Y.; Huang, J.-C.; Lin, T.-T.; Mya, K.-Y.; Zhang, X.-H. J Am Chem Soc 2004, 126, 7792-7793.

40. Xiao, Y.; Liu, L.; He, C.-B.; Chin, W.-S.; Lin, T.-T.; Mya, K.-Y.; Huang, J.-C.; Lu, X.-H. J Mater Chem 2006, 16, 829-836.

41. Tonzola, C. J.; Alam, M. M.; Bean, B. A.; Jenekhe, S. A. Macromolecules 2004, 37, 3554-3563.

42. Chen, F.; Mehta, P. G.; Takiff, L.; McCullough, R. D. J Mater Chem 1996, 6, 1763-1766.

43. Abdou, M. S. A.; Lu, X. T.; Xie, Z. W.; Orfino, F.; Deen, M. J.; Holdcroft, S. Chem Mater 1995, 7, 631-641.

44. Ding, A. L.; Pei, J.; Lai, Y.-H.; Huang, W. J Mater Chem 2001, 11, 3082-3086.

45. Siddiqui, S.; Spano, F.C. Chem Phys Lett 1999, 308, 99–105.

Chapter 5 Conclusion and future work

5.1 Conclusions

In summary, a systematic study of the effect of incorporation of POSS on the properties, especially the optical characteristics, of luminescent nano-particles and hyper-branched polymers has been conducted by using three series of materials purposely designed and synthesized in this study.

1) Well defined POSS luminescent dots were designed and synthesized, in which conjugated oligomers with precise molecular structure and lengths were directly grafted onto eight vertexes of a POSS cage. All the luminescent units on each vertex of POSS were protected by alkyl / or alkoxy chains to eliminate inter- molecular interaction. As a result, intra- molecular interactions were suppressed. A further confirmation of the non-aggregation characteristic is the PL quantum efficiency of film which is much higher than that in solutions. Moreover, the diameter of POSS luminescent dots could be precisely controlled, and were in the range of 2-4 nm. Based on this unique set of POSS luminescent dots, we have gained fundamental understanding of the effect of incorporating POSS on the light emitting characteristics of the resulting luminescent nano-particles. It has been found that excitons are confined in each arm of luminescent units and hence can be treated as excitons confined within each individual nano-particle light emitting dot. It can be thought that isolated chromospheres are obtained. Quantum confinement effects are expected to be demonstrated by these novel nano-particles because the size of isolated chromospheres are in a range of 2-4nm. The quantum confinement effects have indeed been confirmed by the size effect, i.e. absorption and photoluminescence regularly red shift with the increase of size, and

a time-resolved PL study in which the exciton decay time readily increased with the molecular size. The PL and absorption spectra of these hybrid nano-particles, in contrast to conjugated polymers and dendrimers, are not red shift in the condensed state in comparison with solutions. The light emitting characteristics are strongly influenced by the interaction with local environment such as solvent polarities. By incorporating POSS, the resulting light emitting nano-particles are amorphous. The thermal stability of these hybrid luminescent dots is also improved compared with the conjugated chains.

2) Highly regioselective bromination of octaphenyl-POSS has been achieved at room temperature under mild conditions. The green POSS light emitting dots based on this structure have been synthesized to achieve well defined nano-particles with precisely controlled structures and sizes. The organic luminescent units are confined between two barriers with higher band gaps which are the POSS cage and surrounded alkyl chains. The structures, similar with blue light emitting dots as above mentioned, demonstrated quantum confined characteristics, as both intra- and inter- molecular interactions are prevented and excitons are localized on each arm of eight conjugated chains anchored onto POSS cage. The UV absorption and PL spectra hardly shifted from solutions to films. The PL spectrum is further studied by adding one polymer to this hybrid dot by gradually changing the polymer/dot ratio. The PL spectrum of a green light emitting dot overlaps with the PL spectrum of the polymer, but its spectrum hardly shifts regardless whether in solid/blend, neat film or in solution. A time-resolved PL study has shown that the exciton decay times of the green light emitting dot in dilute solution, condensed state, and in blend form with other polymer are quite similar, indicting a strong quantum confinement effect as the diameter of

light emitting unit is around 4 nm. Furthermore, hydrophilic green light emitting dots have been prepared to demonstrate the possibility of its bio-application.

3) Functional POSS were incorporated into red hyper-branched conjugated polymers. It was found that incorporation of POSS into the red hyper-branched conjugated polymers significantly reduced the potential intra- and inter-chain interactions, and hence reduced the chances of non-radiative combination of excitons. As a result, POSS based hyper-branched polymers demonstrated greatly improved thermal stabilities, higher PL quantum yield, lower crystallinity, narrower electroluminescent spectrum, lower turn-on voltage, higher electroluminescent brightness, etc. In addition, physically blending POSS with the same light emitting polymer also showed an enhancement in PL quantum efficiency, possible due to disruption of the packing of the polymer chain.

5.2. Direction of future work

The unique materials obtained in this study are homogenous isolated chromospheres with high PL quantum efficiency and stable luminescence regardless whether in solutions or in condensed state. The tunable and controllable structures and emission wavelengths are other advantageous properties in sensing applications. The challenges for conventional nano-particles sensing materials, as mentioned in Chapter 1, are how to develop nano-particles with optical stablilty, homogeneity, robustness, less toxicity, high efficiency, diversity of emission range, and affordable prices. The next step of work is to explore the sensing applications by synthesizing a series of hybrid luminescent nano-particles as sensors for toxic chemical environments, chemical weapons, and air-pollution detectors.

The nano-sensors will have star-like structures using POSS as a core and will be tethered with alkyl / alkoxy chains protected chromospheres on eight vertexes. The PL spectrum in film and solution will be identical. The new nano-particle based sensors will offer superior optical properties over organic dye sensors, such as having brighter luminescent signals with higher photo-stability, as well as higher resolutions. The unique structure and properties of the new materials will overcome the disadvantages of conventional nano-particles, e.g. organic dye sensors, such as aggregation quenching, low PL intensity of luminescence, and low resolution, unstable luminescence due to concentration changing, etc. The new sensors are not sensitive to concentration of solutions hence it will be unnecessary to make extremely dilute solutions to minimize aggregation caused spectrum shift, which will provide significant enhancement in stable emission and luminescent intensity of the sensor.

Using POSS to carry the chromospheres has four advantages. First, POSS is known to be capable of forming air spray, making it suitable for cloud sensing applications. Second, POSS is a nano-cage structure, and attachment of fluorophores to every vertex of this nano-scaffold will generate more sensor groups per unit mass (or unit volume) and offer greater sensitivity than a conventional system. Third, when rigidly attached to a bulky POSS (see Scheme 5.1), a chromosphere is more sterically hindered than it would be if used in “free” small molecule form. Four, alkyl chain protected chromospheres will minimize aggregation hence provide a high density of isolated chromospheres in uniform size and shape of nano-sensors. Thus aggregation and resulting self-quenching of fluorescence would be expected to be minimised in a POSS-fluorophores system.

The fluorescent labels in Scheme 5.1 are examples for this study because their wavelength of fluorescence is highly sensitive to the polarity of their immediate chemical

environment and they are commercially available in forms that react with POSS-amino or POSS-bromo starting compounds under mild conditions.

Scheme 5.1 structures of nano-sensor materials

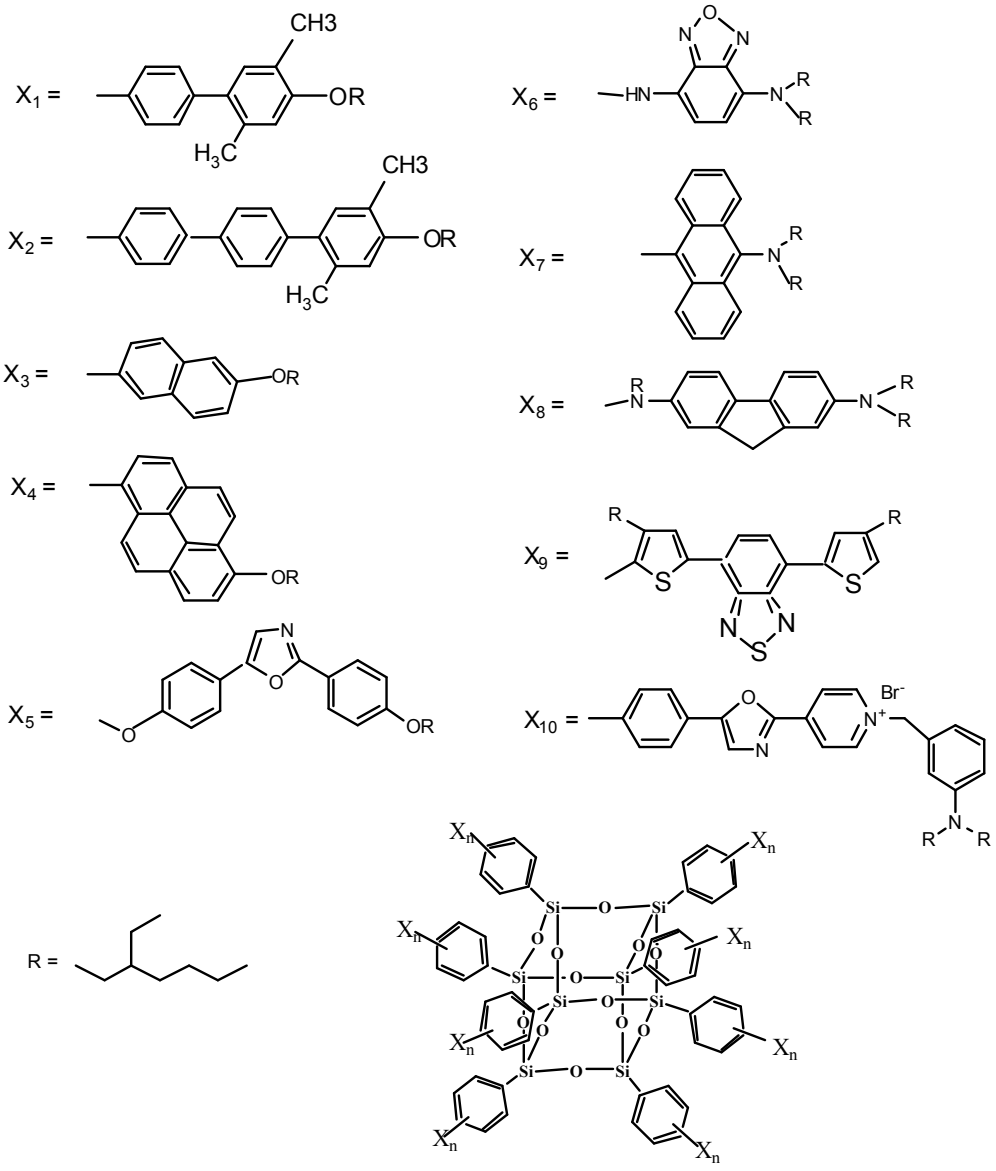

Following are the proposed scopes for further study. 1. To synthesize a series of polyhedral oligosilsesquioxane (POSS) nano-sensors functionalized with luminescent units that change their emissive wavelength in response to their chemical environment. 2. To study the applications by using them to generate fingerprints for a diverse range of analytes

including common organic solvents, air-pollutions, toxic industrial chemicals, chemical weapon agent simulants, and a homologous series of alcohols. To study their sensing capabilities for analytes in solutions, surfaces, and cloud forms. 3. To optimize their compositions and structures to get arrays showing excellent selectivity and being able to distinguish between different alcohols. One-photon fluorescence fingerprints will be constructed by measuring the fluorescence spectra of nano-sensor - analyte pairs in solution. Two-photon fluorescence fingerprints will be generated by remotely interrogating nano-sensor - analyte pairs using a laser and a stand-off fluorimeter.

The POSS compounds are usually thermally and chemically stable and can be modified by conventional synthetic methods. The commercial availability of a wide range of simple monomers will help to further research in these areas more rapidly. The use of POSS as scaffold in building nano-structures will be of particular interest for many new applications.

A1 – Instrument summary

The chemical structures and purities of synthesized materials are characterized by several instrumental techniques such as proton (^{1}H), carbon (^{13}C), and silicon (^{29}Si) nuclear magnetic resonance (NMR) spectroscopy, elemental analysis (EA), mass spectroscopy (MS), Matrix-assisted laser desorption/ionization time-of-flight (MALDI-TOF) mass spectra, fourier-transform infrared spectroscopy (FTIR). These techniques are used to confirm the chemical structures and purities of compounds synthesized in this work. The chemical, physical, and optical properties of materials synthesized in this work are characterized by some other instrumental methods such as gel permeation chromatography (GPC), high performance liquid chromatography (HPLC), differential scanning calorimetry (DSC), thermogravimetric analysis (TGA), X-ray diffraction (XRD), ultraviolet-visible spectroscopy (UV-vis), photoluminescence spectroscopy (PL), time-resolved photoluminescence spectroscopy (TRPL), atomic force microscopes (AFM), scanning electron microscope (SEM), transmission electron microscope (TEM), Modeling. All the methods are briefly introduced as follows.

NMR

With NMR, we are focused on the nuclei of atoms, not the electrons. The chemical environment of specific nuclei is deduced from information obtained about the nuclei. The nuclei of many elemental isotopes have a characteristic spin (I). Some nuclei have integral spins (e.g. I = 1, 2, 3 ....), some have fractional spins (e.g. I = 1/2, 3/2, 5/2 ....), and a few have no spin, I = 0 (e.g. 12C, 16O, 32S, ...). Isotopes of particular interest are ^{1}H, ^{13}C, ^{19}F and ^{31}P, all of which have I = 1/2. Since the analysis of this spin state is fairly straight fore-ward, our discussion of NMR will be limited to these and other I = 1/2 nuclei. A spinning

charge generates a magnetic field. In the presence of an external magnetic field, two spin states exist, +1/2 and -1/2. The magnetic moment of the lower energy +1/2 state is aligned with the external field, but that of the higher energy -1/2 spin state is opposed to the external field. When a radiofrequency is applied to the system and being absorbed, some nuclei in the low energy states are promoted to the higher energy states. The absorptions are characterized by chemical shifts which reflect the local environment of the nuclei. A plot of the peak frequencies of the absorptions against peak intensities forms a NMR spectrum.[1]

^{1}H, ^{13}C, ^{29}Si NMR data in this work were obtained by Bruker Avance 400 spectrometer.

EA

EA is the primary request for confirm the composition of a substance. It provides the information of elemental components and weight ratio of an unknown substance by the weight loss of selected elements in sample through controlled combustion.

Elemental micro-analysis was carried out by the Microanalysis Laboratory of the National University of Singapore.

MS

MS is basically the sorting out of charged gas molecules according to their masses. The sample is first ionised by knocking one or more electrons off to give a positive ion. The ions are accelerated so that they all have the same kinetic energy. The ions are then deflected by a magnetic field according to their masses. The lighter they are, the more they are deflected. The amount of deflection also depends on the number of positive charges on the ion - in other words, on how many electrons were knocked off in the first stage. The more the ion is charged, the more it gets deflected. The beam of ions passing through the machine is detected electrically. The amount of deflection for a given sideways force depends on the

mass of the ion. If one knew the speed of the ion and the size of the force, one could calculate the mass of the ion if the sort of curved path it was deflected through is known.[2]

Mass analysis was carried out by the Mass Spectrometry Laboratory of the National University of Singapore.

MALDI-TOF

The general principle of MS is using, traditionally, thermal vaporization methods to transfer molecules into the gas phase and the methods for ionization are electron impact (EI) and chemical ionization (CI). Most biomolecules, however, undergo significant decomposition under the conditions of both methods. So, the application of MS to bio-material analysis had been limited. MALDI as a principle for analysis of large biomolecules was introduced. In MALDI-MS, the sample is embedded in the crystalline structure of small organic compounds (matrix) and deposited on a conductive sample support. The co-crystals are irradiated with a focused laser beam, either in the UV or infra-red ranges, which can "evaporate" compounds from the solid phase. The laser energy causes structural decomposition of the irradiated crystal and generates a particle cloud (the plume) from which ions are extracted by an electric field. The resulting ions are injected into a tube and accelerated and allowed to drift towards a detector. Ion masses (mass-to-charge ratios [m/z]) are typically calculated by measuring their time-of-flight (TOF) which is longer for larger molecules than for smaller ones. Because predominantly single-charged, non-fragmented ions are generated, parent ion masses can easily be determined from the resulting spectrum.[3]

Our matrix-assisted laser desorption/ionization time-of-flight (MALDI-TOF) mass spectra were obtained on a Bruker Autoflex TOF/TOF instrument using dithranol as a matrix and silver trifluoroacetate as an ionizing salt. The sample was prepared as: a solution of

sample in THF (2mg / ml) was mixed with matrix solution in THF (1mg / ml) and silver trifluoroacetatesolution in THF (1mg / ml) in a ratio (v/v) of sample : matrix : Ag+ = 5 : 3 : 1.

FTIR

Fourier Transform Infrared Spectroscopy (FTIR) is a powerful tool for identifying types of chemical bonds (functional groups). The wavelength of light absorbed is characteristic of the chemical bond. By interpreting the infrared absorption spectrum, the chemical bonds in a molecule can be determined. FTIR spectra of pure compounds are generally so unique that they are like a molecular "fingerprint".[4]

Our FTIR spectra were recorded on a Bio-Rad FTS 165 spectrometer by dispersing samples in KBr disks. The sample was ground with KBr powder and made into a pellet before testing.

GPC & HPLC

GPC / Size-exclusion chromatography (SEC) is a technique which separates molecules on the basis of their sizes or hydrodynamic volumes with respect to the average pore size of the packing. This method uses the principle that a larger molecular size (three dimensional volume) sample elutes faster. The basic process involves the introduction of the sample into a stream of mobile phase that flows through a bed of a stationary phase. The sample molecules will distribute so that each spends some time in each phase. The stationary phase consists of small polymeric or silica-based particles that are porous and semirigid to rigid. Sample molecules that are smaller than the pore size can enter the stationary-phase particles and, therefore, have a longer path and longer retention time than larger molecules that cannot enter the pore structure. Very small molecules can enter virtually every pore they encounter

and, therefore, elute last. Larger molecules are excluded and, therefore, are rapidly carried through the system.[5]

GPC analysis in this work was carried out with a Shimadzu SCL-10A and LC-8A system equipped with two Phenogel 5μ 50 and 1000Å columns in series and a refractive detector, using THF as a eluent at a flow rate of 0.3ml/min at 40ºC. Monodispersed poly(ethylene glycol) were used as standards.

HPLC is basically a highly improved form of column chromatography. Instead of a solvent being allowed to drip through a column under gravity, it is forced through under high pressures of up to 400 atmospheres. That makes it much faster. It also allows the user to use a very much smaller particle size for the column packing material which gives a much greater surface area for interactions between the stationary phase and the molecules flowing past it. This allows a much better separation of the components of the mixture. The other major improvement over column chromatography concerns the detection methods which can be used. These methods are highly automated and extremely sensitive.[5]

HPLC analysis in this work was carried out with a Waters 2996 Separation Module linked simultaneously to a Waters 2996 Photodiode Array Detector. The mobile phase is THF/Acetonitrile (80:20 v/v). The column of reverse phase (SymmetryShield^{TM} PP8 5μm, 4.6x150mm) thermostat was set at 30°C. The flow rate was 1ml/min throughout the whole separation. The absorption of the column eluent was monitored at 254nm. The sample was prepared as: dissolve 2mg of sample in 2ml THF and filter the solution through a filter syringe (0.45 μm).

DSC

DSC is a thermoanalytical technique in which the difference in the amount of heat required to increase the temperature of a sample and reference is measured as a function of temperature. Both the sample and reference are maintained at nearly the same temperature throughout the experiment. Generally, the temperature program for a DSC analysis is designed such that the sample holder temperature increases linearly as a function of time. The reference sample should have a well-defined heat capacity over the range of temperatures to be scanned.[6]

DSC measurements were performed under nitrogen flow of 30 ml/min on a TA Instruments 2920 differential scanning calorimeter equipped with a cooling accessory and calibrated using indium. The powder sample was tested as received without any treatment. The weight range for each testing is 3-5mg.

TGA

TGA is a simple analytical technique that measures the weight loss (or weight gain) of a material as a function of temperature. As materials are heated, they can lose weight from a simple process such as drying, or from chemical reactions that liberate gasses. Some materials can gain weight by reacting with the atmosphere in the testing environment. Since weight loss and gain are disruptive processes to the sample material or batch, knowledge of the magnitude and temperature range of those reactions are necessary in order to design adequate thermal ramps and holds during those critical reaction periods.[6]

TGA was conducted, in this work, on a Perkin-Elmer thermogravimetric analyzer TGA 7 under a heating rate of 15 °C/min and a nitrogen flow rate of 40 cm^3/min

XRD

X-ray diffraction analysis (XRD) is a non-destructive method for the structure analysis of crystals. The sample is irradiated with monochromatic X-ray light and the stray radiation recorded. XRD analysis uses the property of crystal lattices to diffract X-ray light which involves the occurrence of interferences of the waves scattered at the successive planes. The processes are described by Bragg's equation: nL = 2d sina (n = 1,2,3,4,...) where L is the wavelength and d is the lattice plane distance and a is half the diffraction angle. This equation is used for the structure analysis of crystals getting d spacing and other information. The detector is a position-sensitive proportional counter.[7]

Our XRD data was recorded on a Bruker GADDS under a voltage of 40 kV and a current of 40 mA using CuK_α radiation (λ = 0.15418nm). The sample used for testing is a big piece of free standing bulk compound without any sample holder.

UV

A spectrophotometer is employed to measure the amount of light that a sample absorbs. The instrument operates by passing a beam of light of 200 nm – 800 nm through a sample and measuring the intensity of light reaching a detector. The beam of light consists of a stream of photons. When a photon encounters a molecule which is being studied, there is a chance that the analyte will absorb the photon. This absorption reduces the number of photons in the beam of light, thereby reducing the intensity of the light beam.[8] The energy (or wavelength) of light absorbed is characteristic of molecular electronic structures, e.g. band gap, of semiconducting materials.

UV-Vis spectra were recorded on a Shimadzu 3101 spectrophotometer.

PL

PL is a process in which a substance absorbs photons (electromagnetic radiation) and then re-radiates photons. This can be described as an excitation to a higher energy state and then a return to a lower energy state accompanied by the emission of a photon.[10] The wavelength of light absorbed by analyte and the wavelength of light emitted is a reflection of molecular electronic structures and optical properties of materials being studied.[8]

PL measurement was carried out on a Perkin-Elmer LS 50B luminescence spectrometer with a xenon lamp as a light source at room temperature and an UV laser at 325nm for low temperature PL measurement.

Time-resolved PL (TRPL)

Time-resolved photoluminescence (TRPL) is a method where the sample is excited with a light pulse whose photon energy is higher than the semiconductor band-gap and the created electrons and holes recombine and luminesce during all their life time and then the decay in photoluminescence with respect to time is measured.[9]

The time-resolved PL measurements were conducted with the excitation of the frequency doubled output of a Ti:sapphire femosecond laser (Sunami, Spectra Physics). The pulses were centered at 400 nm with pulse duration of 100 fs and pulse repetition rate of 82 MHz. The time evolution of the luminescence was recorded using a streak scope (Hamamatsu, C4334) with time resolution of 15 ps. The samples were kept in vacuum and the experiments were conducted at room temperature. Power of excitation is 12 W/ cm^2. The solution sample was prepared following the same procedures for sampling of PL testing.

AFM

AFM is a very high-resolution type of scanning probe microscopy, with demonstrated resolution of fractions of a nanometer. The AFM is one of the foremost tools for imaging,

measuring, and manipulating matter at the nano-scale. The information is gathered by "feeling" the surface with a mechanical probe. Piezoelectric elements that facilitate tiny but accurate and precise movements on (electronic) command enable the very precise scanning.[10]

Film morphology was examined by Digital Instruments Nanoscope IV multimode AFM (USA).

SEM

SEM is a type of electron microscope that images the sample surface by scanning it with a high-energy beam of electrons in a raster scan pattern. The electrons interact with the atoms that make up the sample producing signals that contain information about the sample's surface topography, composition and other properties such as electrical conductivity.[11]

Film morphology was examined by SEM (JEOL JMS 6700, JAPAN).

TEM

Transmission electron microscopy (TEM) is a microscopy technique whereby a beam of electrons is transmitted through an ultra thin specimen, interacting with the specimen as it passes through. An image is formed from the interaction of the electrons transmitted through the specimen; the image is magnified and focused onto an imaging device, such as a fluorescent screen, on a layer of photographic film, or to be detected by a sensor such as a CCD camera.[12]

TEM sections were collected in a Philips CM300 – FEG operating at an accelerating voltage of 200 kV on carbon coated Copper grids.

Reference

1. Lambert, J. B., Shurvell, H. F., Lightner, D. A., & Cooks, R. G. (1998). *Organic Structural Spectroscopy*. Prentice-Hall, Inc. New Jersey.
2. Clark J. (2000). THE MASS SPECTROMETER [On-line]. Available: http://www.chemguide.co.uk/analysis/masspec/howitworks.html
3. van den Boom, D., Beaulieu, M., Oeth, P., Roth, R., Honisch, C., Nelson, M. R., Jurinke, C., & Cantor, C. (2004). MALDI-TOF MS: a platform technology for genetic discovery. *International Journal of Mass Spectrometry,* 238, 173-188.
4. Pavia, D. L., Lampman, G. M., & Kriz, G. S. (1996). *Spectroscopy*. Harcount Brace College Publishers, 2nd edition.
5. Korhammer, S. A., Bernreuther, A. (1996). Hyphenation of high-performance liquid chromatography (HPLC) and other chromatographic techniques (SFC, GPC, GC, CE) with nuclear magnetic resonance (NMR): A review. *Fresenius Journal of Analytical Chemistry*, 354, 131-135.
6. Bourbigot, S., & Flambard, X. (2002). Heat resistance and flammability of high performance fibres: A review. *Fire and Materials,* 26, 155-168.
7. X-Ray Diffraction Analysis (XRD) [On-line]. Available: http://www.fz-juelich.de/zch/en/xrd
8. Khanna, R. K., Cui, H. (1993). Optical-properties of a novel carbon-carbon chain polymer with pendent poly(thiophene)s. *Macromolecules,* 26, 7076-7078.
9. Heller, C. M., Campbell, I. H., Laurich, B. K., Smith, D. L., Bradley, D. D. C., Burn, P. L., Ferraris, J. P., & Mullen, K. (1996). Solid-state-concentration effects on the optical absorption and emission of poly(p-phenylene vinylene)-related materials. *Physical Review B*, 54, 5516-5522.

10. Alessandrini, A., Facci, P. (2005). AFM: a versatile tool in biophysics. *Measurement Science & Technology,* 16, R65-R92.
11. Drzazga, W., Paluszynski, J., Slowko, W. (2006). Three-dimensional characterization of microstructures in a SEM. *Measurement Science & Technology,* 17, 28-31.
12. Electron Microscopy. [On-line] Available: http://www.unl.edu/CMRAcfem/temoptic.htm

A2 - List of Schemes

A2 - List of Tables

A3 - List of Figures

A4 - List of publications

1. Xiao, Y., Liu, L., He, C. B., Chin, W. S., Lin, T. T., Mya, K. Y., Huang, J. C., & Lu, X. H. (2006). Nano-hybrid luminescent dot: synthesis, characterization and optical properties. *Journal of Materials Chemistry*, 16, 829-836.
2. Xiao, Y., Lu, X. H., Tan, L. W. Ong, K. S., & He, C. B. (2009). Thermally Stable Red Electroluminescent Hybrid Polymers Derived from Functionalized Silsesquioxane and 4,7-Bis(3-ethylhexyl-2-thienyl)-2,1,3-benzothiadiazole. *Journal of Polymer Science Part A-Polymer Chemistry*, 47, 5661-5670.
3. Xiao, Y., Lu, X. H., Zhang, X. H., & He, C. H. Synthesis and optical characteristics of organic light emitting dot based on well-defined octa-functionalized silsesquioxane. *Journal of Nanoparticle Research*, Published on line 02 February 2010.
4. Xiong, S. X., Xiao, Y., Ma, J., Zhang, L. Y., & Lu, X. H. (2007). Enhancement of electrochromic contrast by tethering conjugated polymer chains onto polyhedral oligomeric silsesquioxane nanocages. *Macromolecular Rapid Communications,* 28, 281-285.
5. Hussain, H., Mya, K. Y., Xiao, Y., & He, C. B. (2008). Octafunctional cubic silsesquioxane (CSSQ)/poly(methyl methacrylate) nanocomposites: Synthesis by atom transfer radical polymerization at mild conditions and the influence of CSSQ on nanocomposites. *Journal of Polymer Science Part A-Polymer Chemistry,* 46, 766-776.

6. Teo, J. K. H., Teo, K. C., Pan, B. H., Xiao, Y., & Lu, X. H. (2007). Epoxy/polyhedral oligomeric silsesquioxane (POSS) hybrid networks cured with an anhydride: Cure kinetics and thermal properties. *Polymer,* 48, 5671-5680.
7. Hussain, H., Tan, B. H., Gudipati, C. S., Xaio, Y., Liu, Y., Davis, T. P., & He, C. B. (2008). Synthesis and Characterization of Organic/Inorganic Hybrid Star Polymers of 2,2,3,4,4,4-Hexafluorobutyl Methacrylate and Octa(aminophenyl)silsesquioxane Nano-Cage Made via Atom Transfer Radical Polymerization. *Journal of Polymer Science Part A-Polymer Chemistry,* 46, 7287-7298.